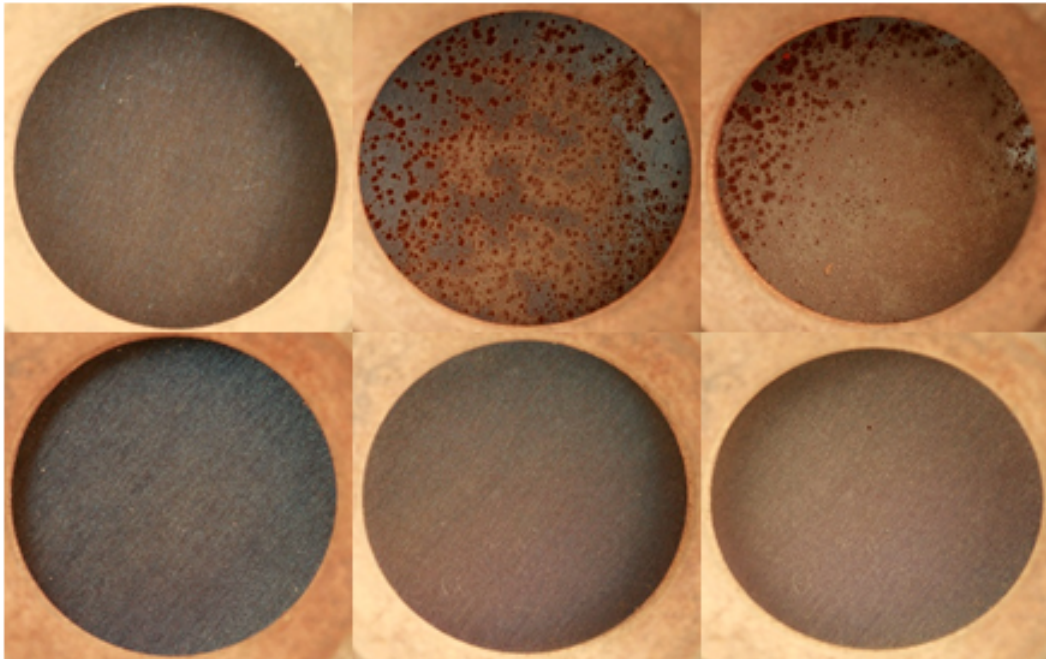




CHALMERS
UNIVERSITY OF TECHNOLOGY



Dual Atmospheric Corrosion of Ferritic Stainless Steels for SOFC Applications

Temperature Dependence of the Dual Atmosphere Effect

Master's thesis in Materials Chemistry

LUKAS HANSEN & OSCAR HJORTH

MASTER'S THESIS 2019

Dual Atmospheric Corrosion of Ferritic Stainless Steels for SOFC Applications

Temperature Dependence of the Dual Atmosphere Effect

LUKAS HANSEN & OSCAR HJORTH



CHALMERS
UNIVERSITY OF TECHNOLOGY

Department of Chemistry and Chemical Engineering
Division of Energy and Materials
The Fuel Cell Group
CHALMERS UNIVERSITY OF TECHNOLOGY
Gothenburg, Sweden 2019

Dual Atmospheric Corrosion of Ferritic Stainless Steels for SOFC Applications
Temperature Dependence of the Dual Atmosphere Effect
LUKAS HANSEN & OSCAR HJORTH

© LUKAS HANSEN & OSCAR HJORTH, 2019.

Supervisors: KEREM ÖZGÜR GÜNDÜZ & CLAUDIA GÖBEL, Department of
Chemistry and Chemical Engineering
Examiner: JAN FROITZHEIM, Department of Chemistry and Chemical
Engineering

Master's Thesis 2019
Department of Chemistry and Chemical Engineering
Division of Energy and Materials
The Fuel Cell Group
Chalmers University of Technology
SE-412 96 Gothenburg
Telephone +46 31 772 1000

Cover: Samples showing dual atmosphere effect.

Typeset in L^AT_EX
Gothenburg, Sweden 2019

Dual Atmospheric Corrosion of Ferritic Stainless Steels for SOFC Applications
Temperature Dependence of the Dual Atmosphere Effect

LUKAS HANSEN & OSCAR HJORTH

Department of Chemistry and Chemical Engineering

Chalmers University of Technology

Abstract

In this study, the dual atmospheric corrosion of solid oxide fuel cell interconnects has been investigated. The promising interconnect material, ferritic stainless steel, specifically AISI 441, has been exposed to two different atmospheres simultaneously, to simulate the operation of a real fuel cell. 0.2 mm thick as received, and ground samples with or without pre oxidation were used. To verify the effect of grinding and to have a clear understanding of temperature dependency of corrosion the samples were pre oxidized at 800°C for 20 minutes. In this process a thin oxide barrier was formed, which will decrease but not severely mitigate permeation of hydrogen. In order to understand the effect of temperature on the corrosion process, exposures between 500 and 800°C were performed both in dual and single atmosphere conditions for 336 hours discontinuously. After 168 hours, the samples were cooled to room temperature and investigated by macro photography to track the corrosion process. After 336 hours the samples were investigated using macro photography, electron microscopy and energy dispersive X-ray spectroscopy. A comparison between the samples exposed to dual, and single atmosphere were conducted. According to the obtained results, samples were highly corroded at 600°C whereas at temperatures below or above 600°C, less corrosion was observed which points out that 600°C is the critical temperature for dual atmosphere corrosion. Furthermore, on the contrary to the results obtained in literature, the dual atmosphere effect was observed at 700°C. Lastly, the effect of grinding was verified and less corrosion was observed on ground samples without pre oxidation compared to the ground and pre oxidized samples.

Keywords: Corrosion, Dual Atmosphere, SOFC, Interconnect

Acknowledgements

We would like to thank our supervisor Kerem Özgür Gündüz for all the help both practically and theoretically. You have given us great support throughout the project and we are thankful for that.

Thank you Claudia Göbel for helping us and Özgür. Without you, we would not have been able to come this far with the project.

Also a big thank you to our examiner, Jan Froitzheim, for giving us the opportunity to work with this project.

Lastly we would like to thank the team of HTC for providing a nice working environment during our thesis work.

Lukas Hansen & Oscar Hjorth, Gothenburg, June 2019

Contents

1	Introduction	1
1.1	Background	1
1.2	Aim	2
2	Theory	3
2.1	Fuel Cells	3
2.1.1	Solid Oxide Fuel Cells	3
2.1.2	Interconnects	4
2.2	Corrosion	5
2.2.1	Thermodynamics	5
2.2.2	Oxide Scale Growth	7
2.2.3	Kinetics	9
2.2.4	Corrosion of Interconnects in Fuel Cells	10
2.3	Dual Atmosphere Effect	11
2.4	Analytical Techniques	12
2.4.1	Broad Ion Beam	13
2.4.2	Scanning Electron Microscopy and Energy Dispersive X-Ray	13
3	Methods	15
3.1	Sample Preparation	15
3.1.1	Grinding	15
3.1.2	Cleaning	15
3.1.3	Pre Oxidation	16
3.2	Exposure	16
3.2.1	Characterization	18
4	Results & Discussion	19
4.1	500°C Exposure	19
4.2	550°C Exposure	22
4.3	600°C Exposure	29
4.4	650°C Exposure	34
4.5	700°C Exposure	41
4.6	800°C Exposure	47
4.7	The Effect of Temperature	51
4.8	The Effect of Surface Treatment	52
5	Conclusion	55

6	Future Works	57
A	Appendix 1	I
A.1	500°C exposure	I
A.2	550°C exposure	III
A.3	600°C exposure	IV
A.4	650°C exposure	VII
A.5	700°C exposure	X
A.6	800°C exposure	XI

1

Introduction

We live in a time where the demand of clean and efficient electricity production is crucial. Due to their high electrical efficiency and fuel flexibility, fuel cells offer an environmentally friendly way of electricity production compared to traditional energy-conversion systems [1, 2]. The basic principle of the fuel cell is based on electrochemistry, where hydrogen or other fuels are oxidized at the anode and oxygen is reduced at the cathode to generate a potential difference between the two electrodes. When hydrogen is employed as a fuel, electricity, water, and heat are produced because of the chemical energy of the reaction that is released [2].

1.1 Background

Solid oxide fuel cells, SOFC, have been studied for several years now, resulting in a reliable base to continue the research on. SOFC are promising devices for production of electricity, there are however two major obstacles for the widespread commercialization of the SOFC, they are expensive, and their lifetime is too short. The progress of the development of the main parts (electrolyte, cathode, and anode) of SOFC systems has resulted in a decrease of operation temperature to 600-800°C, which makes it possible to operate without expensive catalysts. This decrease in temperature also opens the opportunity to use metals, particularly ferritic stainless steels as interconnects. Using ferritic stainless steels instead of other materials previously used is favourable because they are cheaper, easier to manufacture, deformable, and compatible with the main parts of the SOFC. However, the operating temperatures are still very high compared to other fuel cell systems such as the proton exchange membrane (PEM) which has an operating temperature of around 80°C. Although the operating temperatures are high, the extra heat can be used in combined heat and power (CHP) units, or in combination with steam turbines for further energy generation. When re-utilizing water and heat produced as by product, the electrical efficiency of the fuel cell and overall system efficiencies can be increased from around 60% to 90% [3, 4].

The interconnects also work as gas channels, and are therefore exposed to two different atmospheres simultaneously, namely air on one side and fuel (e.g. hydrogen) on the other. This allows for a different type of corrosion called dual atmosphere oxidation, in which it has been shown that when hydrogen is used as fuel the corrosion on the air side is much more severe than the fuel side. It has also been shown that at lower operation temperatures (600°C) the corrosion is more severe compared

to higher temperatures ($>700^{\circ}\text{C}$). However, temperature is not the only parameter that is affecting the dual atmosphere effect, composition, thickness, grain size of the steel, surface finish, pre oxidation and exposure atmosphere (e.g. humidity) also play a big role in the corrosion process. Although there are many studies focused on dual atmosphere oxidation which been published the past 20 years, the exact mechanism leading to dual atmospheric corrosion is not known [5, 6]. Previously, grinding of the samples has shown to have a beneficial effect on the dual atmosphere oxidation [7]. However, not enough experiments were performed, and the effect has not been investigated deeply enough to confirm the effect.

1.2 Aim

Fuel cell interconnects are exposed to two different atmospheres simultaneously, fuel on one side, and air on the other side. This means that hydrogen is permeating from the fuel side to the air side of the steel and leading to severe corrosion through an unknown mechanism. In this project the dual atmosphere effect of ferritic stainless steel (FSS), more specifically AISI 441, used in solid oxide fuel cells (SOFC) as interconnects will be investigated. There are various parameters that affect the dual atmosphere oxidation of FSS (temperature, composition and thickness of the interconnect, surface finish, grain size, etc.). The main focus of the project is to investigate the effect of temperature and surface finish on the dual atmosphere oxidation behavior of FSS interconnects. To understand how the temperature and grinding affect the corrosion of FSS, experiments at different temperatures ($500\text{-}800^{\circ}\text{C}$) were performed on ground and as received samples with or without pre oxidation. After exposures the samples were characterized in terms of elemental distribution, thickness, micro structure and surface topography using macro photography and SEM-EDX.

2

Theory

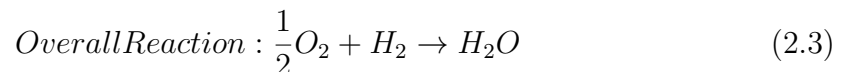
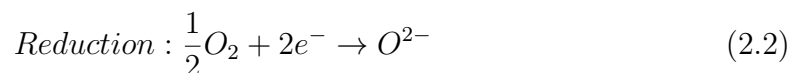
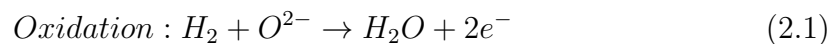
To understand how corrosion in fuel cell applications can be mitigated, an understanding of the behaviour of the corrosion is needed. The following chapter will explain the basic concepts of the fuel cell, high temperature corrosion and the analysis techniques used.

2.1 Fuel Cells

A fuel cell performs like a battery in the sense that it converts chemically stored energy to electricity via an electrochemical reaction without combustion. The first case of a working fuel cell was demonstrated independently by William Grove and Christian Friedrich Schönbein in 1839 [8]. Each cell consists of an anode and a cathode which are separated by an electrolyte. The purpose of the electrolyte is to separate the reaction into oxidation and reduction [9]. Since the electrolyte material is permeable to ions but not electrons, the electrons are forced to migrate through an external circuit. The process is driven by a concentration gradient over the electrolyte, where ion diffusion takes place when the anode and cathode are electrically connected via an external circuit [8]. In order for the reaction to take place, the system needs fuel. This is one advantage over regular batteries, the fuel cell can operate as long as fuel is provided.

2.1.1 Solid Oxide Fuel Cells

In a solid oxide fuel cell the electrolyte is a solid oxide, thus serves as an oxygen ion conductor. Generally, a solid oxide conducts only oxygen ions which allows the usage of different fuels, such as hydrocarbons like methane and diesel, where the fuel is oxidized into both H_2O and CO_2 . When H_2 is used as fuel, H_2 is oxidized to H_2O according to the following reactions:



The hydrogen is oxidized at the anode, and the oxygen is reduced at the cathode. The oxygen ions are diffused through the electrolyte and the electrons are transferred

via an external circuit. These steps, together with an illustration of a fuel cell stack are presented in Figure 2.1. As can be seen in Reaction 2.3 when H_2 is used as a fuel, the only product is water, which makes the fuel cell a fine candidate for future electricity production, both for stationary units as well as for mobile applications and auxiliary power units [9]. Depending on the electrolyte material, different fuels can be used since the electrolyte determines which ions can diffuse through the electrolyte.

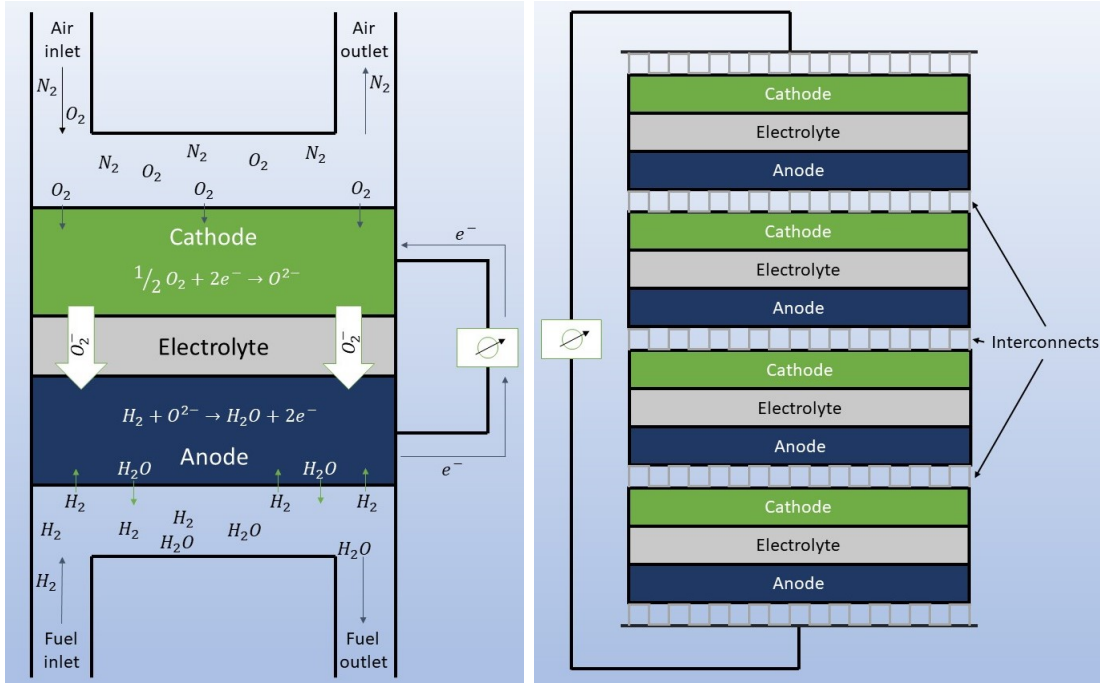


Figure 2.1: Solid oxide fuel cell. Operating principle (left) and Fuel cell stack (right). Drawn by the authors based on [10].

The reason for stacking the fuel cells is that one cell can only produce approximately 1 V [9], however, when they are connected internally they can reach the kW range. This is done by electrically connecting cells in a series via a component called interconnect to form a stack. The interconnect is more described in the next section.

2.1.2 Interconnects

The main purpose of the interconnect is to make an electrical connection between the anode of one cell and the cathode of the next cell. Another function is to separate the fuel and the air between cells in a stack [11]. To ensure reliable performance the interconnect should fulfill a few major requirements:

- Excellent resistance towards gases used on the anode and the cathode.
- High electrical conductivity.
- Low ionic conductivity.
- Good thermal conductivity.
- Compatible coefficient of thermal expansion, CTE, with adjacent components.

Previously, interconnects were made from ceramics. Their high cost, and process difficulties made ceramics as interconnect material undesirable for the commercialization of fuel cells [12]. The drawbacks of the ceramic materials have drawn the attention away from these materials and towards stainless steels which have more desirable properties. Metallic interconnects are easier to manufacture, have a lower cost, higher mechanical strength, and better electrical and thermal conductivity [2]. One requirement for the metallic interconnects is that they can be used at intermediate to low temperatures ($<800^{\circ}\text{C}$), because of the low oxidation rate.

The most suitable material for SOFC interconnects is ferritic stainless steels, because of its good electrical and thermal conductivity, cheap cost, easy formability and compatibility with the main components in terms of thermal expansion. These steels contain chromium that will form a protective layer on top of the interconnect. However at elevated temperatures chromium tends to form volatile species, especially in humidified environments that eventually will poison the cathode at the three phase boundaries. To improve the SOFCs lifetime, metallic interconnects will require some modification, some metals need coatings to avoid chromium evaporation, other need to be doped with other elements [13]. Small additions of oxygen-active elements, such as hafnium, cerium, lanthanum, yttrium, and zirconium, have been proven to provide positive effects on the oxidation behaviour. These elements are often called reactive elements, and small additions of these elements to a chromia forming alloy will result in a higher adherence of chromia scale to the metal. Also, the growth rate of the chromia scale is decreased and the selective oxidation is enhanced, which restricts the formation of iron oxide [13, 14].

2.2 Corrosion

The majority of all metals are generated by reducing ores. That means that under natural conditions, oxides are stable. Therefore, a charge of energy, such as an elevated temperature is necessary to generate a metal. When metals react with oxygen they will return to a more stable state, as an ore. At lower temperatures ($<500^{\circ}\text{C}$) and in the absence of water, the corrosion rate does normally not cause any problems. However, when the temperature increases the corrosion rate will be a larger threat [15]. For our application where ferritic stainless steel is used and at elevated temperatures, a fast growing, non protective iron oxide scale is formed. This may cause the material to break. To understand how the corrosion behaves, knowledge regarding thermodynamics and kinetics are necessary. The fundamentals of high temperature corrosion are described in the following section.

2.2.1 Thermodynamics

To determine the stability of a metal under certain conditions, the Gibbs free energy can be used:

$$\Delta G = \Delta H - T\Delta S \quad (2.4)$$

where G is Gibbs free energy, H is enthalpy, T is temperature and S is entropy. Depending on the value of ΔG the reaction is either in equilibrium, $\Delta G=0$, non-spontaneous, $\Delta G>0$, or spontaneous, $\Delta G<0$. One can also express Gibbs free energy by using the reaction quotient, Q_p :

$$\Delta G = \Delta G^\circ + RT \ln Q_p \quad (2.5)$$

ΔG° represents the free energy under standard conditions and R is the ideal gas constant. The oxidation of metals can be described as:



where M is any given metal. Using Reaction 2.6, the reaction quotient can be written as:

$$Q = \frac{a(M_xO_y)}{a(M)^x a(O_2)^{\frac{y}{2}}} \quad (2.7)$$

here a represents the thermodynamic activity of a specific species. For pure solids, such as the metal and its oxide, the activity can be approximated as unity ($a=1$). If Equation 2.5 is combined with Equation 2.6 the expression for the oxidation of metals is obtained:

$$\Delta G = \Delta G^\circ + RT \ln \left(\frac{a(M_xO_y)}{a(M)^x a(O_2)^{\frac{y}{2}}} \right) \quad (2.8)$$

For equilibrium conditions, ΔG is equal to zero which results in Equation 2.9.

$$\Delta G^\circ = -RT \ln \left(\frac{1}{a(O_2)^{\frac{y}{2}}} \right) \quad (2.9)$$

The oxygen activity can be approximated as the oxygen partial pressure which results in Equation 2.10:

$$p_{O_2} = \exp \left(\frac{\Delta G^\circ}{RT} \frac{2}{y} \right) \quad (2.10)$$

Since the partial pressure, p_{O_2} , together with temperature, T , are important factors in this relation, Equation 2.10 can be used to calculate whether a metal or oxide is thermodynamically stable or not under certain conditions. To visualize the thermodynamic stability of metal oxides and metals, the Ellingham/Richardson diagram can be used. In this diagram the dissociation pressure of metals is shown, this is the oxygen pressure where the metal and metal oxide are in equilibrium. When the oxygen partial pressure falls below the dissociation pressure, the oxide gets reduced to metal, and a partial pressure larger than the dissociation pressure results in oxidation of the metal. As can be seen in Figure 2.2, lines in the lower part of the diagram represent metal oxides with low ΔG . Further up in the diagram, oxides with high ΔG are depicted [16].

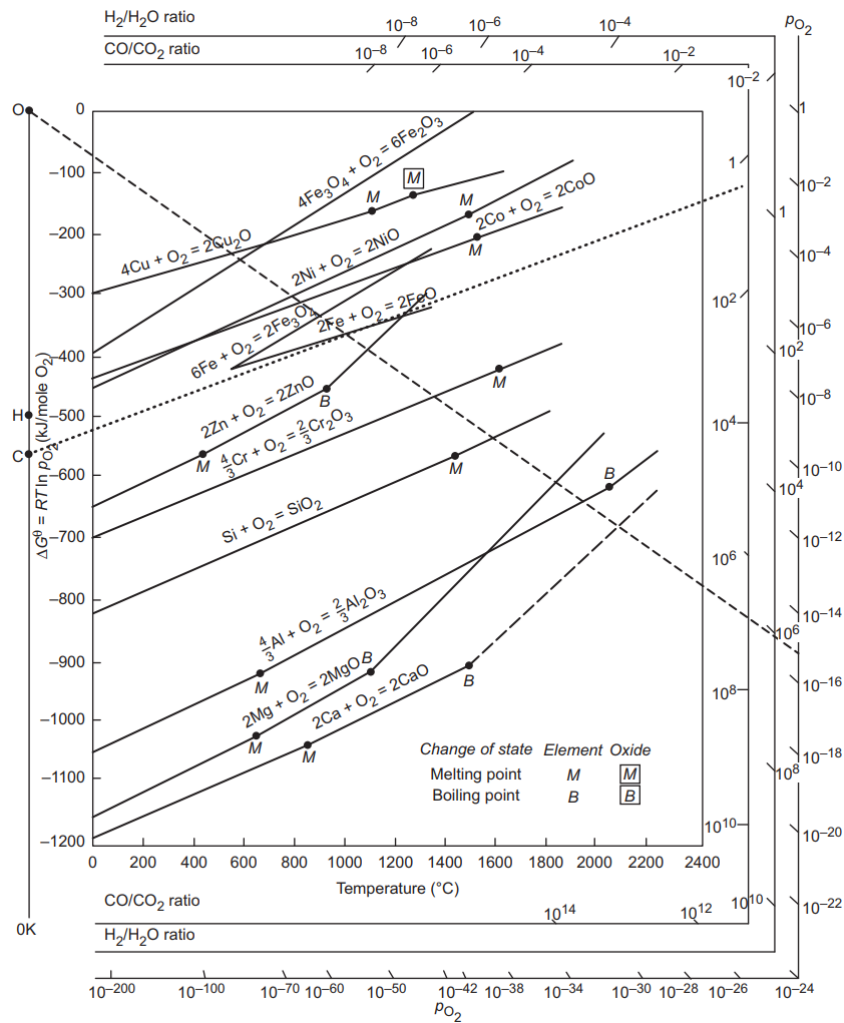


Figure 2.2: Ellingham/Richardson diagram showing different metals and their oxides for different parameters [17].

This diagram illustrates the standard free energy of formation versus temperature. In the left most part of the diagram guiding points can be seen. These points together with the partial pressure of oxygen allows for quick calculations of the dissociation pressure. This is done by drawing a line between the guiding points and the intersection between the temperature and a specific metal.

2.2.2 Oxide Scale Growth

The initial oxidation process happens in three steps:

- Adsorption of oxygen gas to the surface.
- Formation of a continuous oxide film due to lateral growth of oxide nuclei.
- Growth of the oxide film perpendicular to the metal surface.

The surface conditions play a great part in the oxide scale formation, at least for the first two steps. The growth is dependent on the surface preparation or surface defects, and impurities in the gas or metal. The third step is dependent on the

solid-state diffusion, since the oxide growth relies on the diffusion of metal ions to the oxide-air interface or the diffusion of oxygen anions to the metal-oxide interface [16]. Figure 2.3 illustrates the mechanism for oxide scale growth.

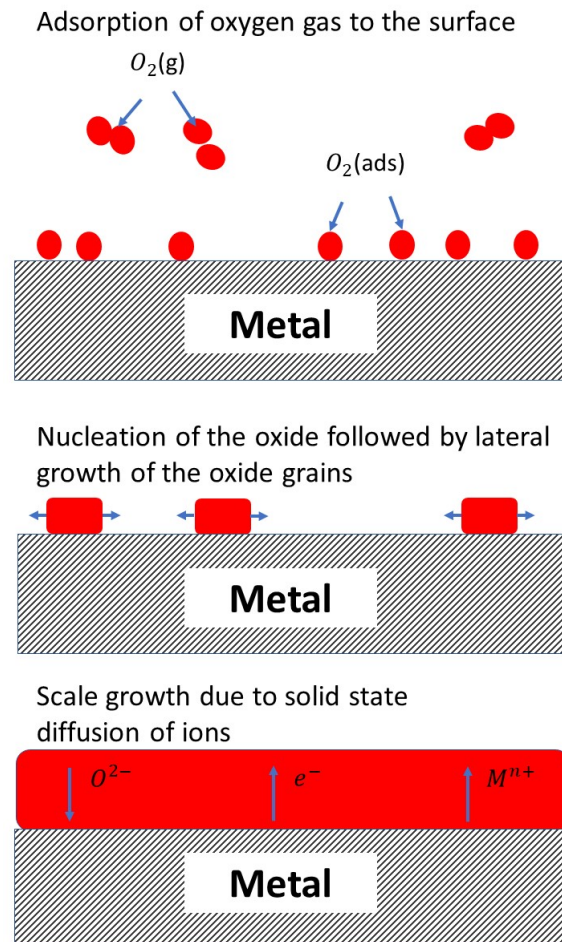


Figure 2.3: Schematic of the oxide scale growth. Drawn by the authors based on [10].

Defects in the oxide scale will determine whether the diffusion through the scale is dominated by oxygen ion diffusion or metal ion diffusion. This in turn will also determine in which direction and rate the oxide scale will grow. Since oxides often are classified as by their semiconductor properties, they can be said to be n- or p-type depending on the predominant defect type. N-type oxide semiconductors are either oxygen deficient or have excess metal ions. Since the metal excess oxides have interstitial cations in the lattice, the cations must be compensated by an equal charge, this is done by the electrons in the conduction band. This allows the cations to be conducted through the lattice via changes in the interstitial sites. If the n-type oxide instead have oxygen vacancies, the net charge is positive, this positive charge is also compensated for by electrons in the conduction band. Following the same reasoning, p-type oxides have a net negative charge due to the lack of metal ions

or excess of oxygen. This is compensated for by electron holes in the valence band. By changing interstitial sites, excess ions can diffuse through the oxide, and also, ion vacancies can diffuse in the lattice which results in vacant ion species becoming conductive. For the n-type oxides, they are said to be outwards growing if they have a metal excess, and inward growing if they have anion vacancies. For p-type oxides, an oxygen excess indicates an inwards growing oxide and cation vacancies means that the oxide is outwards growing [14, 18].

2.2.3 Kinetics

As the Ellingham/Richardson diagram shows, when the temperature increases the thermodynamic stability of metals also increases. For a kinetic evaluation of a reaction, different rate laws can be applied. Which rate law that is chosen is dependent on the mass gain against time, which is presented in Figure 2.4.

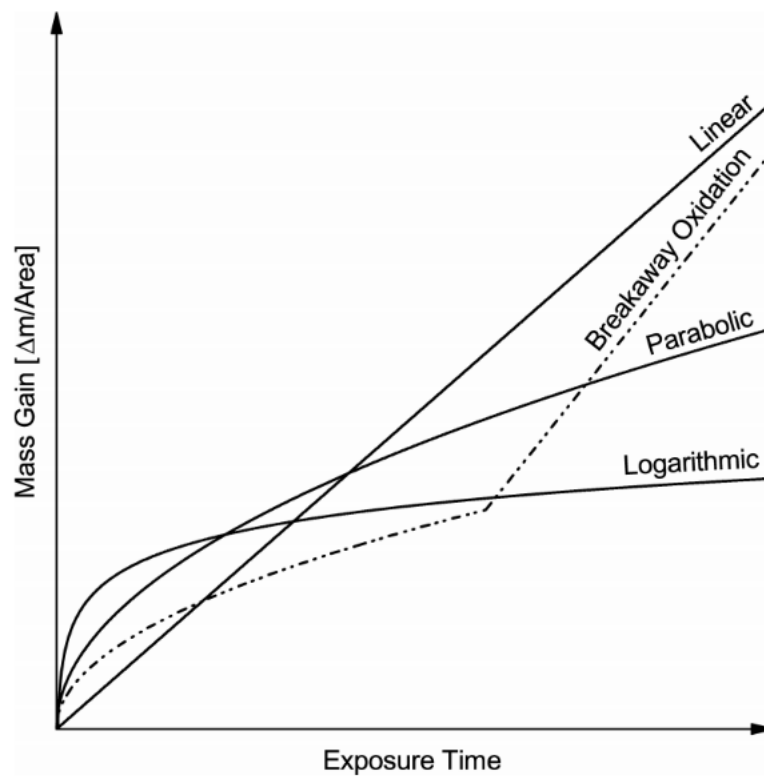


Figure 2.4: Dependence of mass gain for different rate laws [10].

Parabolic Rate Equation: At elevated temperature, above 400°C, the oxidation of metals usually follows a parabolic rate law, Equation 2.11.

$$\Delta m^2 = k_p t + A \quad (2.11)$$

In this equation Δm is the mass gain, k_p is the parabolic rate constant, t represents the time of exposure and A is a constant. At high temperatures the oxide scale

growth is controlled by solid-state diffusion through the scale. Equation 2.11 describes the parabolic behaviour, the diffusion through the scale becomes slower as the thickness of the oxide grows thicker, hence the parabolic behaviour [16, 19].

Linear Rate Equation: When the oxidation rate of a metal is constant, it follows the linear rate law,

$$\Delta m = k_l t \quad (2.12)$$

where Δm represents the thickness of the oxide scale, k_l is the linear rate constant and t is the time of exposure. Equation 2.12 is valid when the rate-determining step is a phase-boundary process, or a surface process, e.g. adsorption of oxygen to the metal surface [10, 19].

Logarithmic Rate Equation: When the temperatures are low, lower than 400°C, the initial metal oxide formation can be said to follow the logarithmic rate law. Equations 2.13 and 2.14 describe an initial rapid reaction which soon will decrease to a lower reaction rate.

$$\text{Direct Logarithmic : } \Delta m = k_{log} \log(t + t_0) + A \quad (2.13)$$

$$\text{Inverse Logarithmic : } \frac{1}{\Delta m} = B - k_{il} \log(t) \quad (2.14)$$

A , B , t_0 , k_{log} , and k_{il} are constants at a constant temperature [18].

Breakaway Oxidation: When the parabolic behaviour suddenly is interrupted by a rapid increase in mass, something called breakaway corrosion might occur. This means that the oxide scale follows the parabolic rate law to a certain point in time and changes into a fast growing regime. When the alloy contains chromium or aluminium, breakaway corrosion can be caused by Cr or Al depletion, which will result in the incorporation of iron into the steel and an iron rich spinel will emerge. Through this spinel iron can easily diffuse towards the surface which means that the oxide is not protective anymore and the thickness of the protective part is reduced due to cracking and rupturing of the oxide [16].

2.2.4 Corrosion of Interconnects in Fuel Cells

When it comes to using metal interconnects in fuel cells, different issues may arise. Since the interconnect plays such an important role in the fuel cell, the understanding of the corrosion mechanism is vital. Due to the harsh environment in the SOFC, the interconnects degrade over time. The following section will discuss problems related to corrosion of interconnects and how these problems can be avoided [10]. First of all, most materials that are used in high temperatures protect themselves by forming a protective layer of either Al_2O_3 or Cr_2O_3 . These protective scales offer different properties, while Al_2O_3 forming alloys are very resistant against high temperature

corrosion, Cr_2O_3 forming alloys are less resistant since they suffer from continuous Cr evaporation and the growth rate is higher than for Al_2O_3 forming alloys. Al_2O_3 is naturally an insulator, which is an unwanted feature in SOFC applications since the main purpose of the interconnect is to electrically connect separate cells. Therefore, Cr_2O_3 forming alloys are more suitable as material for interconnects. Three types of Cr_2O_3 forming alloys exist, namely chromium alloys, nickel based Cr_2O_3 forming alloys and Cr_2O_3 forming stainless steels which are divided into ferritic and austenitic stainless steels. These materials are classified according to their crystalline structure.

If the material has a face-centered cubic structure it is called austenitic steel, and if it has a body-centered cubic structure it is called ferritic stainless steel. For interconnects, ferritic stainless steels are more frequently used because its CTE is more compatible with the CTE of the other fuel cell components [20, 21]. To ensure long-term operation of ferritic stainless steel interconnects, some degradation issues must be taken care of. Since the performance of the fuel cell is dependent on the electrical resistance of the interconnect, the Cr_2O_3 formed on the interconnect must grow as slow as possible as a protective oxide since the electrical resistance increase with increasing thickness of the scale. Another issue regarding the thickness of the scale is that the risk of spallation also increases when the scale grows which results in the loss of electrical contact between the interconnect and the electrodes and consume the chromium reservoir of the steel faster [14].

To mitigate corrosion and other issues the steel can be coated using different coating materials. The coating materials have different properties depending on the crystal structure of the oxide. Common coatings are based on perovskites or spinel oxides. One promising spinel coating is $(\text{Mn,Co})_3\text{O}_4$, which shows high electrical conductivity as well as promising Cr-retention. Other ways to mitigate corrosion is addition of alloying elements to the steel. These alloying elements will add different properties to the steel, such as increased resistance against corrosion or better mechanical properties. However, some elements are unwanted in the steel and are remains from the manufacturing process. They are still present because they are too expensive to remove [10, 14].

2.3 Dual Atmosphere Effect

The dual atmosphere effect has been studied for several years, in the first studies the samples were exposed to single atmosphere, either fuel side atmosphere or air side atmosphere. This does not simulate the real conditions of a fuel cell where the interconnect is exposed to two different atmospheres simultaneously and research has now shifted towards dual atmosphere exposures. This has revealed a new problem called the dual atmosphere effect where the air side of the interconnect is more severely corroded compared to single atmosphere exposures. However, the mechanism behind is not yet fully understood [5, 6]. These studies have confirmed that when a ferritic stainless steel is exposed to both air and fuel simultaneously, the corrosion on the air side is more severe than on the fuel side. Suggestions have been made that the effect is due to hydrogen diffusion, since hydrogen has a diffusivity

rate in the mm h^{-1} range through ferritic stainless steels [10, 14].

A study made by Bredvei Skilbred et al. [22] shows that for the tested material Sanergy HT at 800°C , elevated hydrogen concentrations were reported on the air side of the dual atmosphere exposed samples compared to samples exposed to air-only atmosphere. These results propose that the hydrogen actually diffuses through the steel. Other theories regarding the hydrogen diffusion have been proposed by Yang et.al [6]. They suggest that the accelerated corrosion might be a result of an increase in cation transport because of the hydrogen doping of the Cr_2O_3 scale. Furthermore, the authors believe that hydrogen forms hydroxide on an oxygen site resulting in an effective positive charge.

This effective charge might be compensated for by chromium vacancies, this would result in more available sites for cation transport and in turn the iron content at the air side would increase. This is true with the assumption that the Cr_2O_3 scale is a p-type semiconductor under oxidizing conditions [10, 14]. Other work that support this theory have been made by Hultquist et.al [23, 24]. They have shown that, when hydrogen is present in Cr_2O_3 the Cr cation diffusivity in the oxide greatly increases. Further, studies by Alnegren [25, 26] show that at 600°C the dual atmosphere effect is present, however in the temperature dependence study the authors suggest that the effect is more severe at 600°C than at 800°C . They suggest that the negative effect of hydrogen is compensated by the higher Cr diffusivity at higher temperatures. Some results from that study is shown in Figure 2.5 showing the difference between samples exposed to single and dual atmosphere.

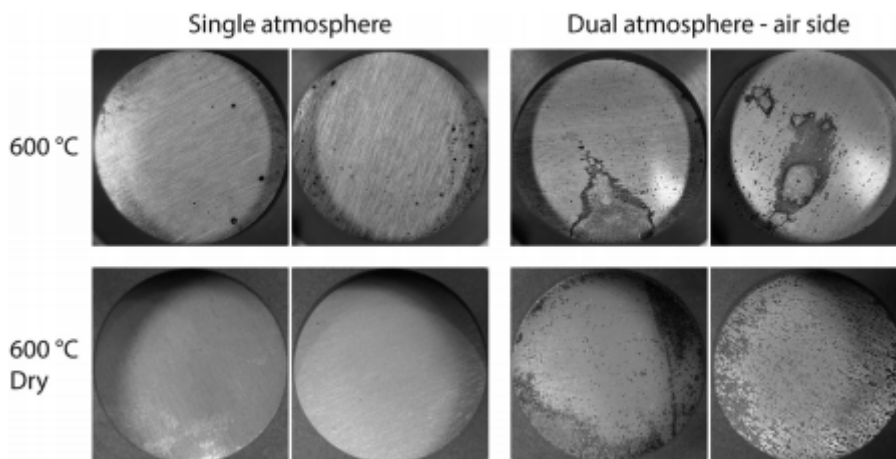


Figure 2.5: Results from dual atmosphere exposure at 600°C [26].

2.4 Analytical Techniques

During this project, different methods have been used to characterize the samples. The theory and working principle of each method are presented in this section.

2.4.1 Broad Ion Beam

In order to achieve a good and qualitative cross section the technique broad ion beam milling can be used. This technique is based on bombarding the cut sample with ions to make the cut smooth by removing layers of the cut surface. The result will be a smooth surface that can be analyzed further and will show less damage when compared to other methods such as mechanical polishing [10]. This was performed to obtain a smooth surface for further analysis using scanning electron microscopy.

2.4.2 Scanning Electron Microscopy and Energy Dispersive X-Ray

Scanning electron microscopy, SEM, is an analytic technique for analyzing surface morphology and topography with high resolution down to the nanometer range. The technique is based on shooting electrons at the sample in a vacuum, the electrons then interact with the sample and generate different types of signals which then can be detected. In Figure 2.6 descriptive images show how primary electrons are turned into secondary electrons, back scattered electrons and characteristic X-rays which then can be detected and used for analysis.

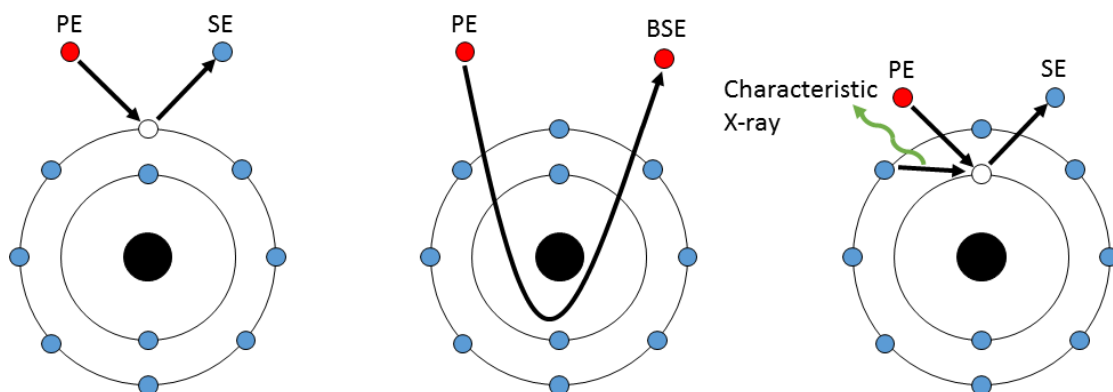


Figure 2.6: Explaining how different SEM signals are generated. Adapted from [27].

The different types of signals depend on how the electron interacts with the sample and how deep into the sample they penetrate. As can be seen in Figure 2.7, different signals have different interaction volumes, which means that they are surface sensitive to different degrees. As secondary electrons have smaller interaction volume makes them more surface sensitive and high resolution compared to characteristic X-rays which have a higher interaction volume and therefore lower surface sensitivity.

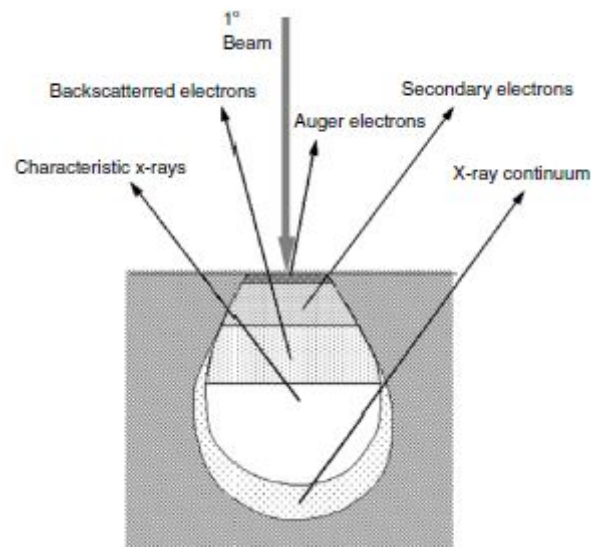


Figure 2.7: Interaction volume of different SEM signals [5].

The different signals generated in SEM give different amount of information. Secondary electrons give information about surface topography while backscattered electrons give information about the chemical composition as they interact differently with different elements. Heavier elements gives a larger amount of backscattered electrons which appear brighter in the image and can therefore be distinguished from lighter elements. If more exact chemical composition is needed then Energy Dispersive X-Ray Spectroscopy, EDX, can be used. EDX uses characteristic X-rays to determine the element as each element sends out a different characteristic X-ray. So when the primary electrons hit different elements the different elements will send out characteristic X-rays with different energies dependent on which element it is. These specific characteristic x-rays can then be detected and the different amount of each element can be determined. The characteristic X-rays have a large interaction volume which makes them less surface sensitive [5].

In this project both secondary electrons, backscattered electrons and EDX was used to analyze the results. This is because information of both the topography and the chemical composition of the sample is important in order to understand the corrosion of the samples.

3

Methods

To evaluate the temperature dependence of the dual atmosphere effect eight different exposures at six different temperatures from 500°C to 800°C were conducted. In this chapter the method and sample preparations will be described.

3.1 Sample Preparation

AISI 441 stainless steel with two different thicknesses, 0.3 and 0.2 mm, was cut and pressed into circles, 21 mm in diameter, using a hydraulic press. The chemical composition of the 0.3 mm, hereinafter called KA, and the 0.2 mm, hereinafter called LA, is displayed in Table 3.1. Both KA and LA come from the same batch and have the same composition.

Table 3.1: Composition of AISI 441 in weight%.

Alloy	Fe	Cr	Mn	Si	Ti	Nb	Ni	C	S	N	P
AISI 441 Batch 64534	Bal.	17.56	0.35	0.001	0.173	0.39	0.26	0.014	0.001	0.017	0.03

3.1.1 Grinding

The KA samples were ground from their original thickness of 0.3 mm to 0.2 mm to be of the same thickness as the LA samples before the exposures started. The grinding was performed on two different grinding machines, Struers RotoPol-31 and Struers TegraPol-31. The grinding was performed with Struers SiC-Paper with four different grit sizes, 500, 800, 1000 and 1200. When grinding the samples it is important that the surface is uniform in order to get comparable results. All KA samples were ground.

3.1.2 Cleaning

When the KA samples had been ground, both the KA and LA samples were washed using an Elmasonic P ultrasonic bath, first in ethanol for 20 minutes and then in acetone for another 20 minutes. After cleaning, the samples were weighed using a Mettler Toledo XP6 scale with 6-digit precision. Since the thickness of the as received LA samples is known (0.2 mm), the thickness of the ground KA samples can be estimated using the weight of the sample as the density of the steel is known.

All samples were estimated to have the same surface area as they were pressed using the same press.

3.1.3 Pre Oxidation

Some of the KA and LA samples were pre oxidized prior to starting the exposure. When pre oxidizing the samples they were put inside a 800°C and 3% humidity furnace on an alumina sample holder for 20 minutes. After removing the samples from the furnace and letting them cool they were weighed again using a Mettler Toledo XP6 scale and after that the mass gain could be calculated. The mass gain is shown in Figure 3.1 and here it can be seen that all the pre oxidations of the different samples were on the same level. The pre oxidation was conducted to see the effect on pre oxidation on the dual atmosphere effect as pre oxidizing the samples creates a protective oxide which the hydrogen has to diffuse through.

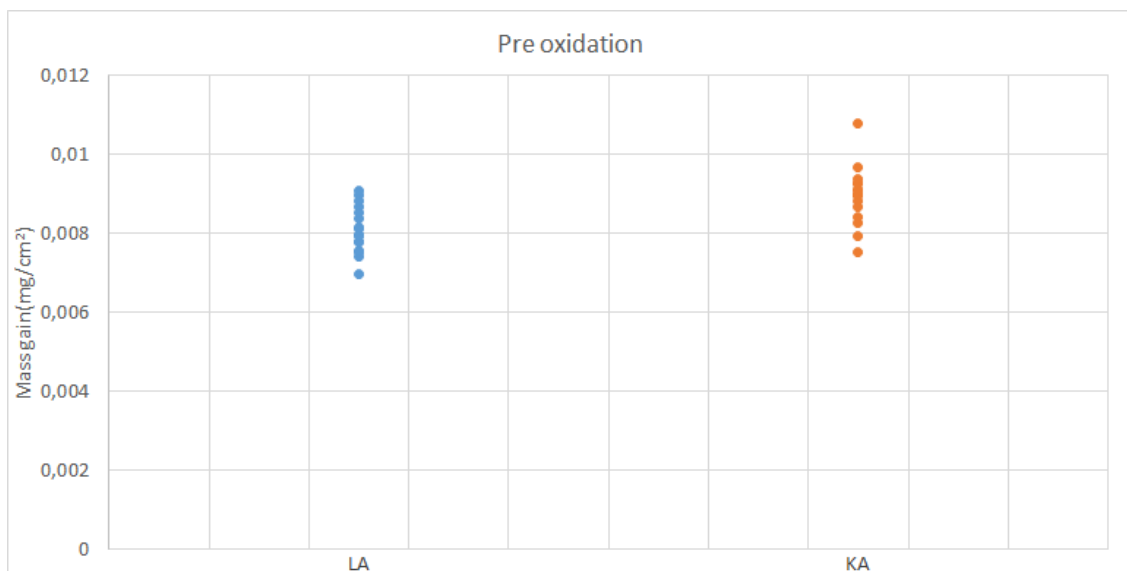


Figure 3.1: Mass gains obtained in pre oxidation step at 800°C for 20 min.

3.2 Exposure

Before the actual exposure was started, a temperature profile had to be made in order to know the exact temperature over the sample holder in the furnace. The furnace is a 3 zone tube furnace made by Entech and had a ramping speed of 1°C/min. The ramping speed was set to this to prevent spallation caused by thermal stresses.

The sample holder was assembled without samples and the temperature over the sample holder was measured using a thermocouple. After the correct temperature had been achieved $\pm 4^\circ\text{C}$, the sample holder was removed and the samples were attached to the holder. The design of the sample holder was based on a design made by the Montana State University and given in Figure 3.2 [28].

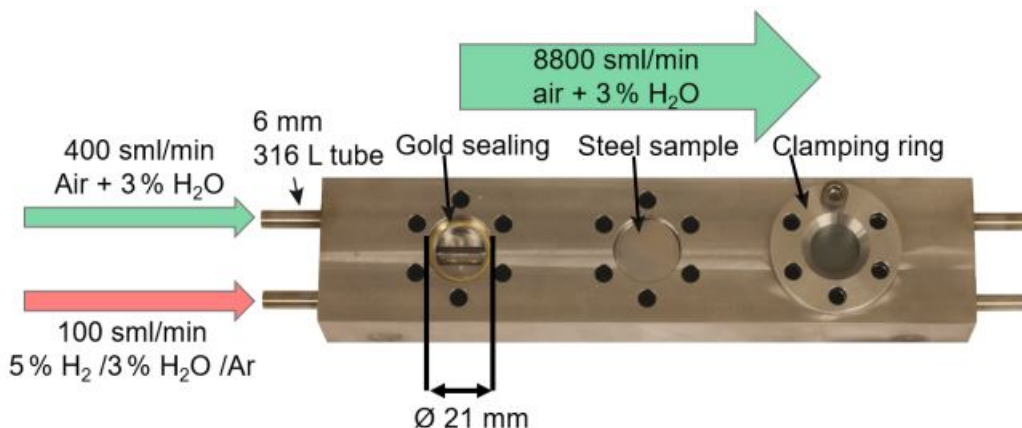


Figure 3.2: Dual Atmosphere Sample holder [10].

The sample holder can fit six samples, three on each side and the tubing can control the flow of gas to three of the samples respectively. For the dual atmosphere exposures, three samples were exposed to hydrogen on one side and air on the other. The other three samples were exposed to air on both sides. Before placing the samples in the holder a gold ring was placed to ensure gas tightness. The sample was then placed on the gold ring and tightened using a clamping ring as can be seen in Figure 3.2.

Table 3.2: Gas flow over sampler holder.

Outer gas	Inner gas 1 (dual atmosphere)	Inner gas 2 (single atmosphere)
8800 sml min ⁻¹ air-3%H ₂ O	100 sml min ⁻¹ Ar-5%H ₂ -3%H ₂ O	400 sml min ⁻¹ air-3%H ₂ O

The gas flows used in the different exposures can be seen in Table 3.2 and the right water content was achieved by bubbling the gas through water with a temperature of 24.4°C which gave 3% humidity in the gas. All exposures lasted 336 hours with a break after 168 hours for taking photographs of the samples. This exposure setup is illustrated in Figure 3.3. The order of exposures was 600°C, 550°C, 650°C, 500°, 700°C, 800°C and lastly repeat runs of 650°C and 550°C.

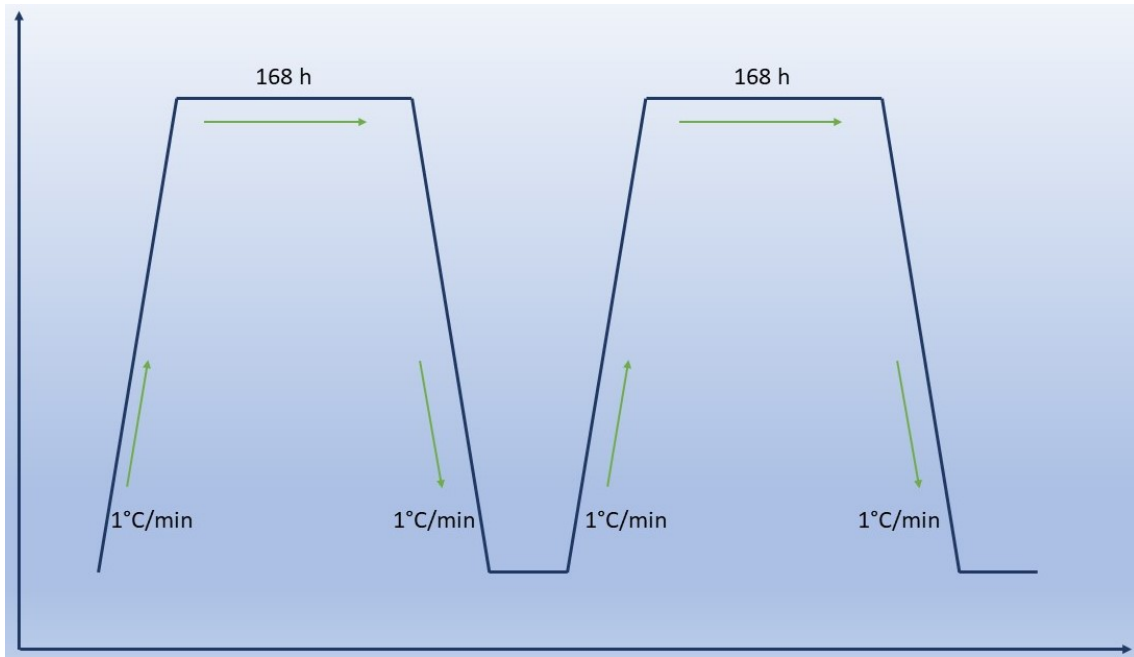


Figure 3.3: Experimental run procedure.

Table 3.3: Sample matrix for the two first exposures.

	Sample 1	Sample 2	Sample 3	Sample 4	Sample 5	Sample 6
Surface finish	As received	Ground	Ground	As received	Ground	Ground
Preoxidation	20 min	20 min	No preox.	20 min	20 min	No preox.
Atmosphere	Dual	Dual	Dual	Single	Single	Single

For the first two exposures, 600°C and 550°C, samples as shown in Table 3.3 were used and for the remaining exposures samples as shown in Table 3.4 were used. The ground sample, which is sample 3 in Table 3.3 was swapped for an as received sample, which is sample 3 in Table 3.4 to have a sample that would corrode more to make it easier to compare the dual atmosphere effect for different temperatures.

Table 3.4: Sample matrix for the remaining exposures.

	Sample 1	Sample 2	Sample 3	Sample 4	Sample 5	Sample 6
Surface finish	As received	Ground	As received	As received	Ground	As received
Preoxidation	20 min	20 min	No preox.	20 min	20 min	No preox.
Atmosphere	Dual	Dual	Dual	Single	Single	Single

3.2.1 Characterization

The samples were photographed before, after 168 hours and after completed exposure with a Canon EOS 1D mk III camera, equipped with a Canon 100 mm f/2.8 macro lens. Further characterization was made by SEM and EDX using a FEI Quanta FEG 200 ESEM equipped with an energy dispersive X-ray detector. The samples where cross sections where preformed a Leica EM TIC 3 X was used.

4

Results & Discussion

In this chapter the results of the different exposures will be shown and discussed. Some results similar to previously presented results will be presented in Appendix 1.

4.1 500°C Exposure

Figure 4.1 shows that there is no obvious dual atmosphere effect affecting the samples at this temperature. This is also confirmed when looking at the samples with SEM, a topview SEM of the pre oxidized sample in dual atmosphere is shown in Figure 4.2 and we can see that the surface is completely free from any breakaway corrosion. This is also the same for the other samples exposed to dual atmosphere which can be seen in Figure A.1 and A.2 in Appendix 1. We can therefore conclude that at 500°C the temperature is too low for the dual atmosphere effect to be observed for this sample.

One reason for this lack of dual atmosphere effect at this temperature might be that the diffusion of hydrogen might be too slow due to the diffusion being a thermally activated process which is obeying the Arrhenius law. This will result in that only protective oxide is formed on the surface. Further, this gives us the information that at 500°C no obvious dual atmosphere effect is present for AISI 441 stainless steel with the thickness of 0.2 mm.

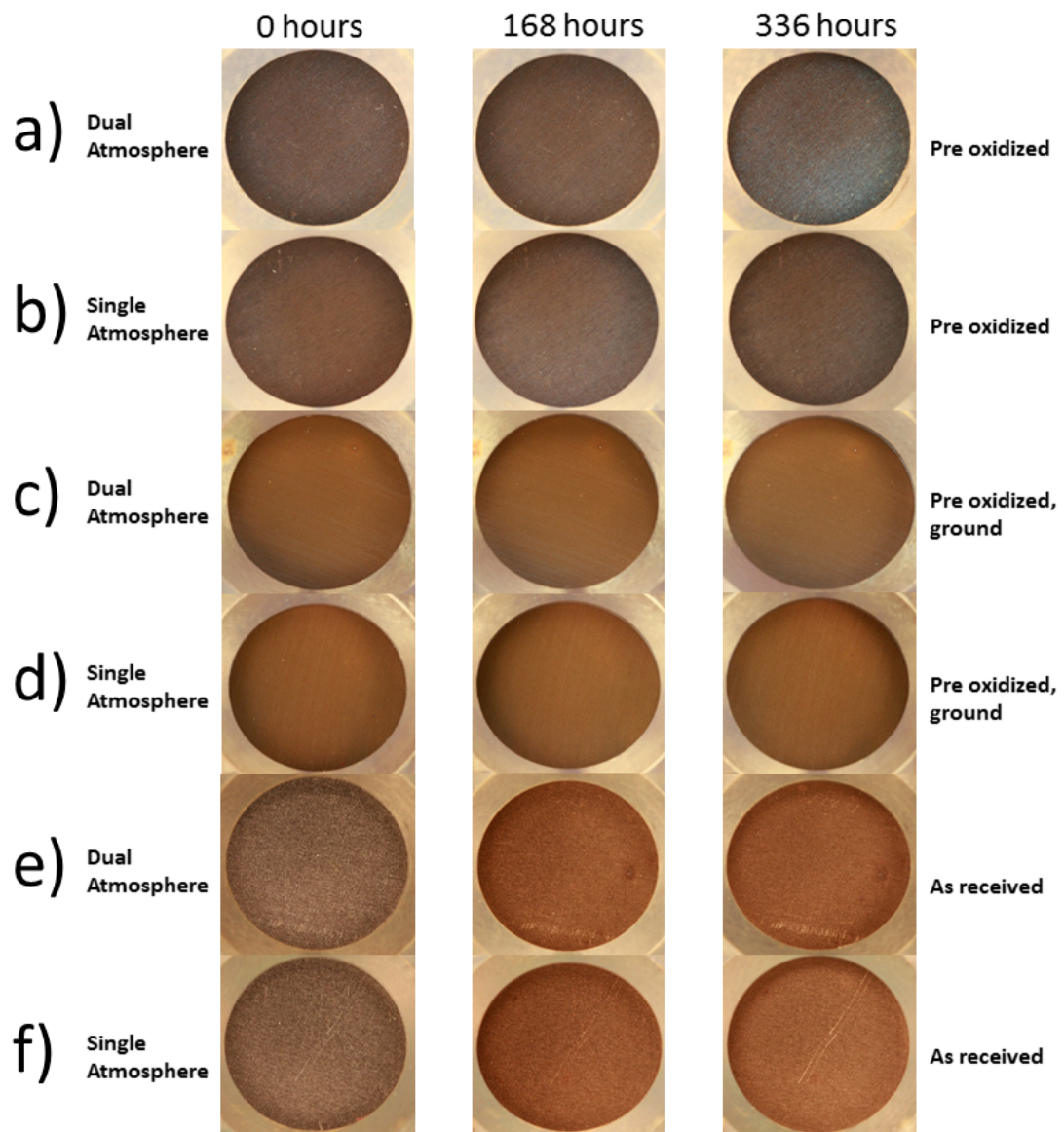


Figure 4.1: Results from the 500°C exposure. a) Pre oxidized sample in dual atmosphere, b) Pre oxidized sample in single atmosphere, c) Pre oxidized ground sample in dual atmosphere, d) Pre oxidized ground sample in single atmosphere, e) As received sample in dual atmosphere, f) As received sample in single atmosphere.

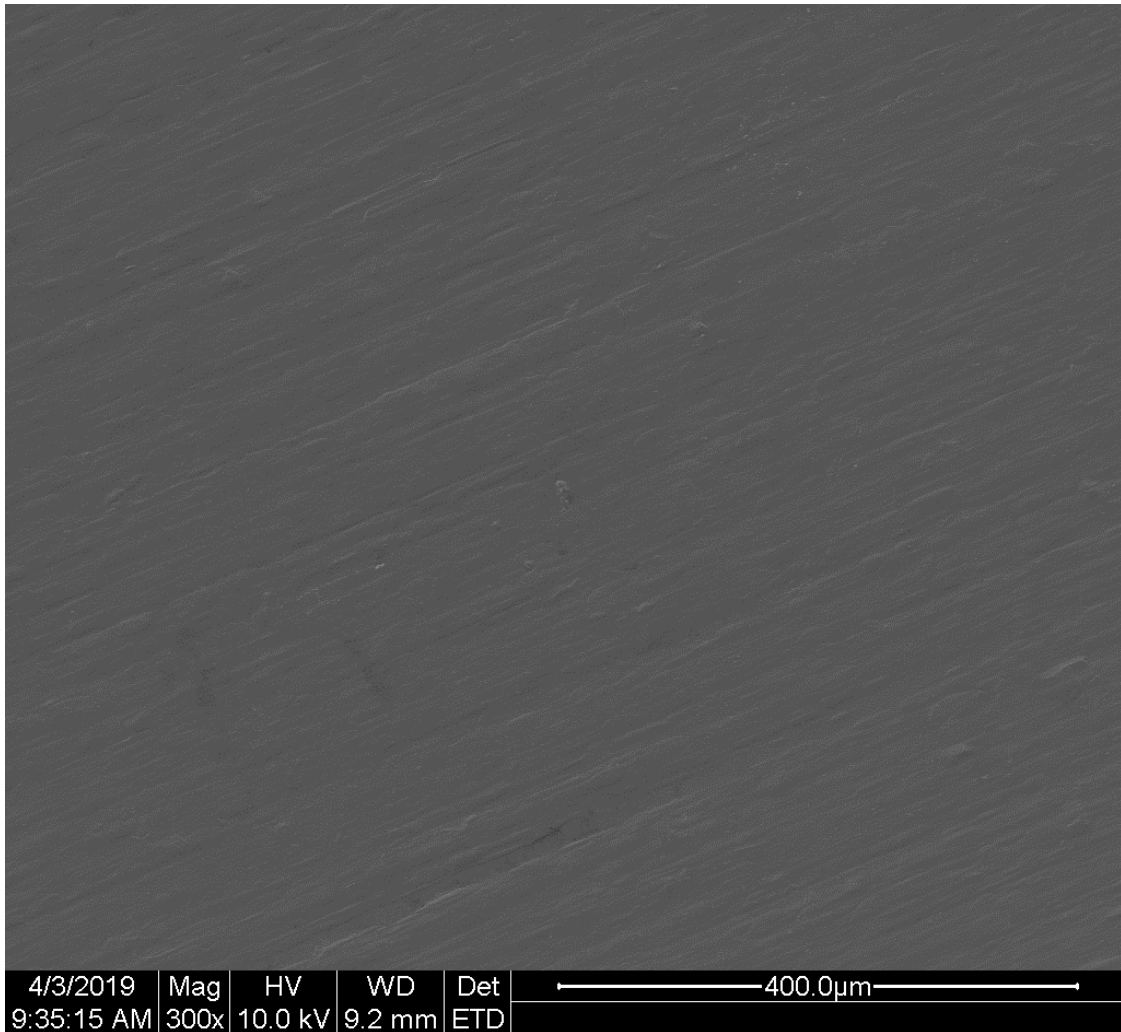


Figure 4.2: Top view SEM image of the pre oxidized sample a) after 336 hours.

4.2 550°C Exposure

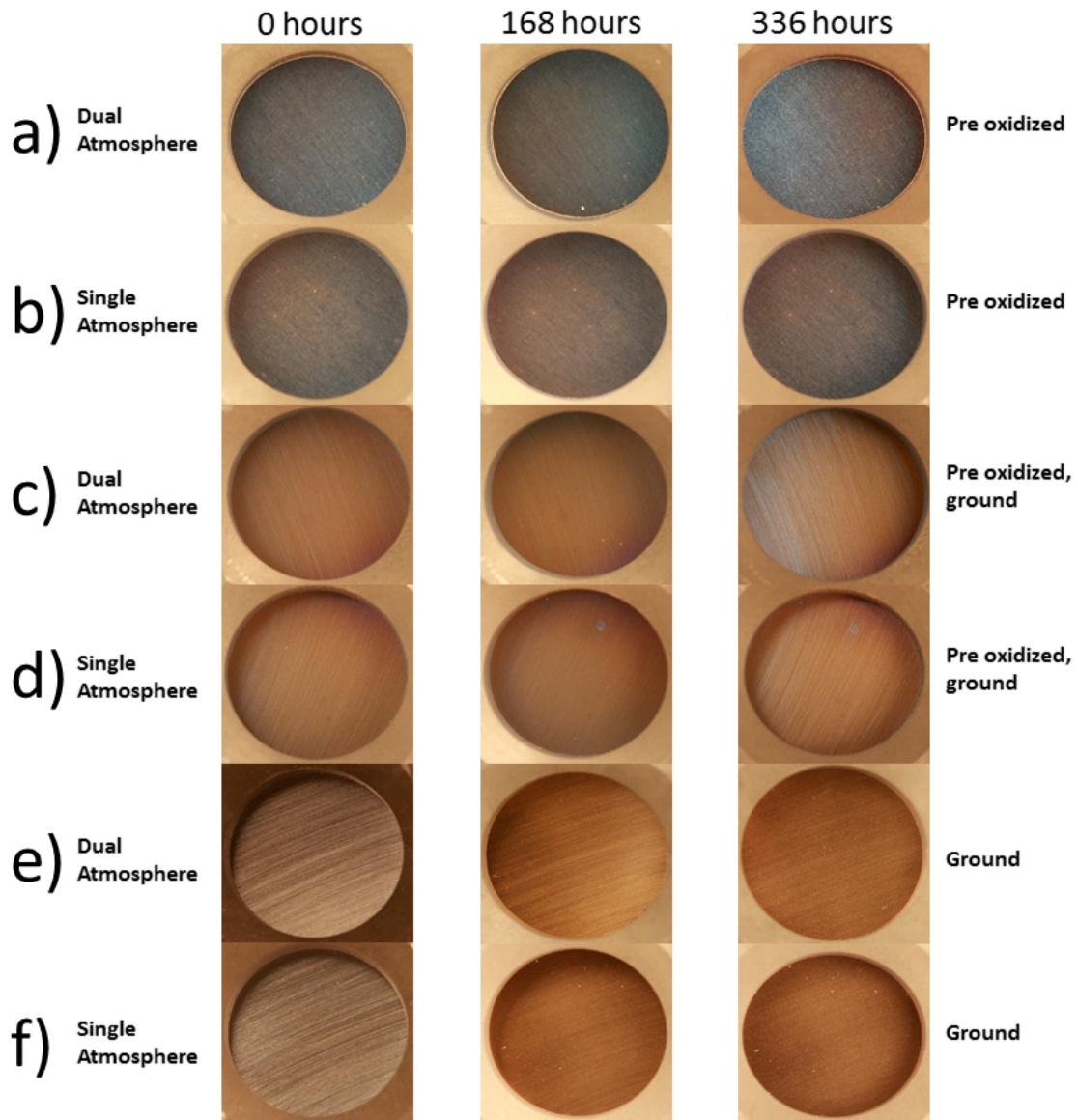


Figure 4.3: Results from the 550°C exposure. a) Pre oxidized sample in dual atmosphere, b) Pre oxidized sample in single atmosphere, c) Pre oxidized ground sample in dual atmosphere, d) Pre oxidized ground sample in single atmosphere, e) Ground sample in dual atmosphere, f) Ground sample in single atmosphere.

The macroscopic photographs that are presented in Figure 4.3 of the 550°C exposure show no obvious signs of the dual atmosphere effect. To confirm this, SEM images of the samples were taken and they are displayed in Figure 4.4, Figure 4.6 and Figure 4.8.

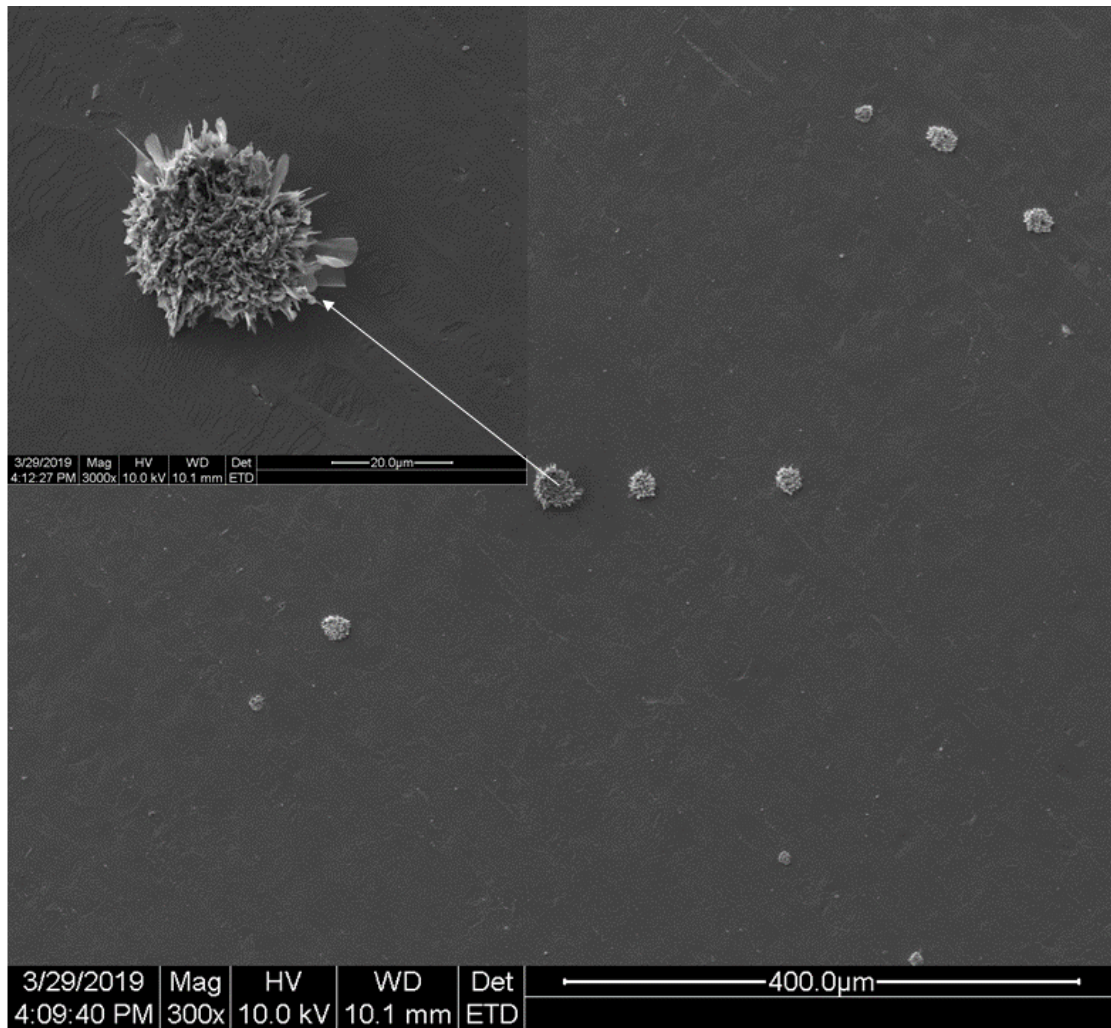


Figure 4.4: Top view SEM image of the pre oxidized sample a) after 336 hours.

In Figure 4.4 we can see that there are some nodules on the surface which indicates that the dual atmosphere effect is present at 550°C even though only to a small extent. It was confirmed by EDX in Figure 4.5 that the nodules are iron oxide and they are believed to be hematite based on previous studies [10]. The results of the EDX analysis are shown in Table 4.1. The same type of results can be seen in Figure 4.6, where we also see a few hematite nodules on the sample surface. These were confirmed to be iron rich oxides using EDX which are shown in Figure 4.7 and Table 4.2.

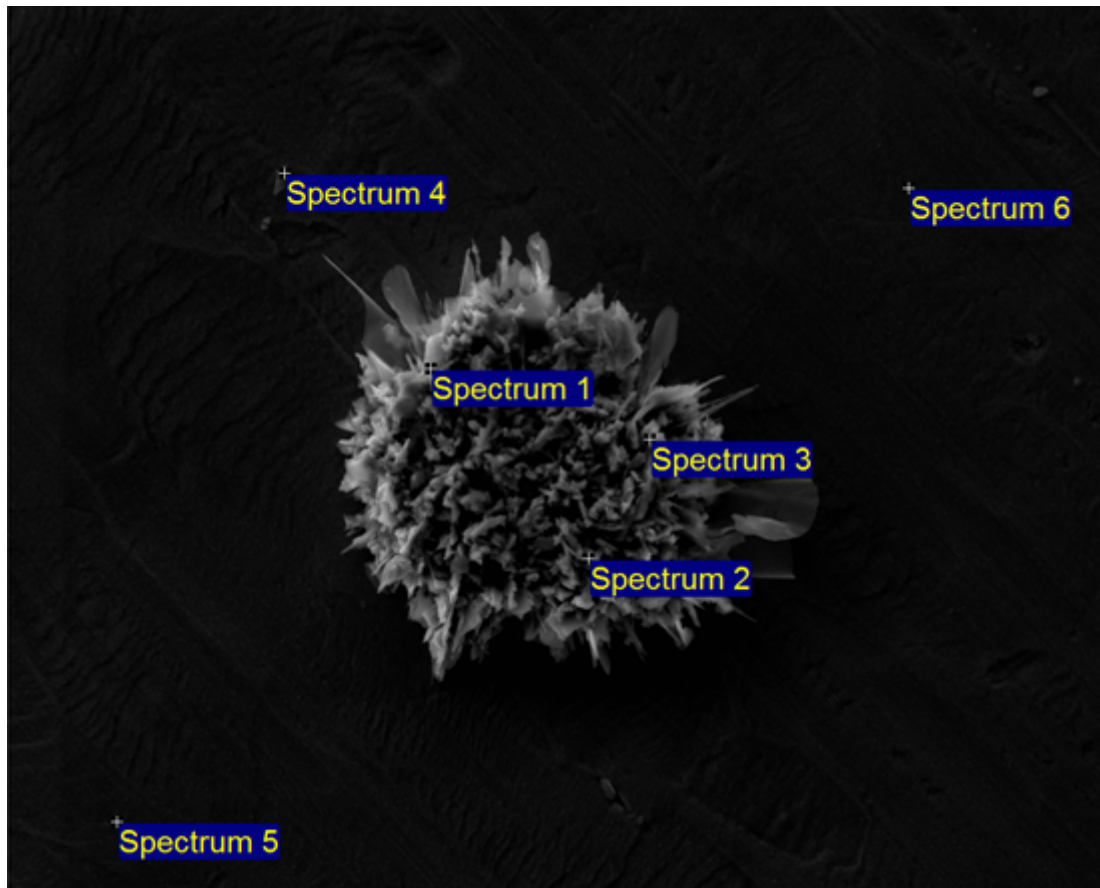


Figure 4.5: EDX image of the pre oxidized sample a) after 336 hours.

Table 4.1: EDX analysis of the pre oxidized sample a) after 336 hours, elements in weight%.

	C	O	Si	Cr	Mn	Fe
Spectrum 1	4	29		11		56
Spectrum 2	5	28		10		57
Spectrum 3	4	29		11		56
Spectrum 4	3	10	1	18	1	67
Spectrum 5	2	3	1	19	1	74
Spectrum 6	2	4	1	19	1	73

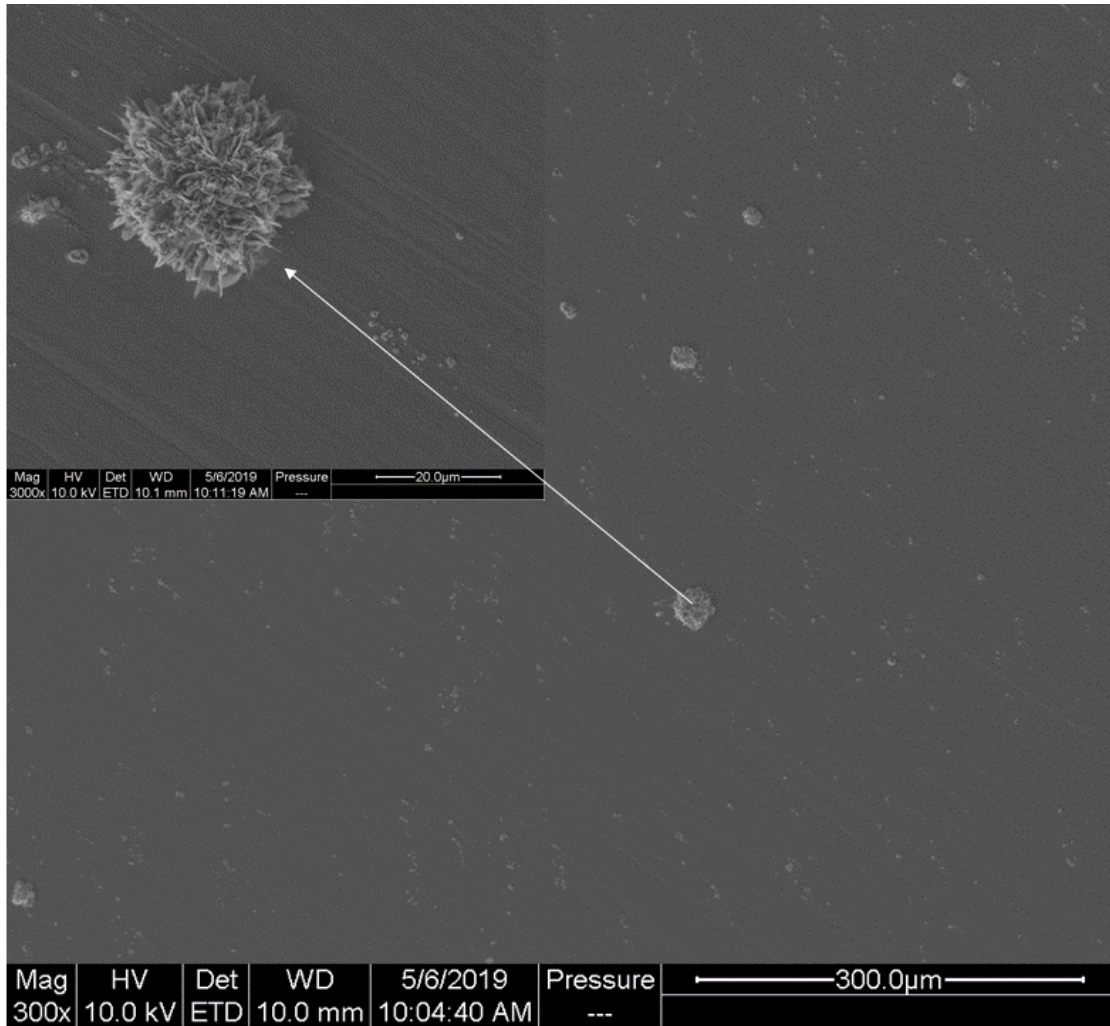


Figure 4.6: Top view SEM image of the ground and pre oxidized sample c) after 336 hours.

After further analysis of the EDX results in Figure 4.7 and Table 4.2 we can see some niobium rich nodules present, which most probably are Laves phase precipitates, this assumption is based on previous studies [14]. Furthermore, according to spectrum 1 and 2, there is a larger hematite nodule present. Spectrum 3 shows similar behaviour, which might indicate that a hematite nodule is nucleated and growing.

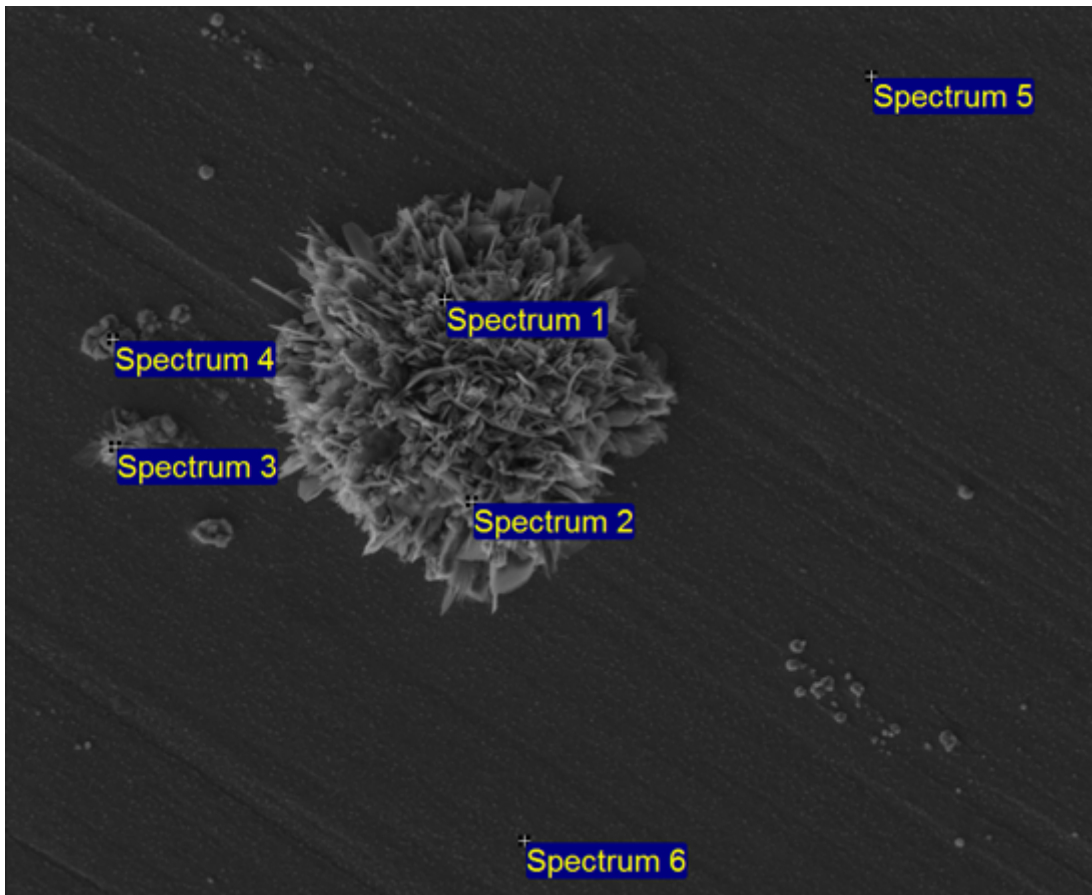


Figure 4.7: EDX image of the ground and pre oxidized sample c) after 336 hours.

Table 4.2: EDX analysis of the ground and pre oxidized sample c) after 336 hours, elements in weight%.

	C	O	Si	Ti	Cr	Fe	Nb
Spectrum 1	2	22			15	61	
Spectrum 2	7	20			15	58	
Spectrum 3	2	19			15	64	
Spectrum 4	2	22		7	20	22	27
Spectrum 5	1	4	1	1	23	70	
Spectrum 6	1	4	1	1	24	69	

The surface of the ground sample presented in Figure 4.8 was found to be covered in a large amount of hematite nodules. We can also observe longer nodules which seem to be growing in the direction of the grinding. The nodules are confirmed to be iron rich oxides and the results from this EDX analysis are shown in Figure A.3 and Table A.1 in Appendix 1.

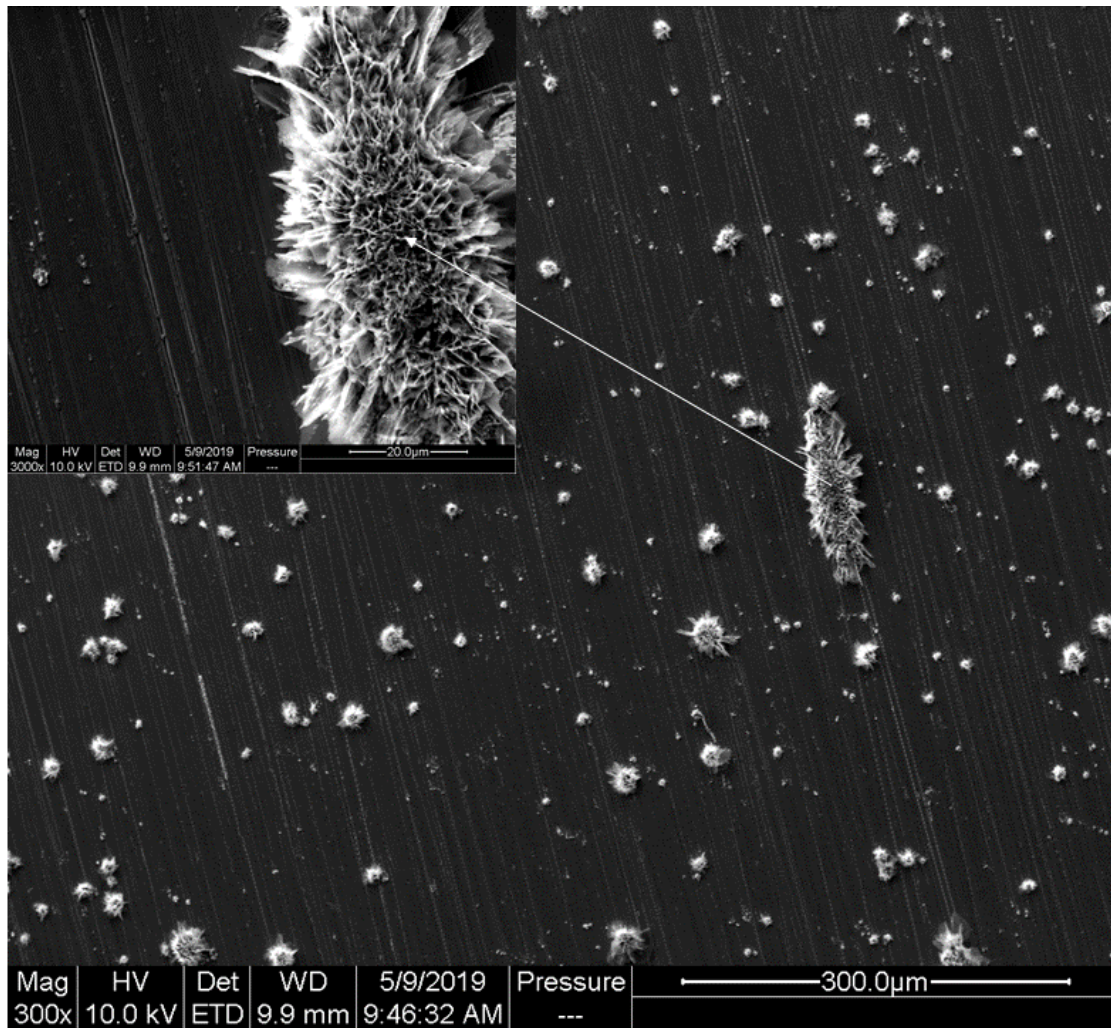


Figure 4.8: Top view SEM image of the ground sample e) after 336 hours.

A comparison between the results from the 550°C exposure and the 500°C exposure was made, and it was found that there is an onset of the dual atmosphere effect somewhere between these temperatures. It can be said that 550°C is the lowest temperature where the dual atmosphere effect can be observed for these samples. The increase from 500°C to 550°C must have increased the thermal energy just enough for the hydrogen diffusion through the steel to impact the oxidation of the air side leading to more severe corrosion on that side.

In order to see the dual atmosphere effect and confirm the results a repeat run of the 550°C exposure was conducted. In Figure 4.9 the results from the as received samples are shown. The other results from the repeat run will not be demonstrated as they were only conducted to confirm the previous results which they did. In Figure 4.9 the dual atmosphere effect is clearly seen when comparing the samples exposed to dual and single atmosphere after 336 hours. The surface of the dual exposed samples has a different color and when looking closer using SEM in Figure 4.10 it is clear that the entire surface of the sample is covered in iron oxide.

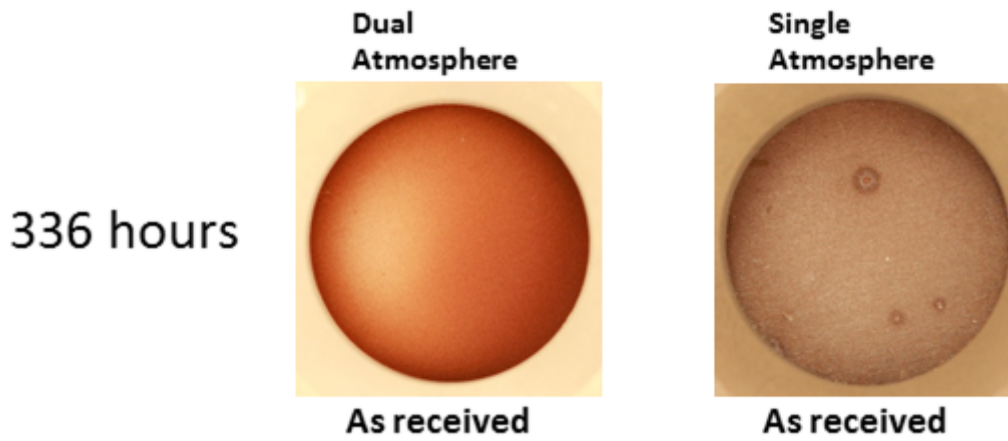


Figure 4.9: Results from the 550°C repeat exposure.

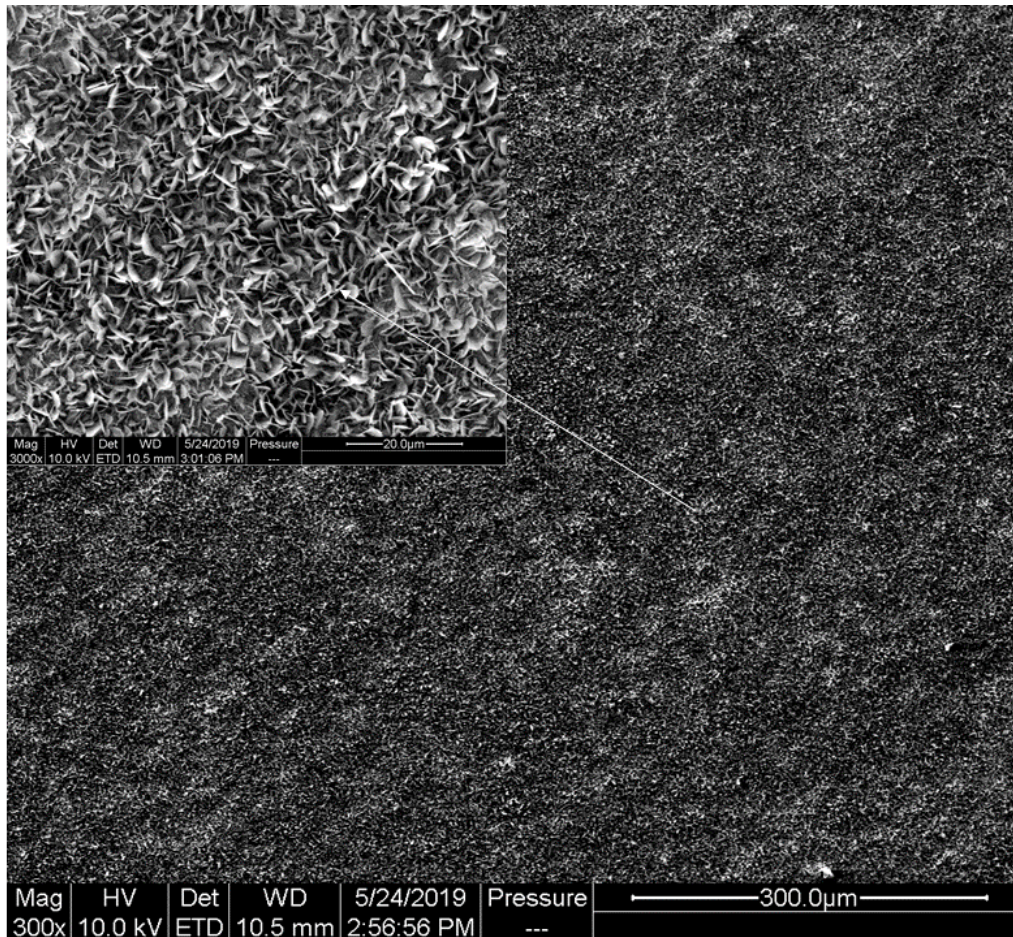


Figure 4.10: Top view SEM image of the as received repeat sample after 336 hours.

If we look closer at the surface in Figure 4.10 we can see that it looks like the surface is covered in one big nodule, we can still see these flakes that we see on the individual nodules and this tells us that the iron oxide layer is probably quite thin as it has just grown to cover the surface and has not yet started to grow more outwards as a

complete layer. If we also compare this result with the one in Figure 4.2 at 500°C we see that the dual atmosphere effect is affecting this sample at 550°C much more compared at 500°C. This shows us that for the as received samples going from 500°C to 550°C makes a big difference for the dual atmosphere effect.

4.3 600°C Exposure

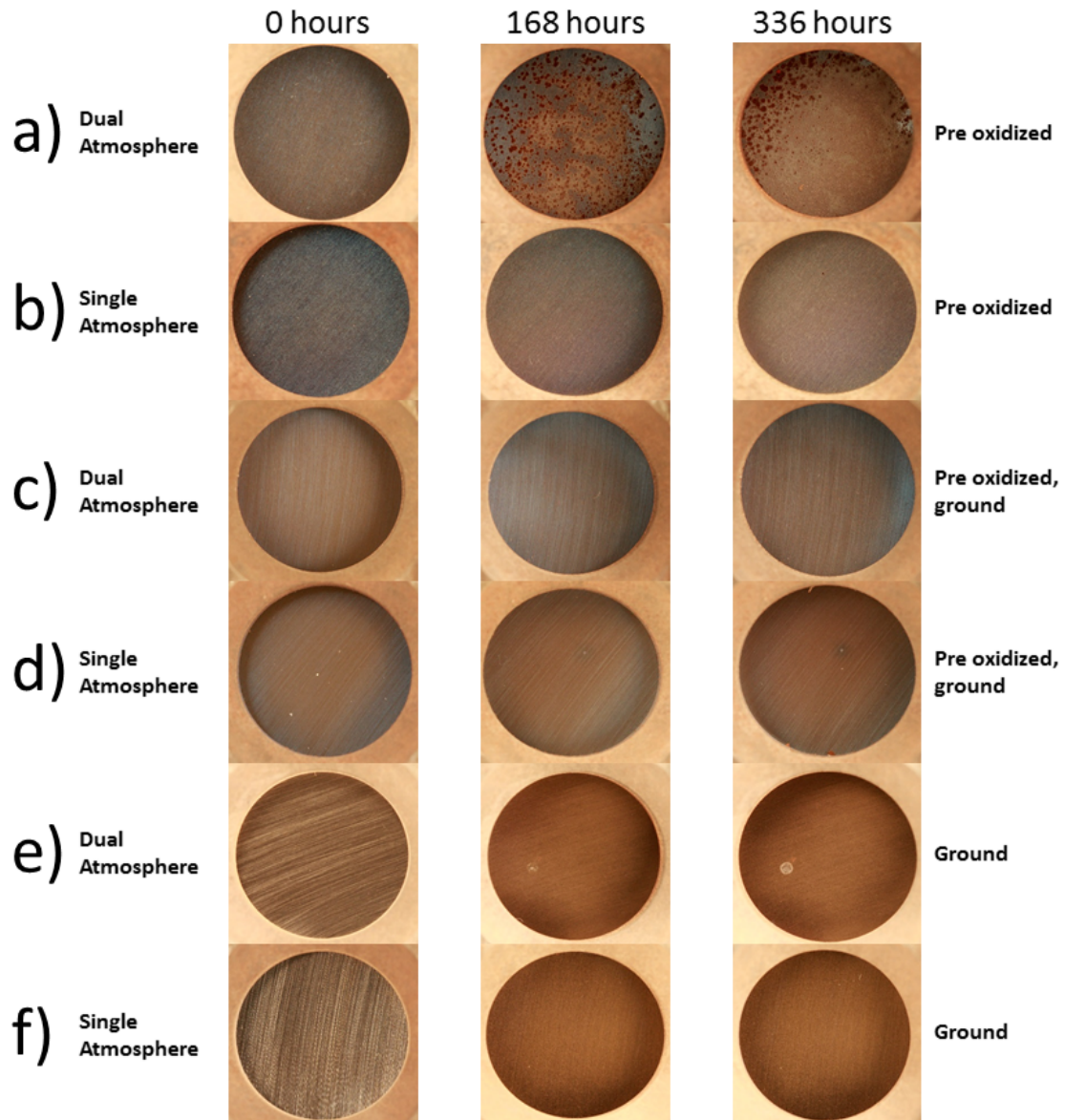


Figure 4.11: Results from the 600°C exposure. a) Pre oxidized sample in dual atmosphere, b) Pre oxidized sample in single atmosphere, c) Pre oxidized ground sample in dual atmosphere, d) Pre oxidized ground sample in single atmosphere, e) Ground sample in dual atmosphere, f) Ground sample in single atmosphere.

In Figure 4.11 the pictures taken before, in the middle and after the 600°C exposure are presented. We can clearly see the dual atmosphere effect when comparing the pictures of the pre oxidized samples in a) and b). Already after 168 hours the sample exposed to dual atmosphere is severely corroded where the single atmosphere sample is still protected. The surface of the pre oxidized sample a) after 336 hours can be seen in Figure 4.12. The dual atmosphere effect can also be seen when comparing the ground and pre oxidized samples c) and d). On c) after 336 hours some nodules can be seen on the surface which is confirmed using SEM in Figure 4.13.

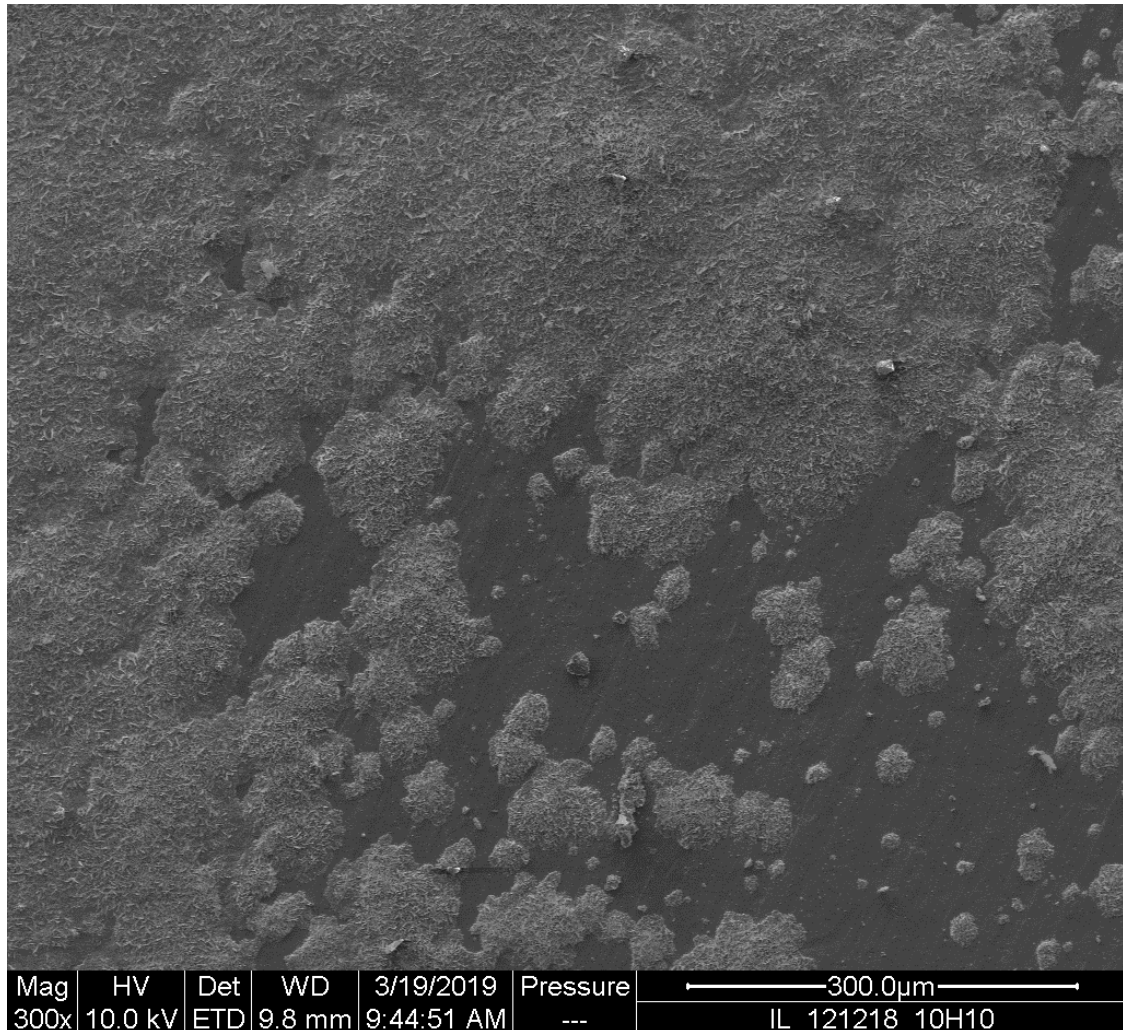


Figure 4.12: Top view SEM image of the pre oxidized sample a) after 336 hours.

Most of the surface of the pre oxidized sample a), is covered in hematite, which can be seen in the macroscopic photo in Figure 4.12, and very little protective oxide is visible. This is also confirmed by EDX analysis, shown in Figure A.4 and Table A.2 in Appendix 1. The EDX shows the chemical composition of a small piece of still protective oxide and the composition of the iron rich oxide as well.

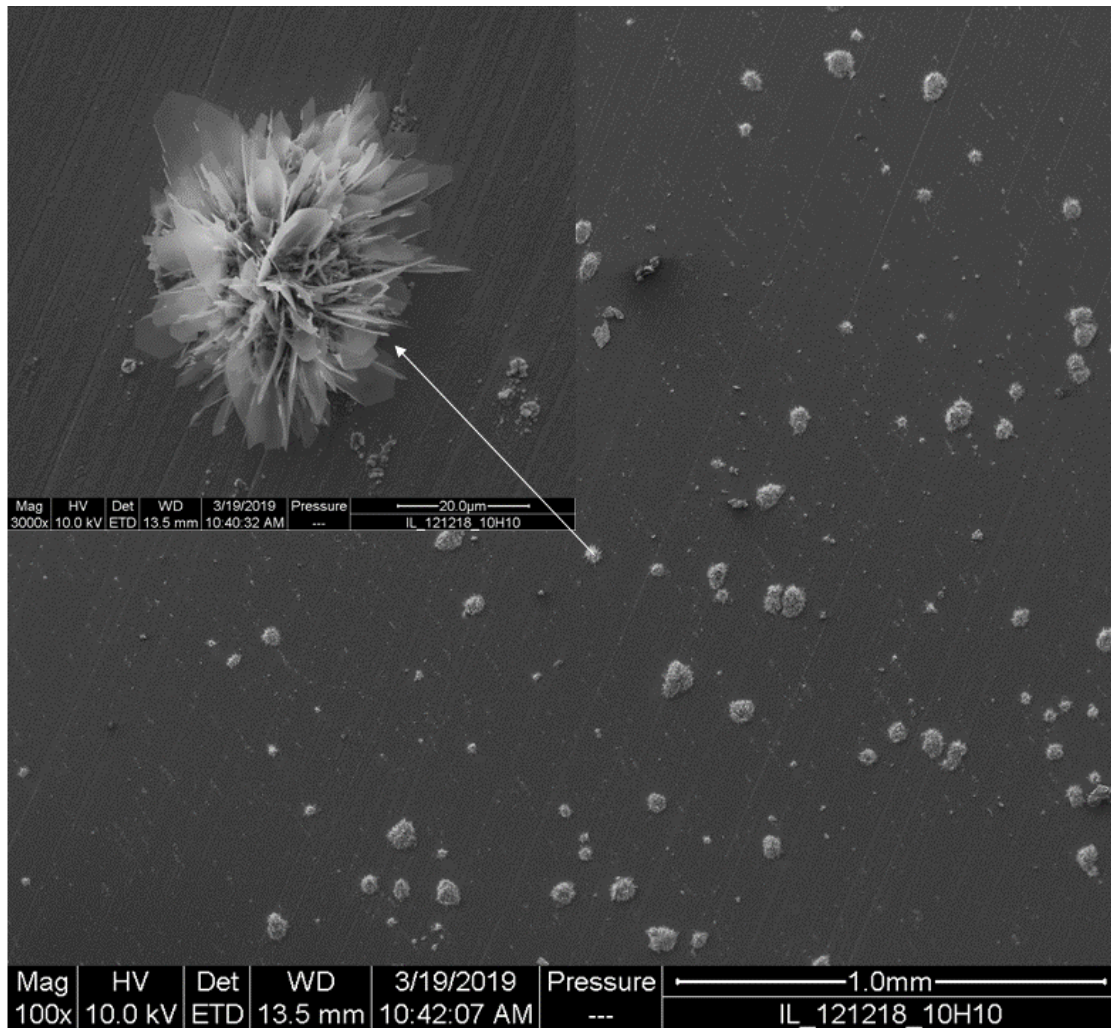


Figure 4.13: Top view SEM image of the ground and pre oxidized sample c) after 336 hours.

To confirm that the nodules on the ground and pre oxidized sample c) were iron oxide, EDX analysis were performed which is presented in Figure A.5. The results of the EDX are displayed in Table A.3 and the EDX analysis shows that iron rich oxide nodules as well as protective oxide have grown on the surface.

Figure 4.14 shows a top view SEM of the ground sample e) after 336 hours. The presence of iron rich nodules can be confirmed both visually and by the EDX shown in Table A.4 and Figure A.6 in Appendix 1. Another interesting thing that can be observed is that there are nodules growing in the direction of the grinding as can be seen in the 550°C exposure.

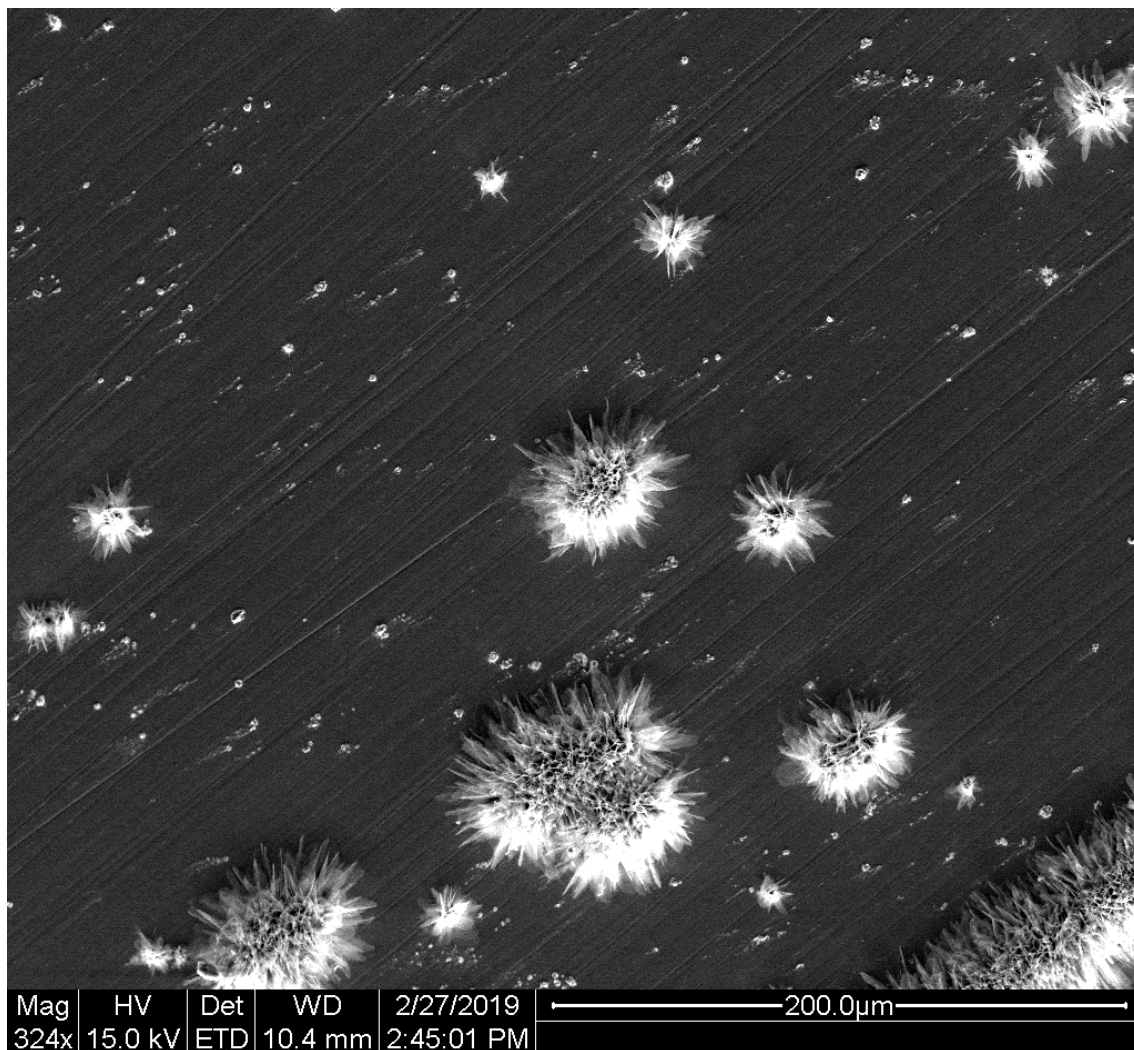


Figure 4.14: Top view SEM image of the ground sample e) after 336 hours.

All the samples exposed to dual atmosphere have shown to contain iron oxide rich nodules on the surface. This is shown in the SEM images for the pre oxidized, ground and pre oxidized and the ground samples, samples, a), c), and e). Worse is for sample a) which is only pre oxidized. This tells us that grinding the samples have a big impact in mitigating the onset of corrosion. Also, what can be said is that at 600°C the dual atmosphere effect is present and a real factor to consider.

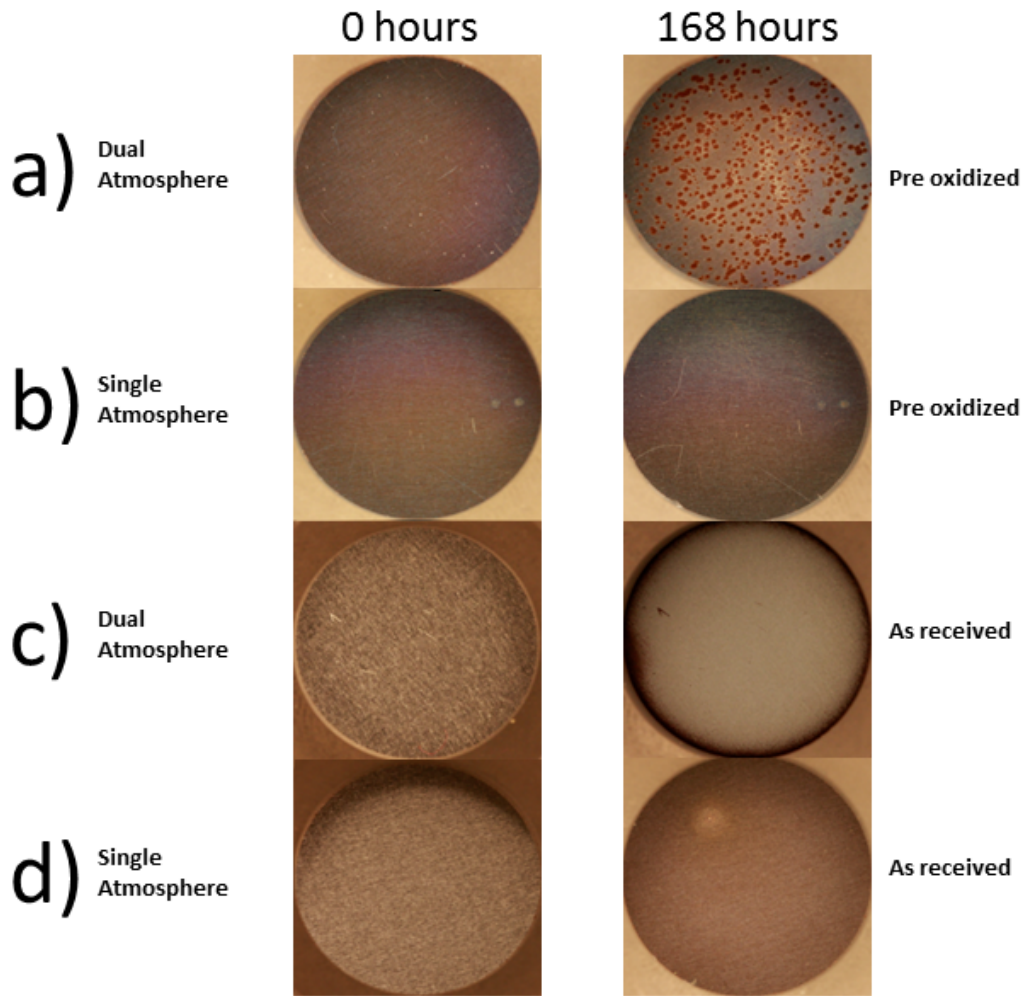


Figure 4.15: Results from the 600°C deuterium exposure [29]. a) Pre oxidized sample in dual atmosphere, b) Pre oxidized sample in single atmosphere, c) As received sample in dual atmosphere, d) As received sample in single atmosphere.

In Figure 4.15 we can see the results of another dual atmosphere exposure at 600°C done by Dr. Kerem Özgür Gündüz where instead of hydrogen, deuterium has been used [29]. These results are comparable to the results in Figure 4.11 since the pre oxidized samples, for both exposures, have a similar behaviour. The as received samples presented in Figure 4.15 are completely covered in iron oxide after 168 hours in dual atmosphere conditions. However, this behaviour cannot be seen for the sample exposed only to single atmosphere, which proves that the dual atmosphere corrosion has occurred for the as received sample.

4.4 650°C Exposure

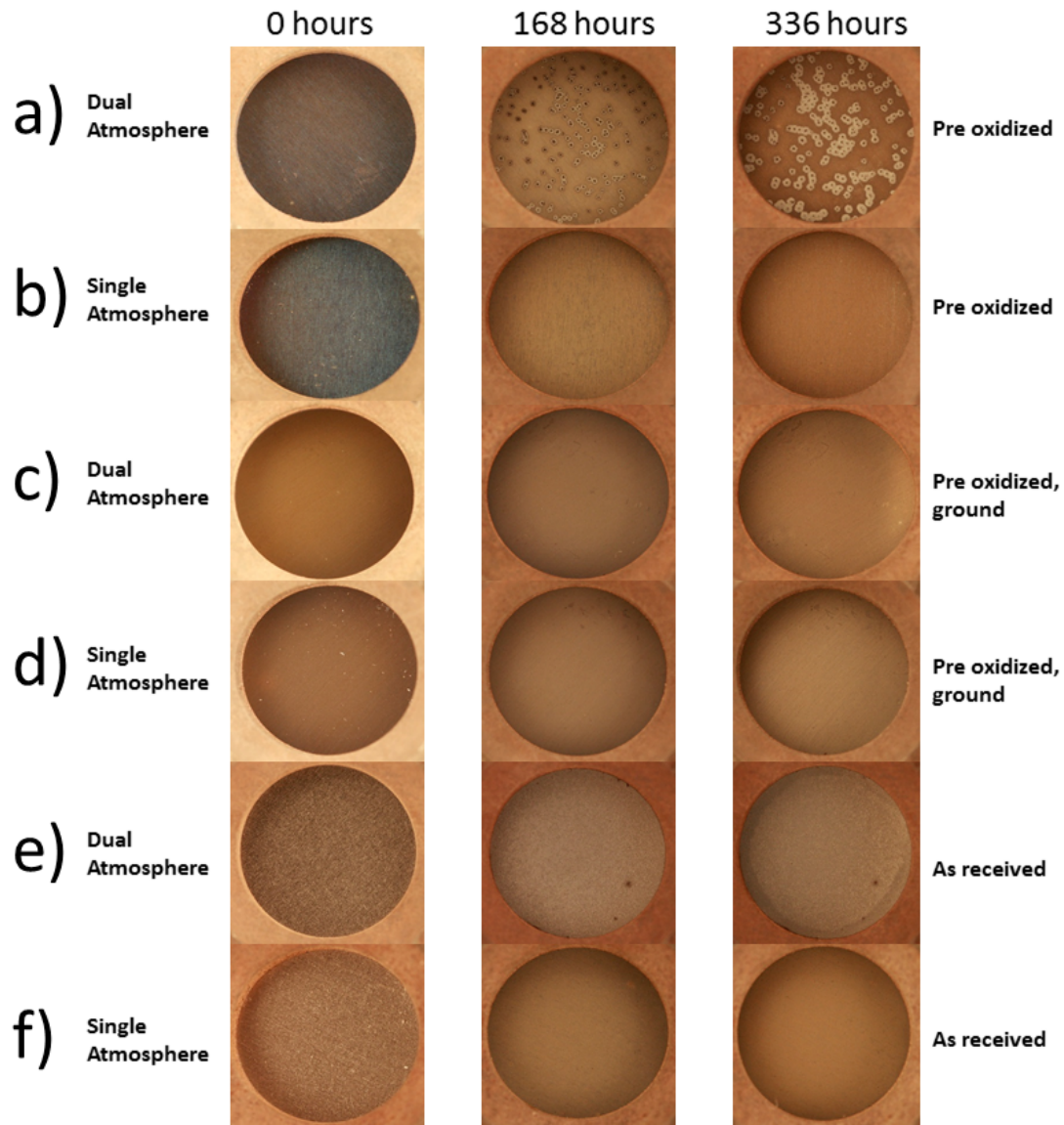


Figure 4.16: Results from the 650°C exposure. a) Pre oxidized sample in dual atmosphere, b) Pre oxidized sample in single atmosphere, c) Pre oxidized ground sample in dual atmosphere, d) Pre oxidized ground sample in single atmosphere, e) As received sample in dual atmosphere, f) As received sample in single atmosphere.

Figure 4.16 clearly shows that the dual atmosphere effect is present at 650°C. When comparing the pre oxidized samples a) and b) we can see that at both 168 and 336 hours the dual atmosphere effect is clearly shown. This is also true when comparing samples e) and f) as well which are only as received and no pre oxidation. The surface of e) after 336 hours is completely covered with iron oxide while sample f) is still protected.

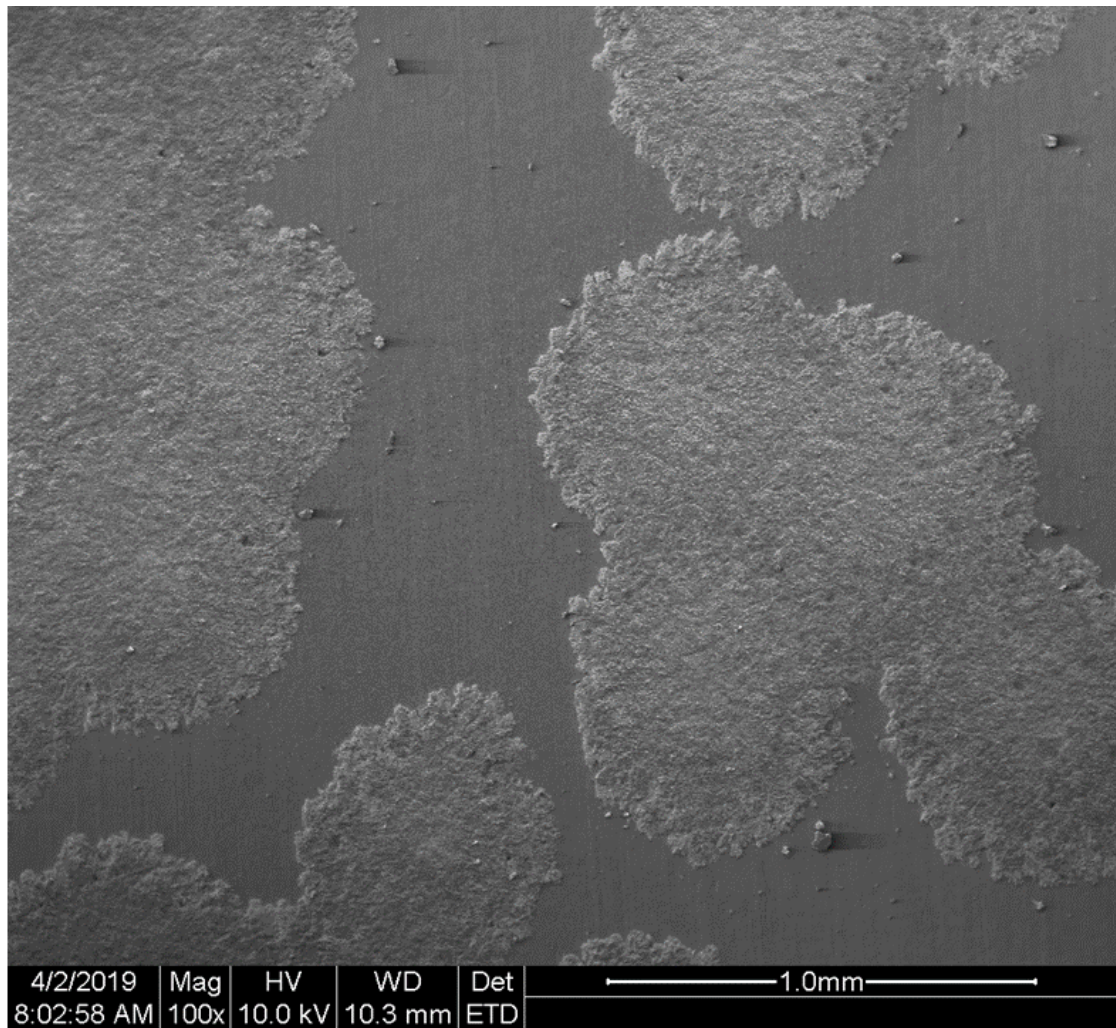


Figure 4.17: Top view SEM image of the pre oxidized sample a) after 336 hours.

The SEM image in Figure 4.17 presents the presence of breakaway corrosion on the pre oxidized sample sample a). We can see that most of the surface is covered and there is only little protected surface left. Closer images of the surface can be seen in Figure 4.18. The surface was analyzed with EDX to confirm the presence of iron oxide and the results are shown in Figure A.7 and Table A.5 in Appendix 1.

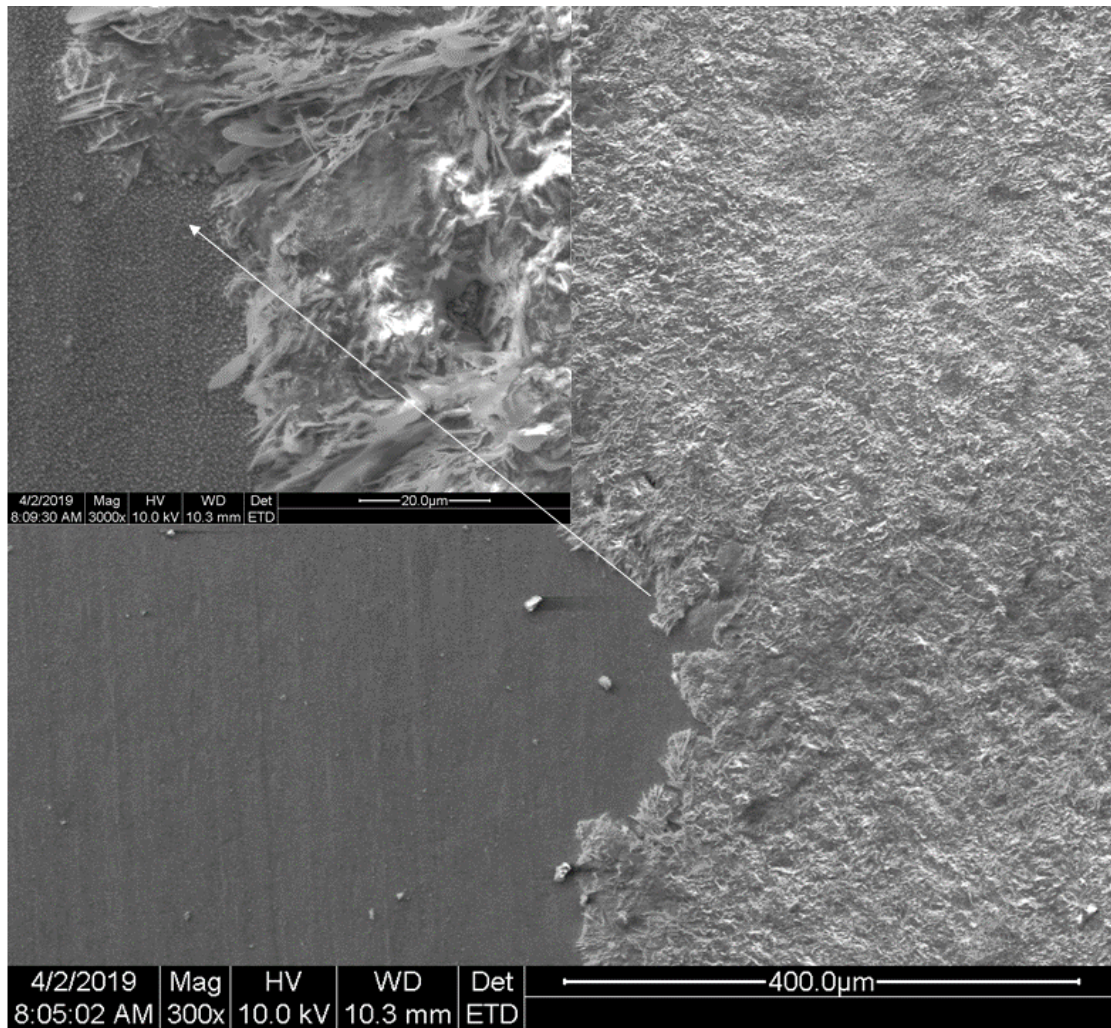


Figure 4.18: Top view SEM image of the pre oxidized sample a) after 336 hours.

When analyzing the surface with SEM, only one nodule was found on the ground and pre oxidized sample c) after 336 hours, presented in Figure 4.20. The rest of the surface was covered with protective oxide. The surface was further analyzed with EDX which can be seen in Figure 4.21 and Table 4.3. We can see that the nodule is rich in chromium, iron and oxygen when looking at spectrum 1 and 6. Similar results are also seen in spectrum 3. This chromium iron oxide has not been seen in previous EDX analysis and is probably due to inward growing iron and chromium rich oxide. Since the EDX signal is not surface sensitive it will penetrate into the sample and get signals from there as well as the outwards growing iron oxide. We can also see what seem to be the onset of iron rich oxide in spectrum 2.

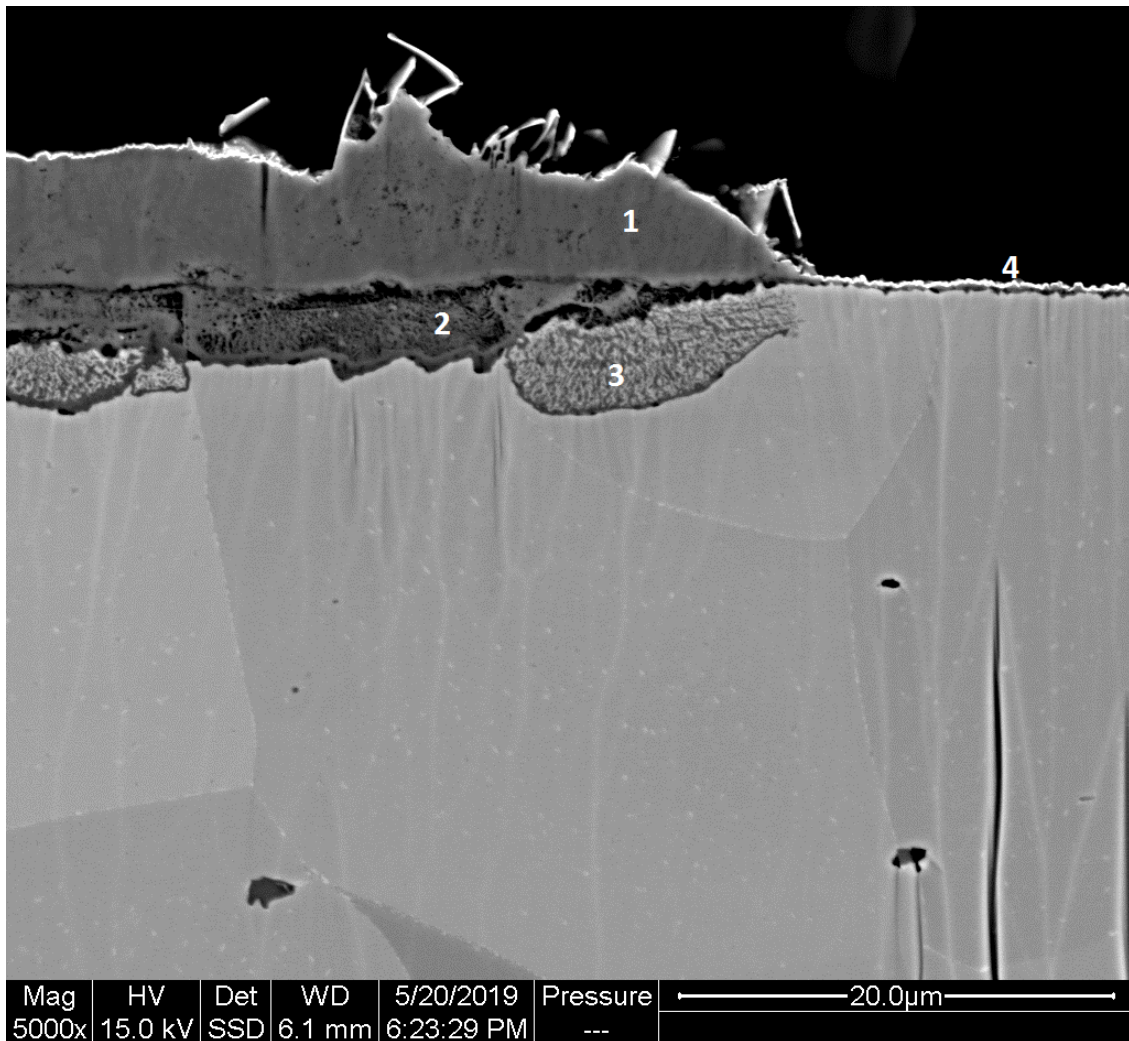


Figure 4.19: Cross section SEM image of the pre oxidized sample a) after 336 hours.

To further analyze the pre oxidized sample a) a cross section was made with Broad Ion Beam milling and analyzed using SEM. The resulting cross section is displayed in Figure 4.19. In this figure different oxides can be observed. Oxide number 1 is the outward growing Fe_2O_3 , also called hematite. This is what is observed when viewing the top view SEM images of this sample. Oxide number 2 is the inwards growing $(\text{Fe,Cr})_3\text{O}_4$ spinel and number 3 is not an oxide but the reaction zone where the internal oxides are formed. Number 4 is the very thin protective oxide which still covers some parts of the sample. These results were confirmed using EDX which is shown in Figure A.8 and Table A.6 in Appendix 1.

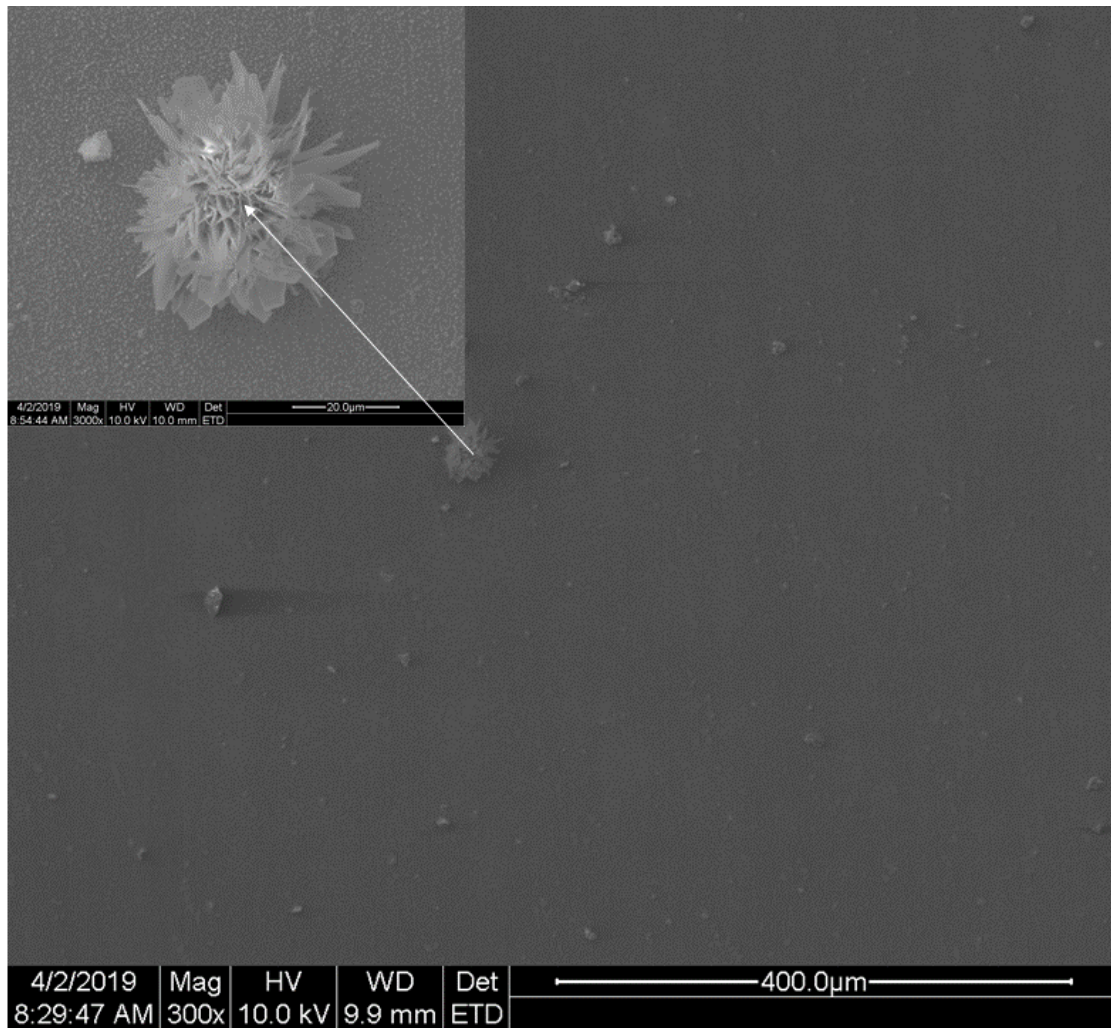


Figure 4.20: Top view SEM image of the ground and pre oxidized sample c) after 336 hours.

In a comparison between the ground and pre oxidized samples c) from Figure 4.11 and 4.16 we could see many hematite nodules on the surface of the sample exposed at 600°C but at 650°C we could only see one nodule. This tells us that the dual atmosphere effect is more severe at 600°C than at 650°C. We could also see that the grinding is beneficial at reducing the dual atmosphere effect when comparing the pre oxidized samples a) and c). This might be due to that when the sample is ground new defects such as dislocations and vacancies are introduced to the surface of the sample which will make it easier for the chromium in the bulk to diffuse to the surface to form the protective oxide.

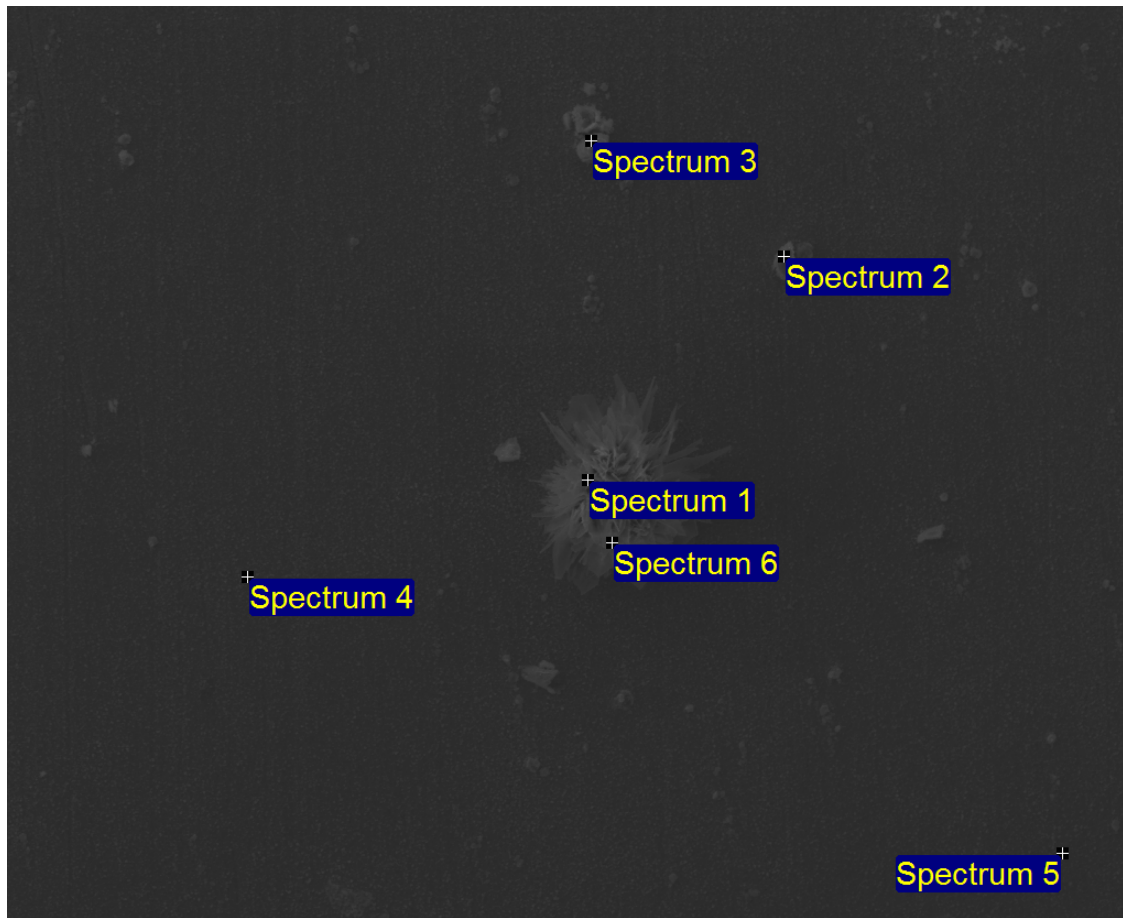


Figure 4.21: EDX of the ground and pre oxidized sample c) after 336 hours.

Table 4.3: EDX analysis of the ground and pre oxidized sample c) after 336 hours, elements in weight%.

	C	O	Si	Ti	Cr	Mn	Fe
Spectrum 1	1	11			46	1	41
Spectrum 2	2	16			5	1	76
Spectrum 3	4	30	1		33	1	31
Spectrum 4	2	10	1	1	19	2	65
Spectrum 5	2	7	1	1	19	1	69
Spectrum 6	3	22			40	1	34

The EDX result of the ground pre oxidized sample, c) is shown in Figure 4.21 and Table 4.3. When looking at Spectrum 1 and 6 a high content of chromium is observed. This is probably due to the fact there might be an inwards growing iron chromium oxide spinel beneath the nodule like seen in Figure 4.19. Since the interaction volume of the EDX is large, signals from this affects the EDX results.

In Figure 4.22 we can see that the surface of the as received sample is completely covered in hematite. This result is also shown when looking at the EDX results in Figure A.9 and Table A.7 in Appendix 1. If we compare this result to the one in

4. Results & Discussion

Figure 4.10 we see that this layer of iron oxide seems to be thicker comparing to the sample exposed at 550°C. This is probably due to the increased thermal activity at higher temperature.

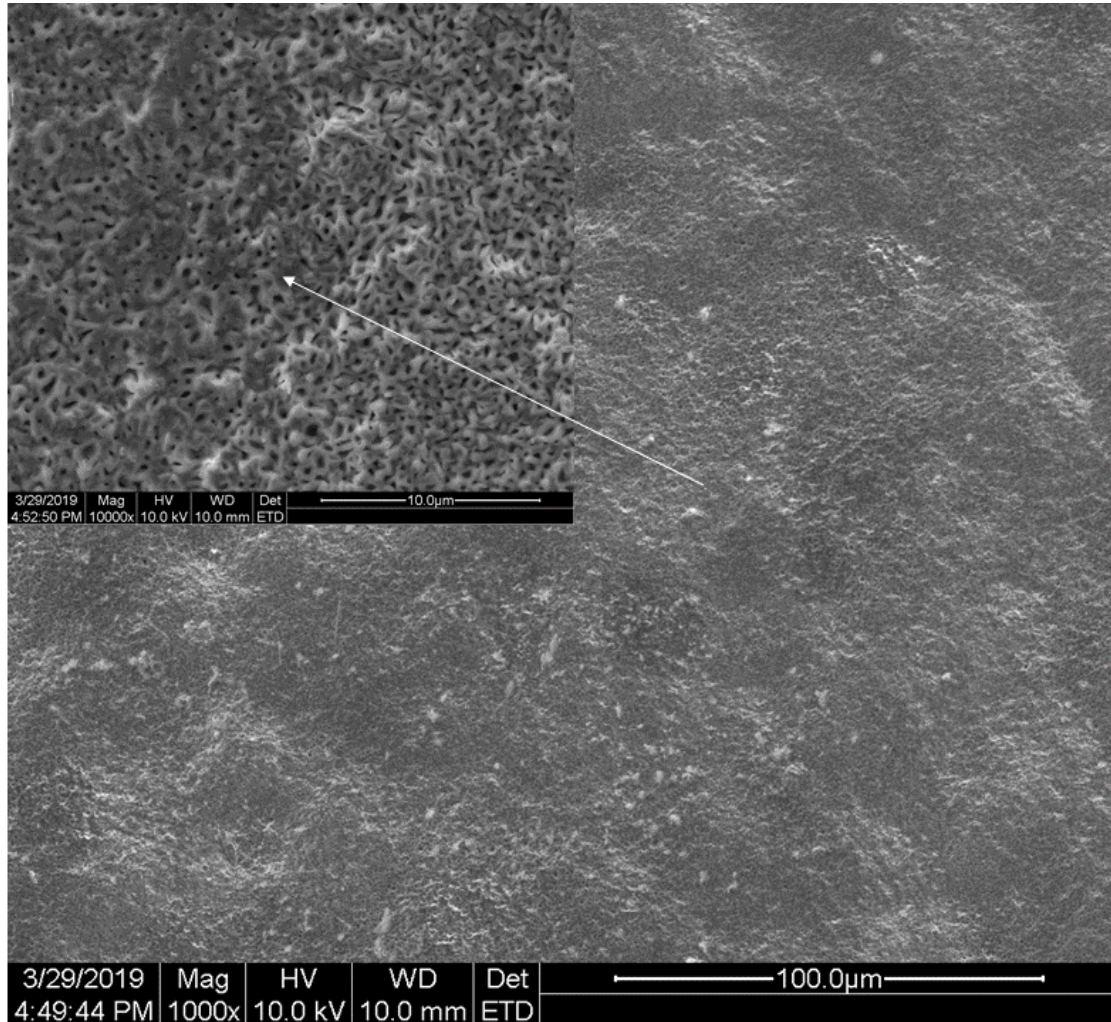


Figure 4.22: Top view SEM image of the as received sample e) after 336 hours.

For the 650°C exposure, the dual atmosphere effect is confirmed since there are some nodules present. However, the effect is less severe than it was for the 600°C exposure. When comparing the pre oxidized samples a) and c) in Figures 4.11 and 4.16 we can see that the dual atmosphere effect is more severe at 600°C and this is also confirmed by the SEM and EDX results.

4.5 700°C Exposure

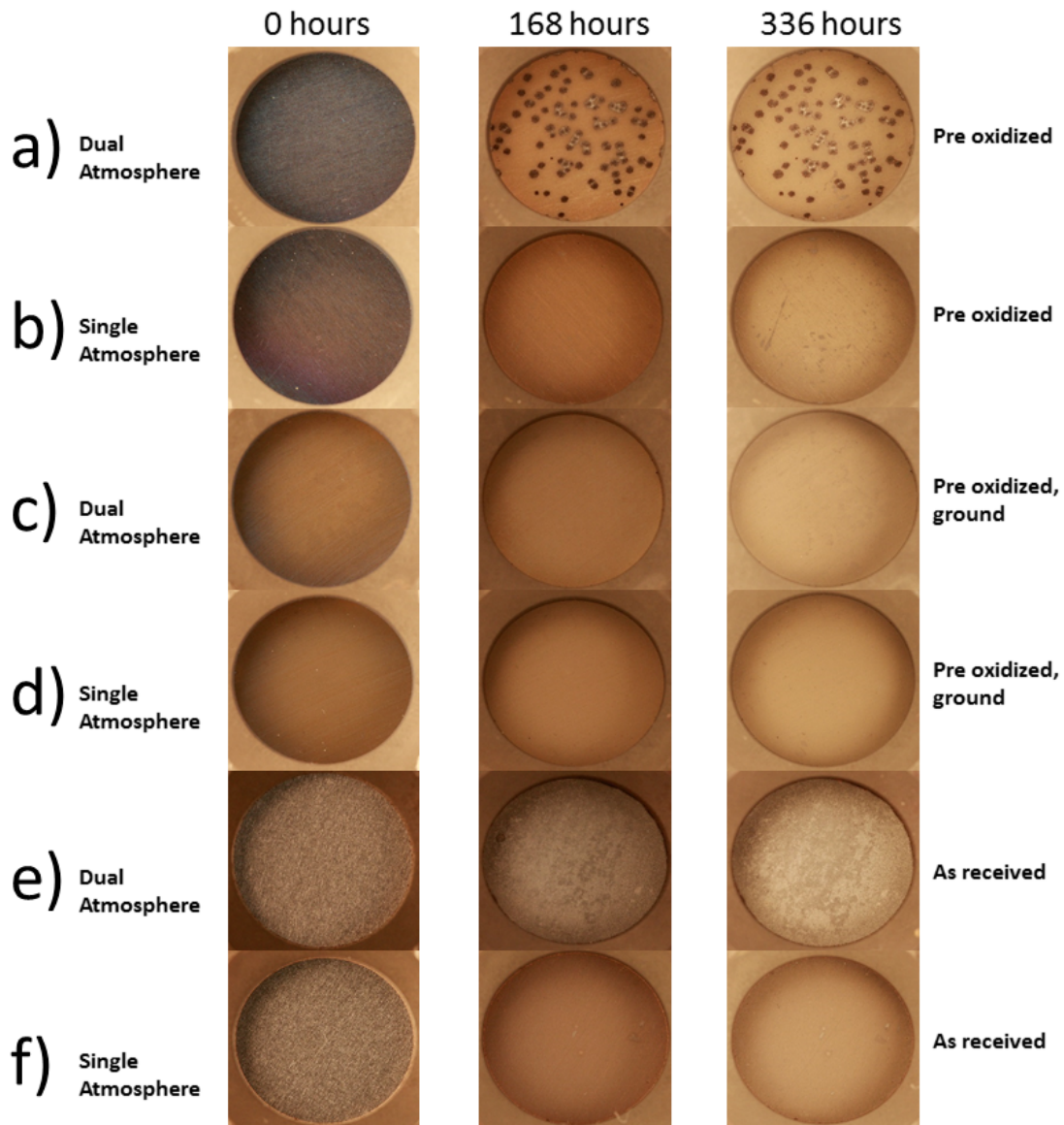


Figure 4.23: Results from the 700°C exposure. a) Pre oxidized sample in dual atmosphere, b) Pre oxidized sample in single atmosphere, c) Pre oxidized ground sample in dual atmosphere, d) Pre oxidized ground sample in single atmosphere, e) As received sample in dual atmosphere, f) As received sample in single atmosphere.

In Figure 4.23 we can clearly see that at 700°C the dual atmosphere effect is present. This is understood when comparing the pre oxidized samples a) and b) and the as received samples e) and f). One can not determine anything by only looking at the ground and pre oxidized samples c) and d), in this case further investigation would be necessary to be able to draw any conclusions.

Figure 4.24 shows the top view SEM image of the pre oxidized sample a) after

336 hours. We can clearly see the area of the surface covered by hematite. What is also noticeable is that some of the surface is still covered with protective oxide.

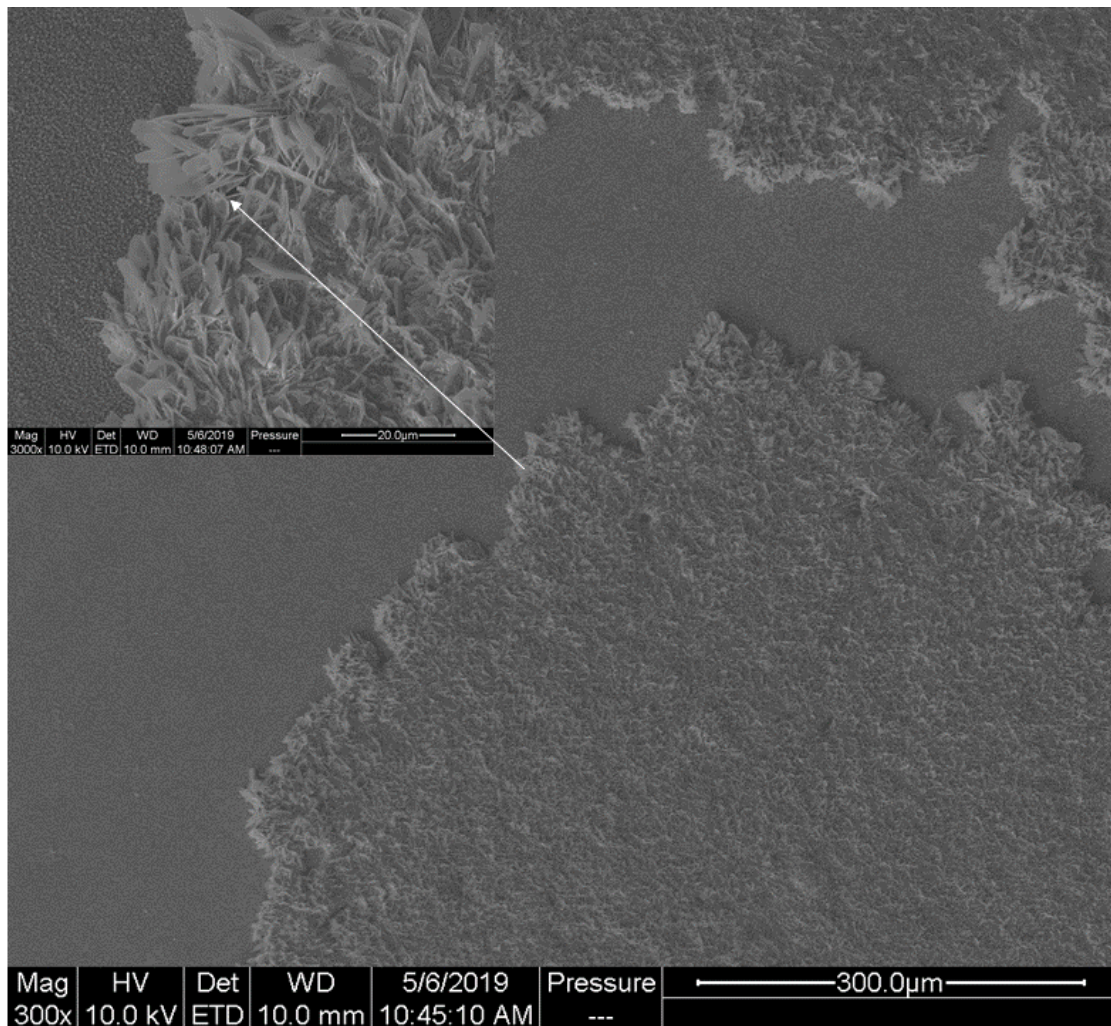


Figure 4.24: Top view SEM image of the pre oxidized sample a) after 336 hours.

For the pre oxidized sample a), it was found that large areas of iron rich oxide had been formed during the exposure, the composition was confirmed by EDX which is presented in Figure 4.25 and Table 4.4. What the EDX also shows is that the protective oxide contains high amounts of manganese and chromium which most probably means that it is an outward growing MnCr_2O_4 spinel.

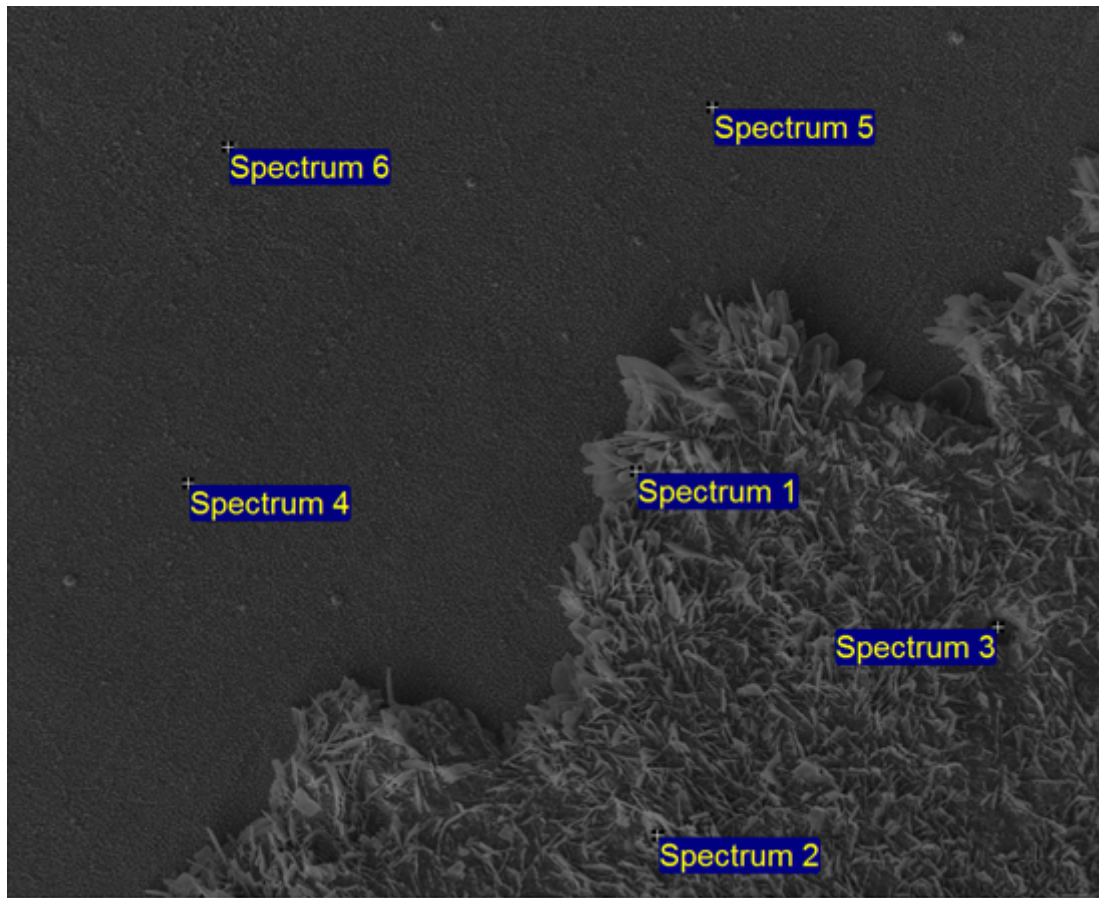


Figure 4.25: EDX of the pre oxidized sample a) after 336 hours.

Table 4.4: EDX analysis of the pre oxidized sample a) after 336 hours, elements in weight%.

	C	O	Si	Ti	Cr	Mn	Fe
Spectrum 1	1	31			22		46
Spectrum 2	1	24			25		50
Spectrum 3	1	28	3	5	27	13	23
Spectrum 4	1	25	1	2	36	25	10
Spectrum 5	1	26	1	2	31	25	14
Spectrum 6	1	22	2	2	36	22	15

Figure 4.26 shows the surface of the ground and pre oxidized sample c) after 336 hours. This sample has a granular kind of surface, no nodules are present anywhere on the surface. This surface is confirmed to be chromium and manganese rich oxide by EDX analysis which is shown in Figure 4.27 and Table 4.5 .

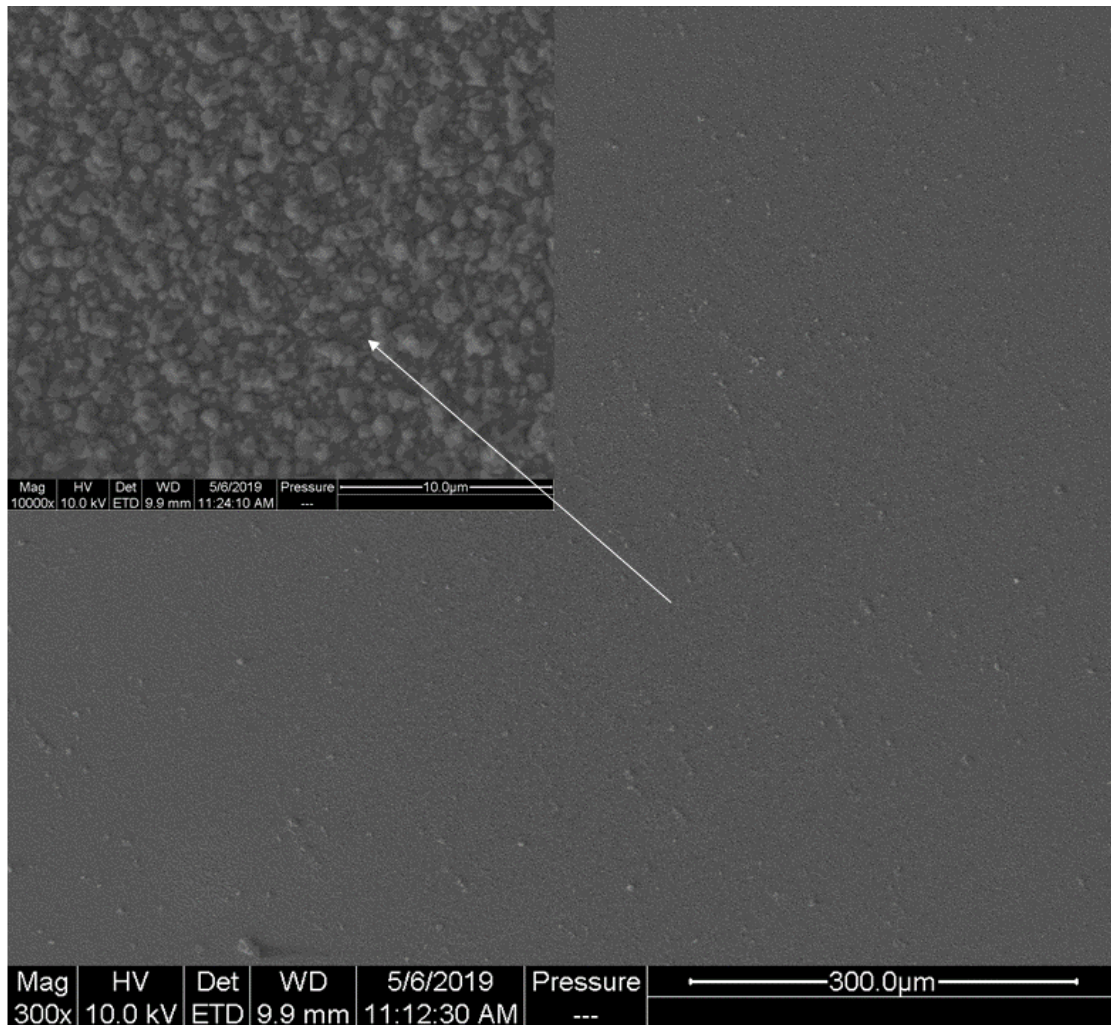


Figure 4.26: Top view SEM image the ground and pre oxidized of sample c) after 336 hours.

In the EDX results we can see that the surface is mostly composed by the MnCr_2O_4 spinel when looking at spectrum 2 and 3. This is a protective oxide so there are no signs of breakaway corrosion on the surface. This also shows that grinding has a big effect on reducing the dual atmosphere effect when comparing sample a) and c) where the only difference is that sample c) is ground.

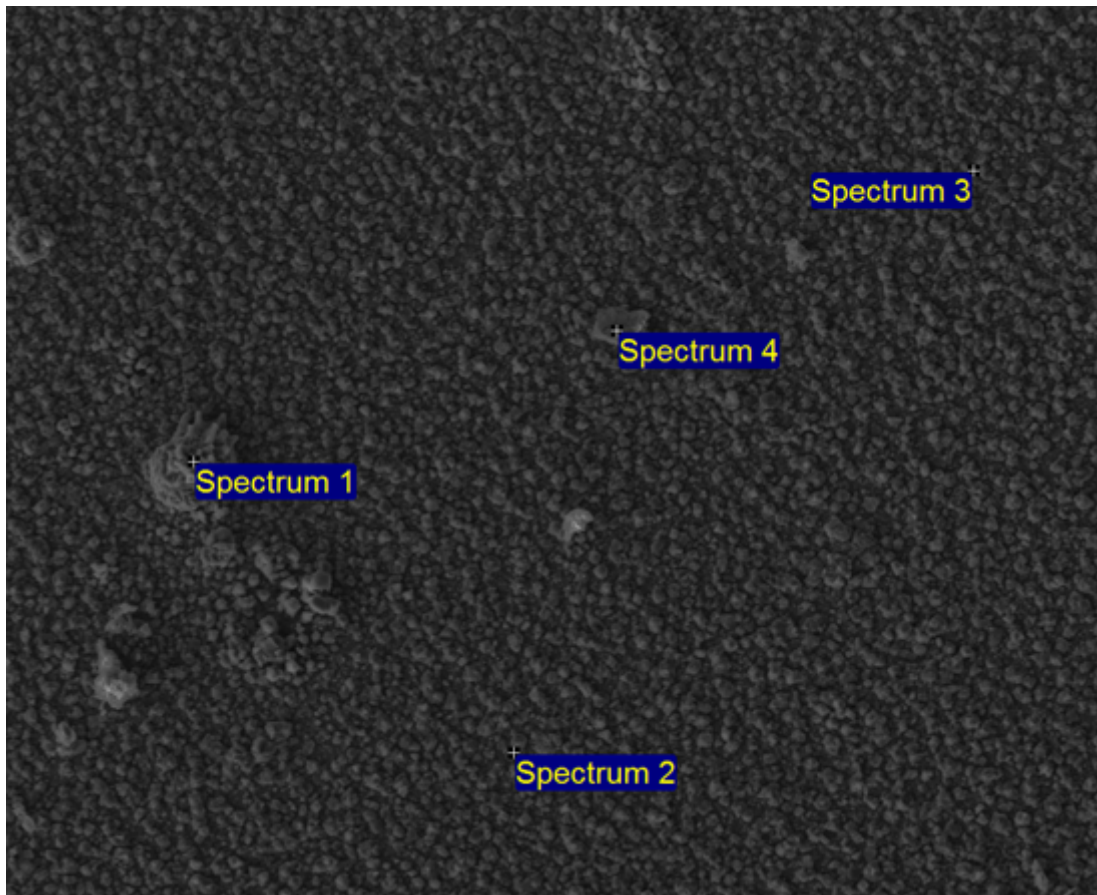


Figure 4.27: EDX of the ground and pre oxidized sample c) after 336 hours.

Table 4.5: EDX analysis of the ground and pre oxidized sample c) after 336 hours, elements in weight%.

	C	O	Si	Ti	Cr	Mn	Fe
Spectrum 1	1	26			58	4	11
Spectrum 2	1	21		2	40	30	6
Spectrum 3	1	19		1	33	38	8
Spectrum 4	1	21	1		44		33

The surface of the as received sample e) obtained from SEM can be seen in Figure 4.28, it is shown that the entire surface is covered with hematite which is also confirmed using EDX which can be seen in Figure A.10 and Table A.8 in Appendix 1.

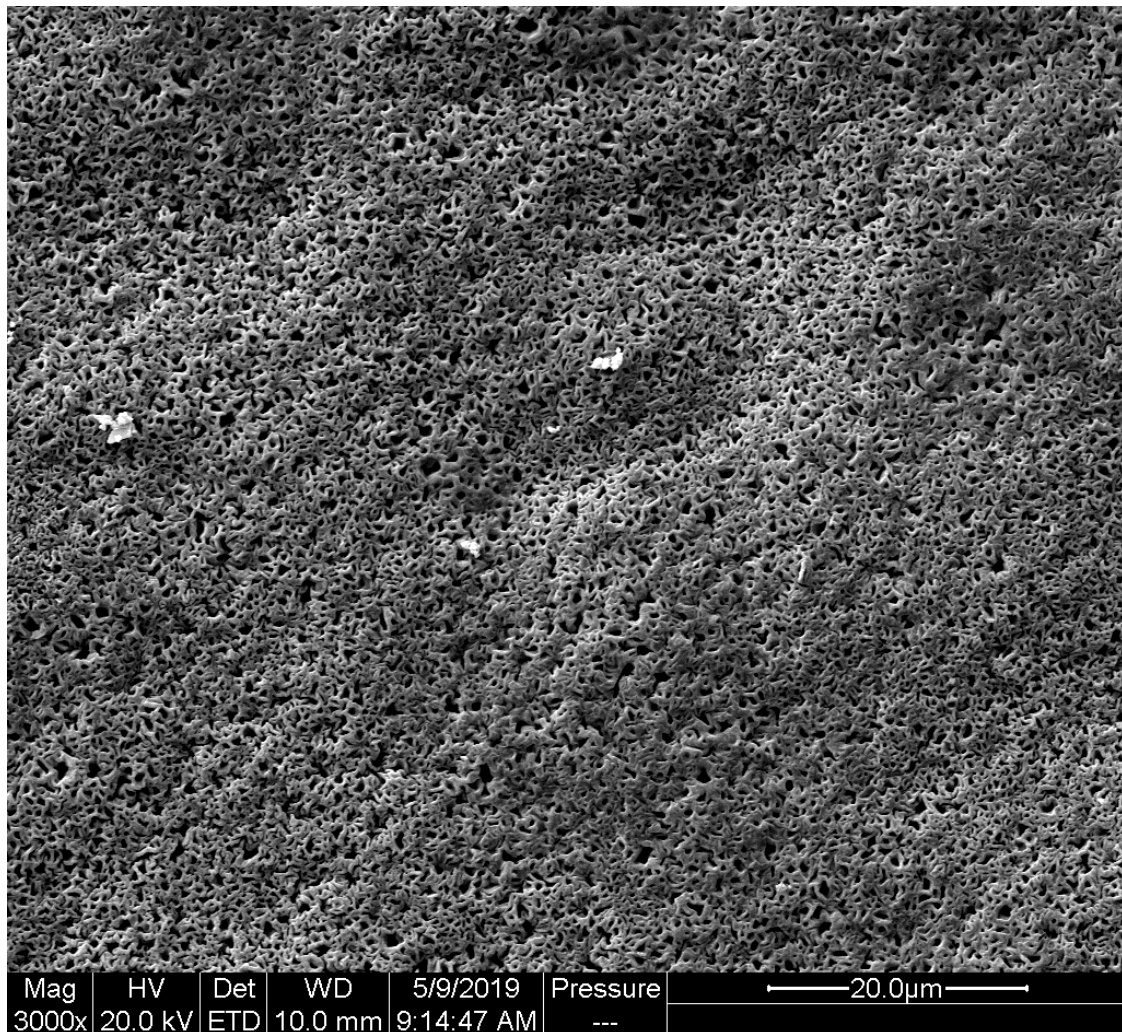


Figure 4.28: Top view SEM image of the as received sample e) after 336 hours.

When comparing the results of the 700°C exposure we can now see that the dual atmosphere effect is less prominent compared to the slightly lower temperatures 600°C and 650°C. The ground and pre oxidized sample c) at 700°C is free from breakaway corrosion. This tells us that at higher temperatures something happens that helps to mitigate the dual atmosphere effect. One theory what this might be is that the increase in temperature will increase the diffusion of chromium and manganese from the bulk to the surface of the steel making it easier to form the protective oxide.

4.6 800°C Exposure

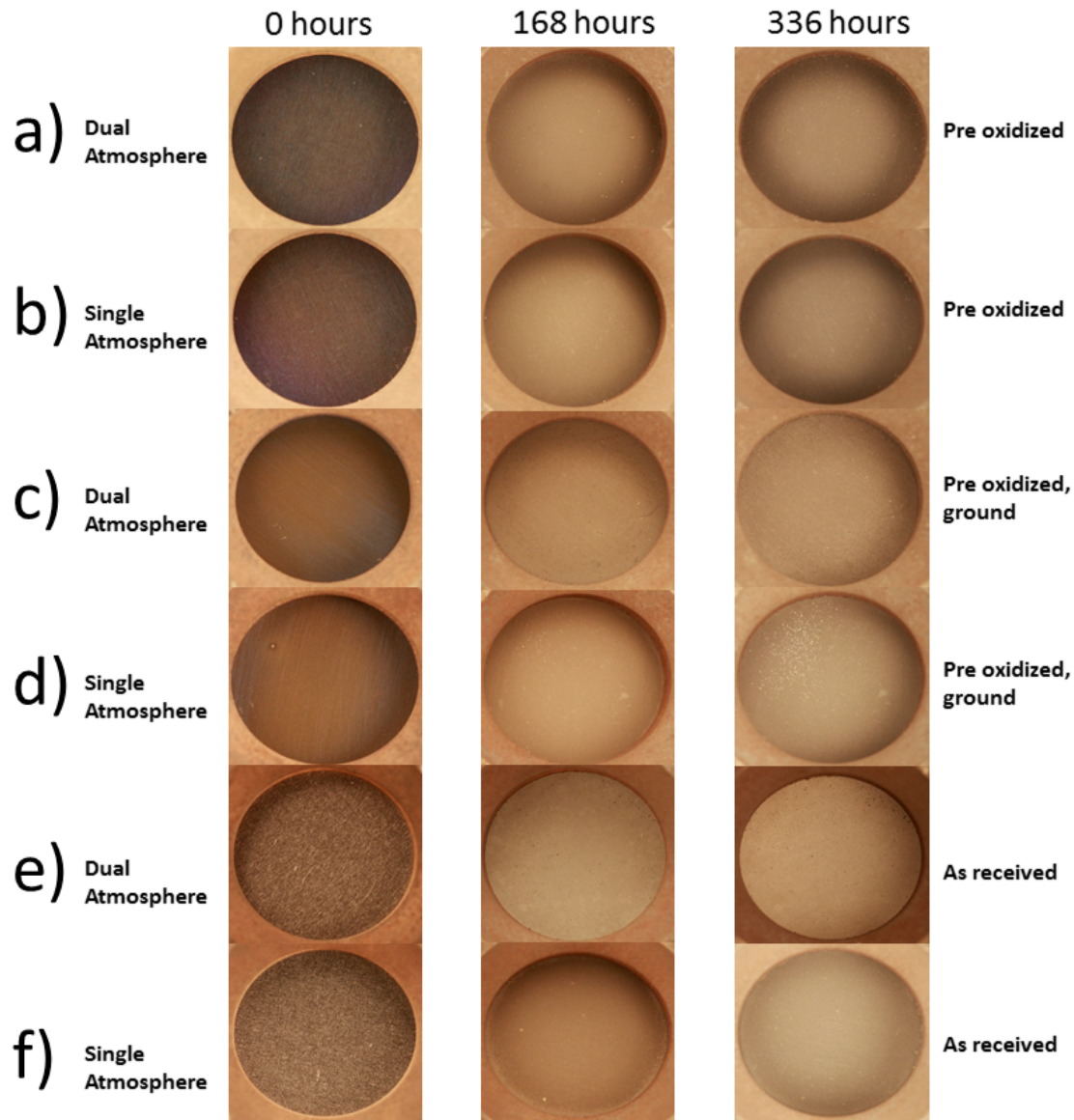


Figure 4.29: Results from the 800°C exposure. a) Pre oxidized sample in dual atmosphere, b) Pre oxidized sample in single atmosphere, c) Pre oxidized ground sample in dual atmosphere, d) Pre oxidized ground sample in single atmosphere, e) As received sample in dual atmosphere, f) As received sample in single atmosphere.

When observing the pictures taken on the samples from the 800°C exposure the dual atmosphere effect can only be observed when comparing the as received samples e) and f). Similar to the exposures at lower temperatures, the surface of sample e) is covered in breakaway corrosion and sample f) still has a protective oxide scale. We cannot see any signs of breakaway corrosion on sample a) as we have seen before but to be sure, SEM analysis has been performed. The top view SEM of the pre

oxidized sample a) is presented in Figure 4.30. We can see that the surface is covered with chromium and manganese rich protective oxide and no iron oxide nodules are present. We can therefore say that at 800°C the dual atmosphere is not clearly affecting this sample. This is also confirmed with EDX analysis which can be seen in Figure A.11 and Table A.9 in Appendix 1.

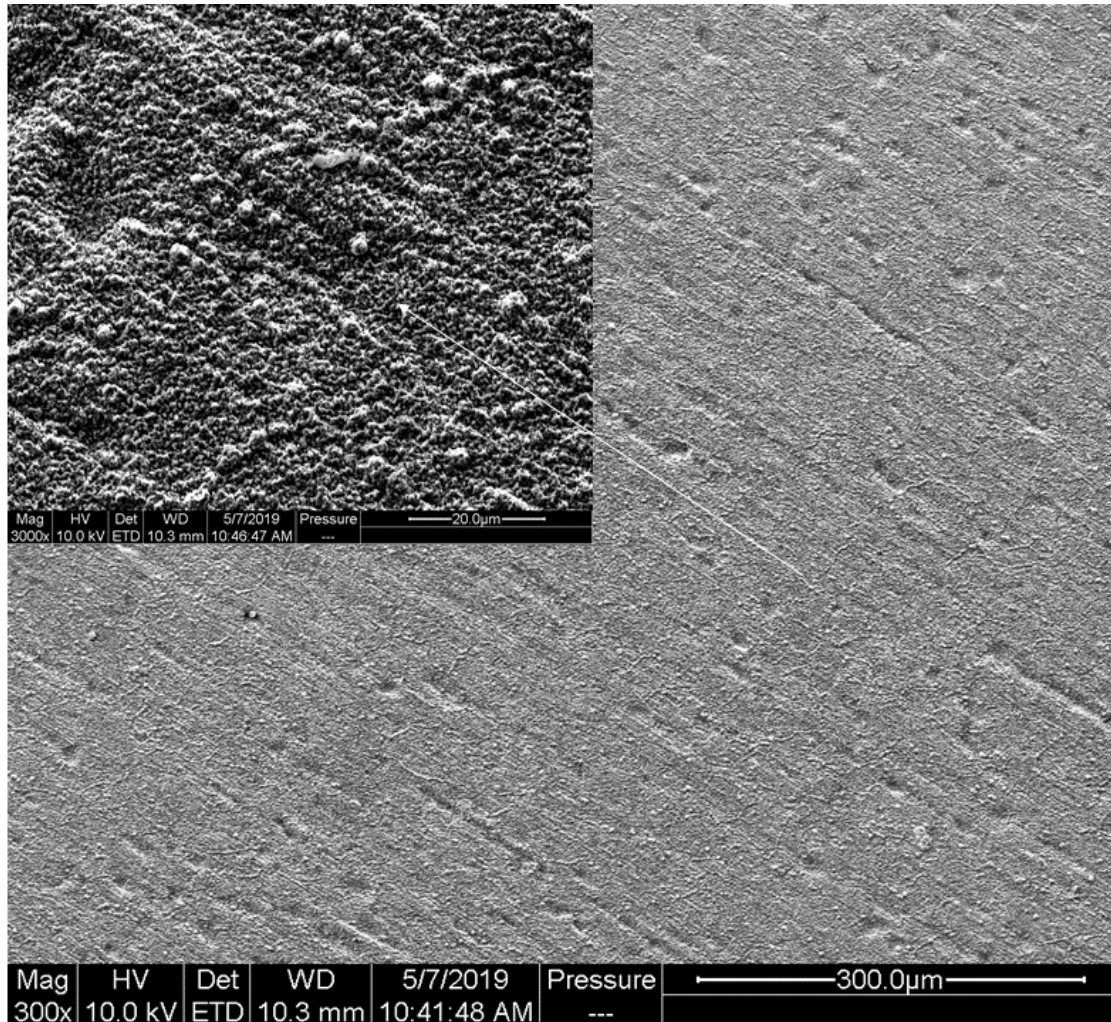


Figure 4.30: Top view SEM image of the pre oxidized sample a) after 336 hours.

Very similar results can be seen when we compare the ground and pre oxidized sample c) with the pre oxidized sample a) using SEM. We can also see that the surface is covered with protective oxide. The oxide is confirmed to be a chromium and manganese rich oxide by using EDX. The result of this EDX analysis can be seen in Figure A.12 and Table A.10 in Appendix 1.

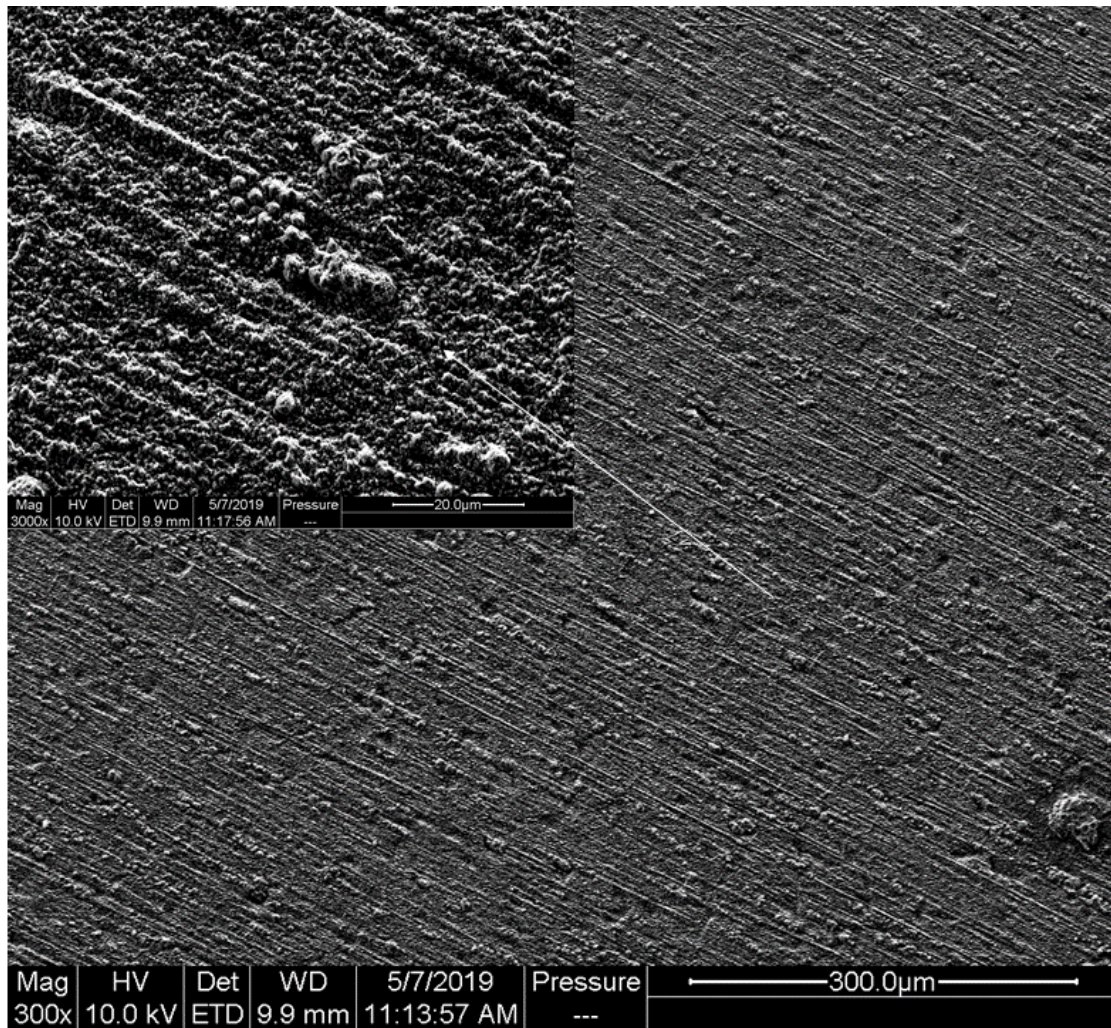


Figure 4.31: Top view SEM image of the ground and pre oxidized sample c) after 336 hours.

Hematite was found on the as received sample e), it was confirmed using SEM and EDX. These results can be seen in Figure 4.29. In Figure 4.32 the surface of the as received sample e) is shown to be completely covered with iron oxide, this is similar to previous results at lower temperatures. This result is confirmed by EDX shown in Figure A.13 and Table A.11 in Appendix 1.

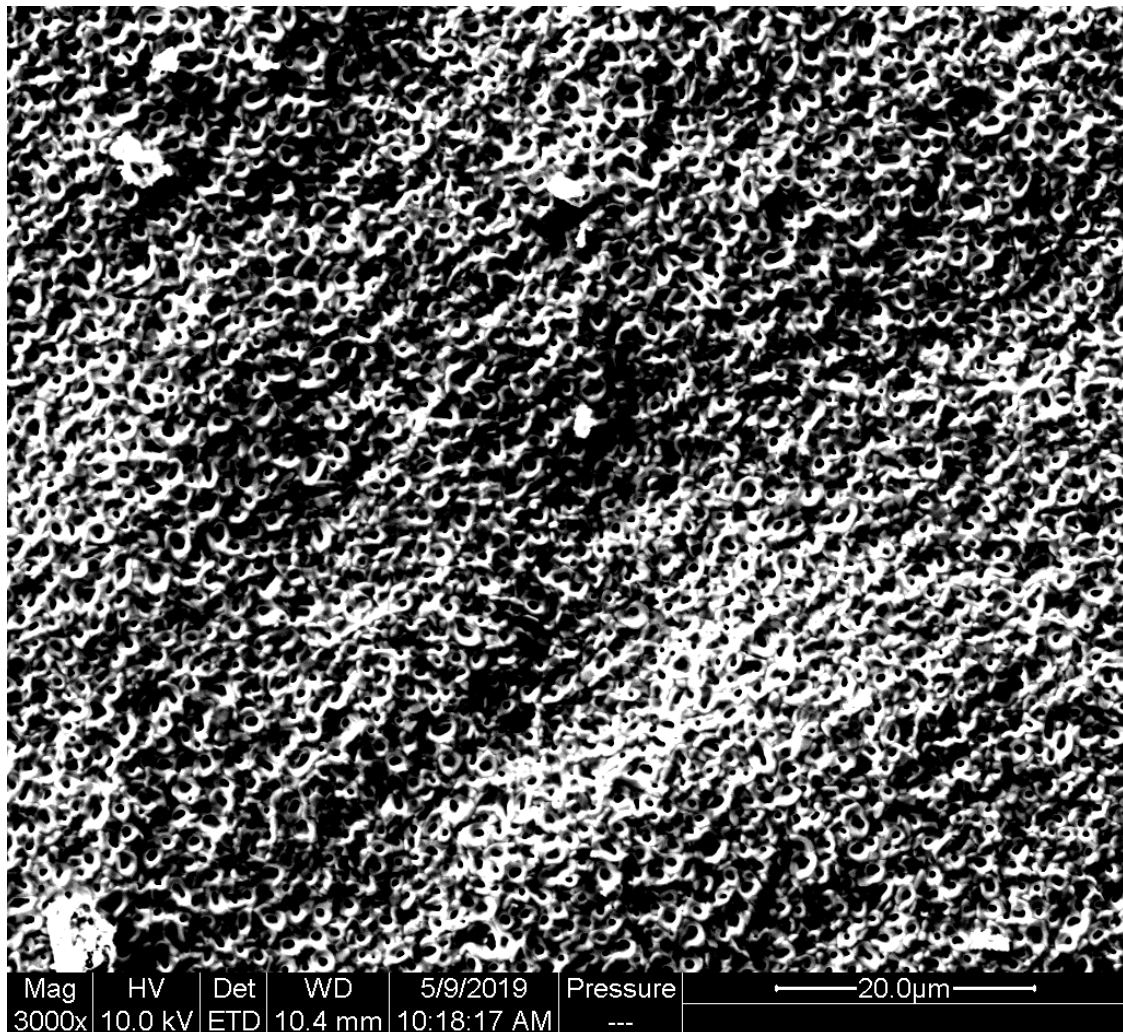


Figure 4.32: Top view SEM image of the as received sample e) after 336 hours.

We can see that the dual atmosphere effect has less of an effect at 800°C compared to the 700°C exposure. At 800°C only the as received sample has signs of dual atmosphere effect. The pre oxidized sample which has shown dual atmosphere effect from 550°C up to 700°C now shows no sign of the dual atmosphere effect. We can now start to make up at which temperatures the different samples are affected by the dual atmosphere effect at these specific experimental parameters. The pre oxidized sample shows to be susceptible to the dual atmosphere effect between the temperatures 550°C up to 700°C while the ground pre oxidized sample only seems to be susceptible between the temperatures 550°C and 650°C with a clear peak at 600°C, at the other two temperatures only a few nodules were seen. The as received sample only seems to survive the dual atmosphere effect at the lowest temperature, 500°C. This indicates that some kind of pre oxidation to form a protective oxide before exposing the sample to dual atmosphere is very important.

4.7 The Effect of Temperature

The results that we have presented show that the dual atmosphere effect is highly temperature dependent but to different extent for the different samples. As mentioned by Alnegren et. al [25] we could also see most effect by the dual atmosphere at 600°C for our samples.

There are several different processes occurring in the sample which all are affected by temperature. There is the formation and growth of the chromia scale on the surface which depends on the diffusion of chromium from the bulk of the sample to the surface. Another temperature dependent process is the diffusion of hydrogen from the fuel side through the sample to the air side. All of these different processes have different activation energies for them to occur and they affect the oxidation on the air side. In what ways we do not yet fully understand. It is believed that the hydrogen diffusion through the sample either interacts with the chromia scale and interferes with the protective scale on the air side or that the hydrogen diffusion through the sample somehow restricts the diffusion of chromium from the bulk to the surface. This would also result in a lack of continuous supply of chromium to maintain the protective oxide.

Depending on the sample conditions the surface had more protective oxide when decreasing the temperature from 600°C to 550 and 500°C. This would indicate that the diffusion of hydrogen is slower at lower temperatures and therefore has less impact on the oxidation on the air side. This is supported by the fact that the diffusion of hydrogen through the steel is a thermally controlled process which follows the Arrhenius law. At lower temperatures the rate of the hydrogen diffusion will be lower and have less of an impact or it could be due to at lower temperatures the scale growth kinetics are slow and a protective oxide can be maintained even with the presence of hydrogen.

When increasing the temperature from 600°C to 650, 700 and 800°C we also see a reduction of the dual atmosphere effect to different extent for the different samples. The reduction of the dual atmosphere effect at elevated temperatures is most likely caused by the fact that at higher temperatures chromium will diffuse faster from the bulk of the steel to the surface to form protective oxides which will hinder the hydrogen diffusion to impact the oxidation on the air side. At 600°C we believe that the conditions are optimal for the dual atmosphere to affect the samples. The temperature is high enough for the thermal energy required for the hydrogen diffusion to impact the oxidation on the air side. The temperature is also low enough for the diffusion of chromium to be slow.

We can also conclude that only increasing the temperatures is not the only thing effecting the dual atmosphere effect. When we compare our as received pre oxidized samples at 700°C with results from Alnegren et. al [26] we can see that our samples show a clear effect of the dual atmosphere at 700°C where the results from Alnegren does not show any obvious signs of the dual atmosphere effect. The main difference

between the samples is the pre oxidation time. Our samples were pre oxidized for 20 minutes while the samples by Alnegren were pre oxidized for 3 hours. This tells us that the pre oxidation time is also very important to mitigate the dual atmosphere effect and this is also reported by Göbel et. al[10].

4.8 The Effect of Surface Treatment

The samples that performed the best, in terms of corrosion resistance, in this study were the samples that were both ground and pre oxidized for 20 minutes. Starting with the lowest temperature, 500°C, no direct difference between the two samples exposed to different environments was observed. Even the SEM analysis showed no signs of the dual atmosphere effect. Going up in temperature the SEM showed more and more iron rich nodules, however this is only true until 600°C was reached. After this temperature, an inverse trend was shown, where less and less iron nodules were present on the surface. Comparing these samples to the pre oxidized as received and the as received samples the conclusion that grinding the surface helps mitigating the corrosion. This is probably due to an increase in defect density of the steel. These defects would make it easier for the alloying elements such as chromium to diffuse faster to the surface and form a protective oxide. A study made by Kurokawa et al. [30] shows that the hydrogen diffusion through a Cr_2O_3 scale is about four orders of magnitude lower than that for iron. It is believed that hydrogen is dissolved as interstitial protons in chromium oxide and that the hydrogen permeation is a diffusion controlled process. A study made by Ardigo-Besnard et al. [7] obtained similar results compared to our study. Their surface finish was however mirror polished and our surface was ground with 1200 grit, disregarding these differences they found differences between the polished samples and the as received samples. The authors suggest that the effect of polishing the surface creates dislocation in the subsurface which promotes the diffusion of chromium and the formation of a protective scale during high temperature exposures. Also, the diffusion coefficient of manganese in Cr_2O_3 is higher than that for chromium which results in the formation of a MnCr_2O_4 . It is suggested that the number of dislocations of the as received samples are too low to ensure the formation of a continuous Cr_2O_3 scale and thus the oxidation of iron can take place resulting in the fast growing iron oxide covering the surface.

The effect of pre oxidation has been proven to mitigate the corrosion behaviour. As mentioned before, the hydrogen diffusion through the Cr_2O_3 scale is much lower than for iron oxide, and by pre oxidizing the samples prior exposure, a thin Cr_2O_3 scale is formed hindering the hydrogen diffusion through the steel. A study made by Göbel et al. [10] also shows that the location of the pre oxidation affects the corrosion. It was found that the samples with a pre oxidized surface facing the fuel side was better at maintaining a protective oxide scale on the air facing side. They suggest that the pre oxidation scale formed acts as barrier against hydrogen diffusion into the steel. In our results it can be seen that the samples with no pre oxidation performed the worst and already at 550°C the sample was completely covered in hematite.

These results suggests that pre oxidation and surface finish help mitigating the corrosion behaviour of the dual atmosphere effect. Both of the surface treatments reduce the hydrogen diffusion in different ways, and since the dual atmosphere effect is believed to be governed by the diffusion of hydrogen, the lack of hydrogen on the air side reduces the corrosion on that side.

5

Conclusion

When AISI 441 stainless steel is exposed to dual atmosphere it will experience more corrosion on the air side of the sample. The effect of this dual atmosphere corrosion depends on many aspects and in this report it has been shown that temperature and surface finish are two very important factors influencing dual atmosphere corrosion.

The dual atmosphere effect is observed to be worst at 600°C. When going down in temperature for our samples the effect is less pronounced and at 500°C the dual atmosphere effect is not present. The dual atmosphere effect also influences the samples less when increasing temperature from 600°C up to 800°C. It is also clear that the surface finish on the different samples play a big role in mitigating the dual atmosphere effect. Samples that were ground and pre oxidized have the smallest temperature range where the dual atmosphere effect is present followed by samples that are only pre oxidized. As received samples show very little protection against the dual atmosphere effect and only survive at the lowest tested temperature, 500°C. These results indicate that the pre oxidation of the samples help to mitigate the diffusion of hydrogen into the steel and that the grinding helps to increase the diffusion of protective alloying elements from the bulk to the surface of the steel.

The different results at the different temperatures show that there is a critical temperature at 600°C where the dual atmosphere effect is most prominent. At lower temperatures the kinetic energy needed for the diffusion of the hydrogen through the steel sample may be too low to effect the oxidation on the air side and at higher temperatures the diffusion of elements is higher and the protective alloying elements can therefore diffuse from the steel bulk to the surface to form protective oxides which mitigates the effect of the dual atmosphere effect.

6

Future Works

To further investigate the dual atmosphere effect of ferritic stainless steel studies regarding the parameters should be performed. These studies should focus on changing the hydrogen concentration in the flow to see if that has an effect. Another possible parameter to be checked is the flow rate, to see how it affects the corrosion behaviour.

There are some studies on coatings regarding the dual atmosphere effect, but we would like to further investigate coatings of different types to gain more knowledge about the mechanisms behind the dual atmosphere effect.

Future studies should focus on the coating material and the coating placement, where only the fuel side of the sample is coated to prevent initial hydrogen diffusion through the sample.

Reactive elements are used to mitigate corrosion and it would be interesting to look further into these elements and see if the dual atmosphere effect can be reduced.

Bibliography

- [1] Abdalla A. Hossain S. Azad A. Petra P. Begum F. Eriksson S. Nanomaterials for solid oxide fuel cells: A review. *Renewable and Sustainable Energy Reviews*, 82:353–368, 2018.
- [2] Junwei Wu and Xingbo Liu. Recent development of soft metallic interconnect. *Journal of Materials Science & Technology*, 26(4):293–305, 2010.
- [3] Iain Staffell, Andrew Ingram, and Kevin Kendall. Energy and carbon payback times for solid oxide fuel cell based domestic chp. *International Journal of Hydrogen Energy*, 37(3):2509–2523, 2012.
- [4] A. Boudghene Stambouli and E Traversa. Solid oxide fuel cells (sofcs): a review of an environmentally clean and efficient source of energy. *Renewable and Sustainable Energy Reviews*, 6(5):433–455, 2002.
- [5] Weilie Zhou and Zhong Lin Wang. *Scanning microscopy for nanotechnology: techniques and applications*, page 3. Springer, 2007.
- [6] Zhenguo Yang, Matthew S. Walker, Prabhakar Singh, Jeffrey W. Stevenson, and Truls Norby. Oxidation behavior of ferritic stainless steels under soft interconnect exposure conditions. *Journal of The Electrochemical Society*, 151(12):B669, 2004.
- [7] M.R. Ardigo-Besnard, I. Popa, O. Heintz, R. Chassagnon, M. Vilasi, F. Herbst, P. Girardon, and S. Chevalier. Effect of surface finishing on the oxidation behaviour of a ferritic stainless steel. *Applied Surface Science*, 412:196–206, 2017.
- [8] J. Larminie and A. Dicks. Fuel cell systems explained. 2nd ed. *West Sussex: John Wiley & Sons Ltd*, 2003.
- [9] A. Kirubakaran. S. Jain and R. K. Nema. A review on fuel cell technologies and power electronic interface. *Renewable and Sustainable Energy Reviews* 13, 2009;13:2430-2440.
- [10] Claudia Göbel. *Corrosion of Ferritic Stainless Steels Used in Solid Oxide Fuel Cells*. PhD thesis, Chalmers University of Technology, 2018.
- [11] Takehiko Takahashi. Nguyen Quang Minh. *Science and Technology of Ceramic Fuel Cells*, page 165. Elsevier, 1st edition, 1995.
- [12] Joelle C.W. Mah, Andanastuti Muchtar, Mahendra R. Somalu, and Mariyam J. Ghazali. Metallic interconnects for solid oxide fuel cell: A review on protective coating and deposition techniques. *International Journal of Hydrogen Energy*, 42(14):9219–9229, 2017.
- [13] Marta Boaro and Arico Antonino Salvatore. *Advances in Medium and High Temperature Solid Oxide Fuel Cell Technology*. Elsevier, 1st edition, 2017.

- [14] Patrik Alnegren. *Corrosion of Ferritic Stainless Steel Interconnects for Solid Oxide Cells – Challenging Operating Conditions*. PhD thesis, Chalmers University of Technology, 2018.
- [15] Noguchi M. and Yakuwa H. Lecture on fundamental aspects of high temperature corrosion and corrosion protection part 1: basic theory. *Ebara Engineering Review*, 252, 2016.
- [16] Per Kofstad. *High temperature corrosion*. Elsevier Applied Science, 1988.
- [17] David John Young. *High Temperature Oxidation and Corrosion of Metals*, page 39. Elsevier, 2nd edition, 2016.
- [18] N Birks, G. H Meier, and F. S Pettit. *Introduction to the high-temperature oxidation of metals*. Cambridge University Press, 2009.
- [19] Hannes Falk Windisch. *Improved Oxidation Resistance and Reduced Cr Vaporization from Thin-Film Coated Solid Oxide Fuel Cell Interconnects*. PhD thesis, Chalmers University of Technology, 2017.
- [20] Z. Yang and J. W. Fergus. *Solid Oxide Fuel Cells: Materials Properties and Performance*. Taylor and Francis Group, 1st edition, 2009.
- [21] Kevin Kendall and Michaela Kendall. *High-Temperature Solid Oxide Fuel Cells for the 21st Century*. Elsevier, 2nd edition, 2015.
- [22] Anders Werner Bredvei Skilbred and Reidar Haugrud. The effect of dual atmosphere conditions on the corrosion of sandvik sanergy ht. *International Journal of Hydrogen Energy*, 37(9):8095–8101, 2012.
- [23] Bent Tveten, Gunnar Hultquist, and Truls Norby. Hydrogen in chromium: Influence on the high-temperature oxidation kinetics in o₂, oxide-growth mechanisms, and scale adherence. *Oxidation of Metals*, 51(3/4):221–233, 1999.
- [24] Gunnar Hultquist, Bent Tveten, and Erik Hörnlund. Hydrogen in chromium: Influence on the high-temperature oxidation kinetics in h₂o, oxide-growth mechanisms, and scale adherence. *Oxidation of Metals*, 54(1/2):1–10, 2000.
- [25] Patrik Alnegren, Mohammad Sattari, Jan-Erik Svensson, and Jan Froitzheim. Severe dual atmosphere effect at 600 °c for stainless steel 441. *Journal of Power Sources*, 301:170–178, 2016.
- [26] Patrik Alnegren, Mohammad Sattari, Jan-Erik Svensson, and Jan Froitzheim. Temperature dependence of corrosion of ferritic stainless steel in dual atmosphere at 600–800°c. *Journal of Power Sources*, 392:129–138, 2018.
- [27] Ray F Egerton. *Physical principles of electron microscopy*. Springer, 2008.
- [28] Gordon R. Holcomb, Malgorzata Ziomek-Moroz, Stephen D. Cramer, Bernard S. Covino, and Sophie J. Bullard. Dual-environment effects on the oxidation of metallic interconnects. *Journal of Materials Engineering and Performance*, 15(4):404–409, 2006.
- [29] Kerem Gündüz. *Unpublished results*, 2019.
- [30] Hideto Kurokawa, Yukiko Oyama, Kenichi Kawamura, and Toshio Maruyama. Hydrogen permeation through fe-16cr alloy interconnect in atmosphere simulating sofc at 1073 k. *Journal of The Electrochemical Society*, 151(8):A1264, 2004.

A

Appendix 1

A.1 500°C exposure

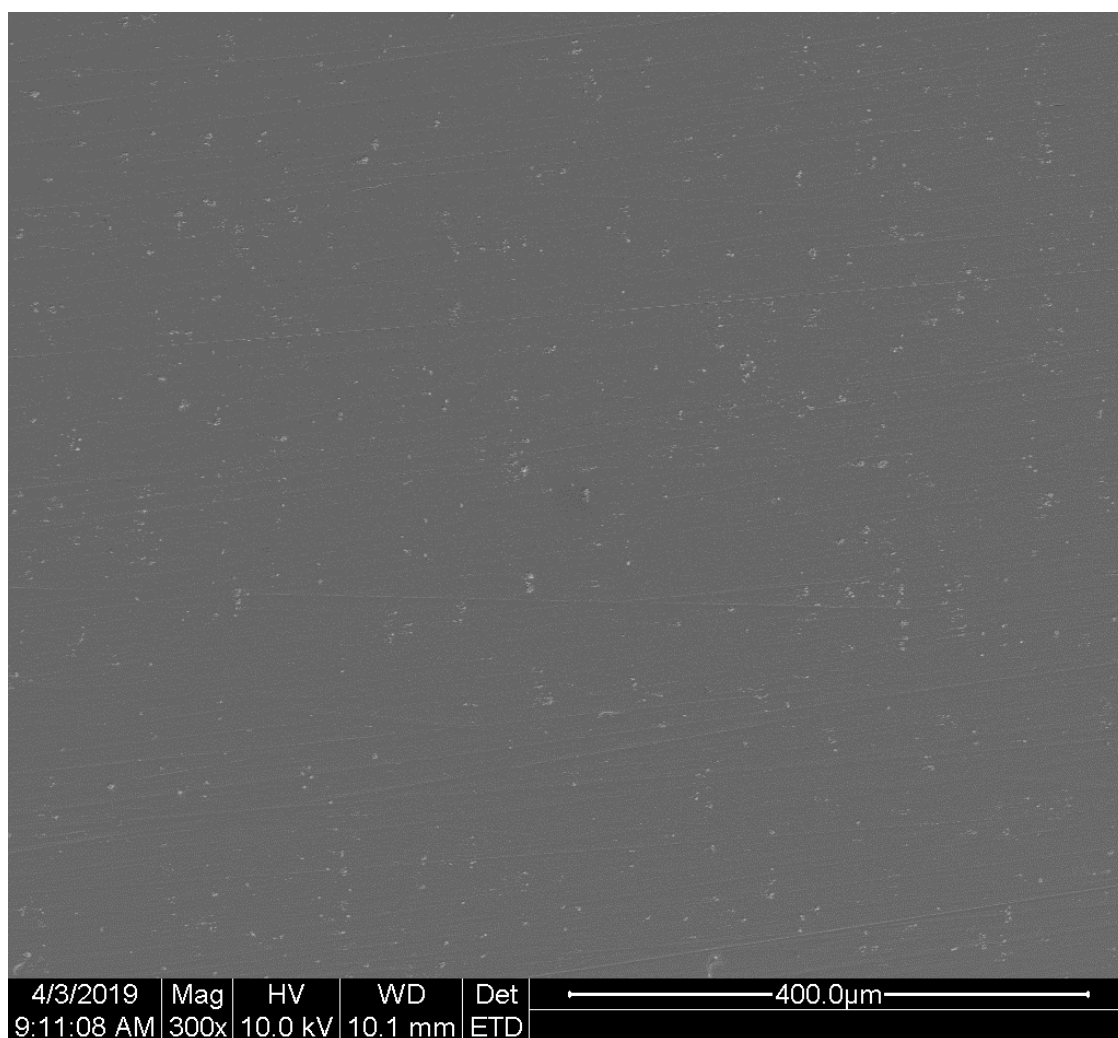


Figure A.1: Top view SEM image of sample c) after 336 hours.

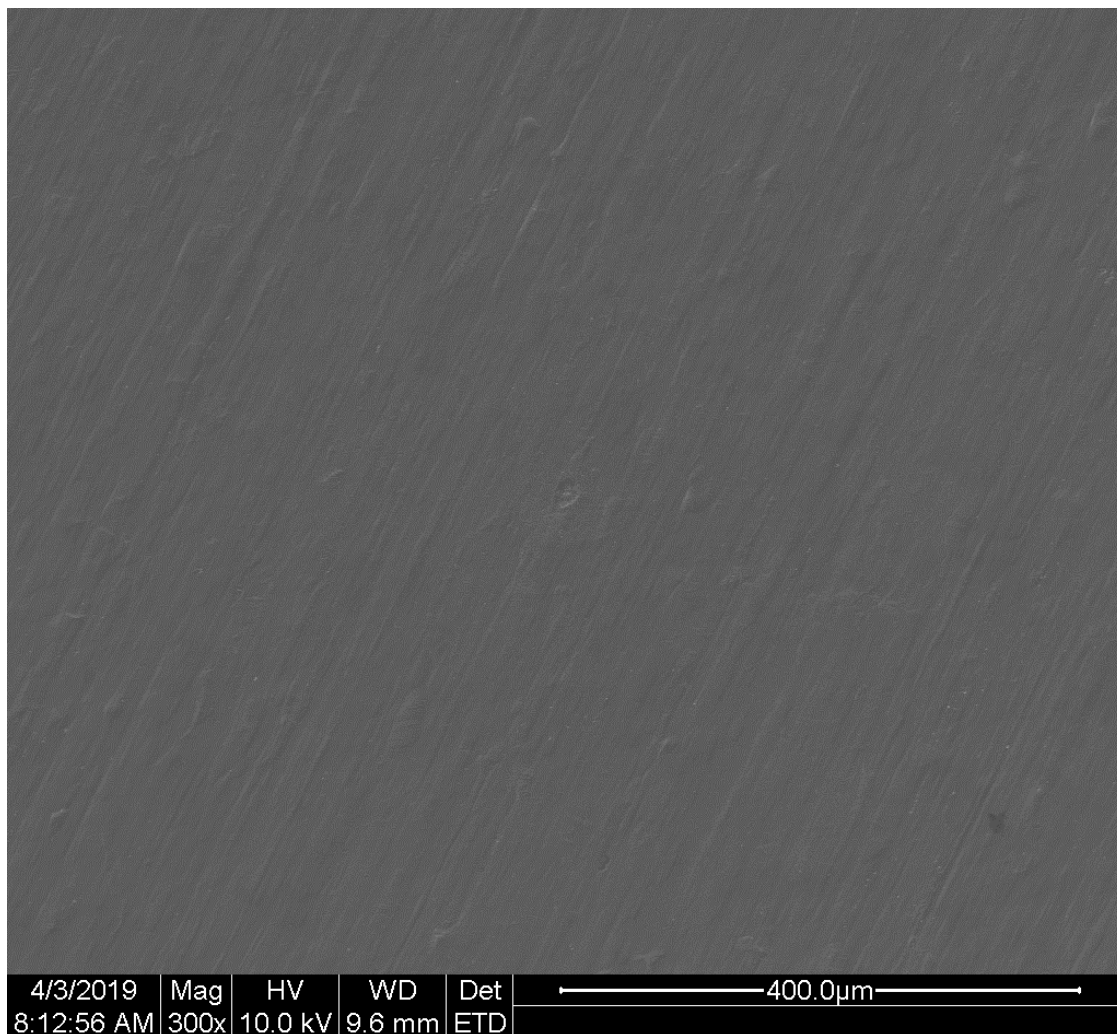


Figure A.2: Top view SEM image of sample e) after 336 hours.

A.2 550°C exposure

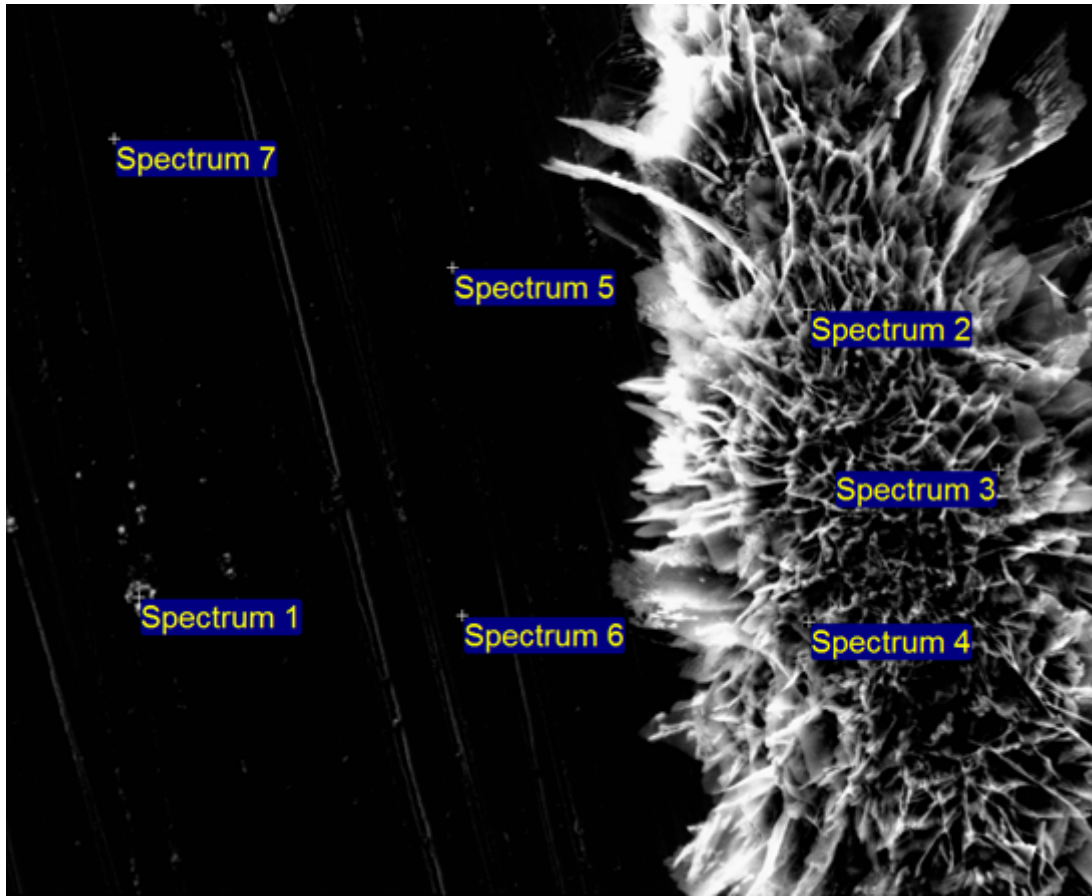


Figure A.3: EDX image of sample e) after 336 hours.

Table A.1: EDX analysis of sample e) after 336 hours, elements in weight%.

	C	O	Si	Ti	Cr	Fe	Nb
Spectrum 1	1	20		4	17	42	15
Spectrum 2	5	17			16	62	
Spectrum 3	2	19			15	64	
Spectrum 4	2	24			11	62	
Spectrum 5	1	6	1		20	72	
Spectrum 6	1	3	1		21	74	
Spectrum 7	1	3	1		20	75	

A.3 600°C exposure

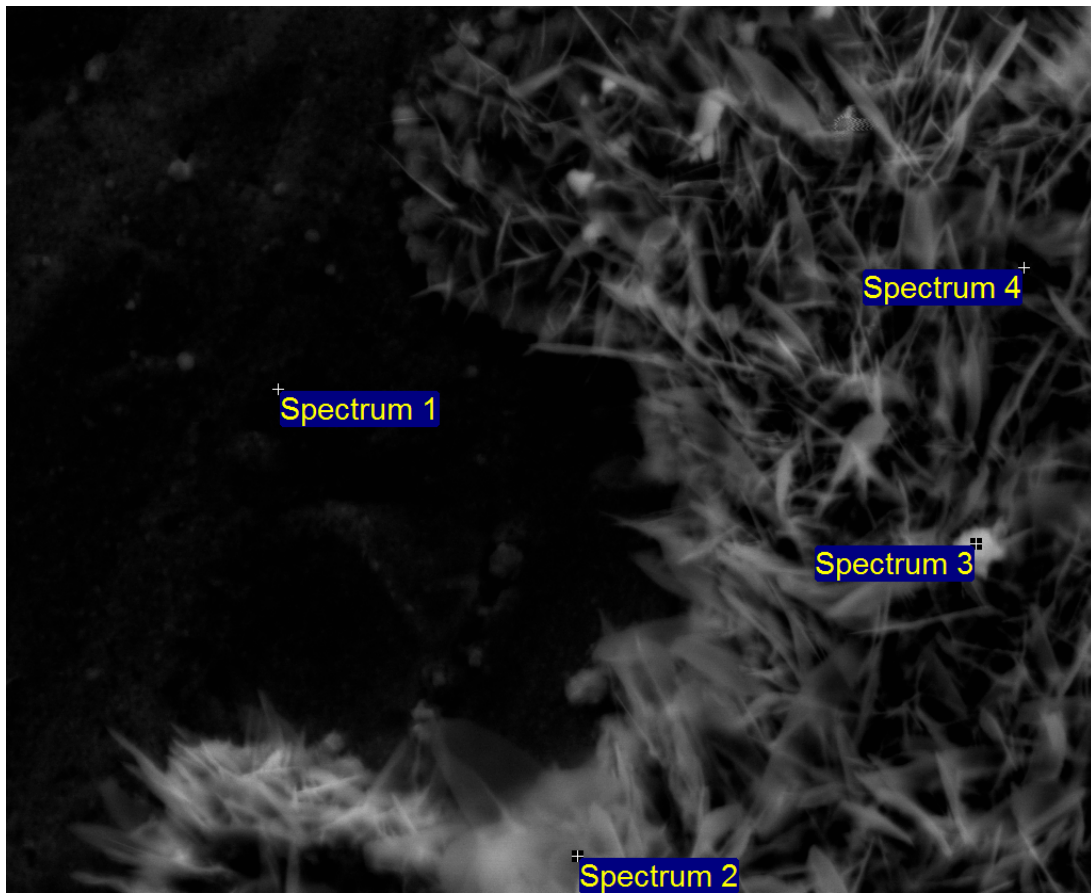


Figure A.4: EDX of sample a) after 336 hours.

Table A.2: EDX analysis of sample a) after 336 hours, elements in weight%.

	C	O	Cr	Mn	Fe
Spectrum 1	3	5	15	1	77
Spectrum 2	3	25	4		68
Spectrum 3	6	36	4		57
Spectrum 4	3	27	3		67

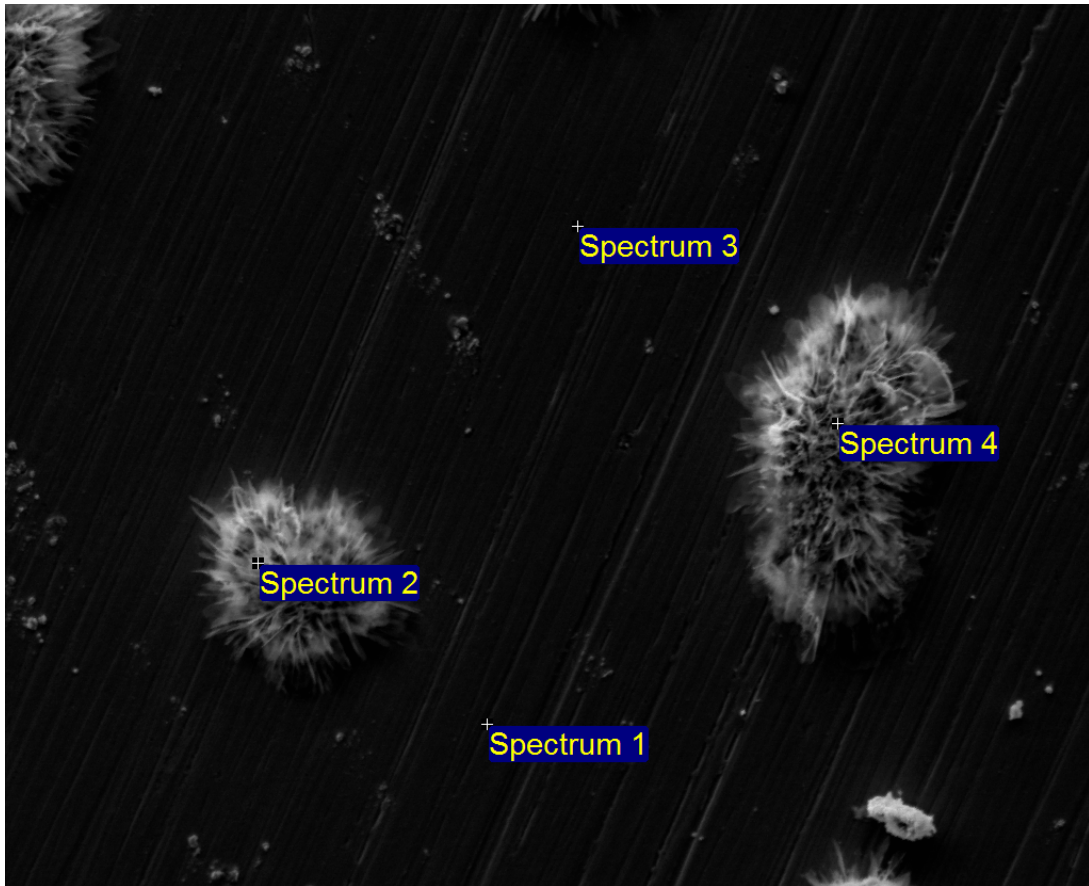


Figure A.5: Top view SEM and EDX image of sample c) after 336 hours.

Table A.3: EDX analysis of sample c) after 336 hours, elements in weight%.

	C	O	Cr	Mn	Fe
Spectrum 1	4	24	8		63
Spectrum 2	4	26	8		62
Spectrum 3	3	4	18	1	74
Spectrum 4	3	22	8		66

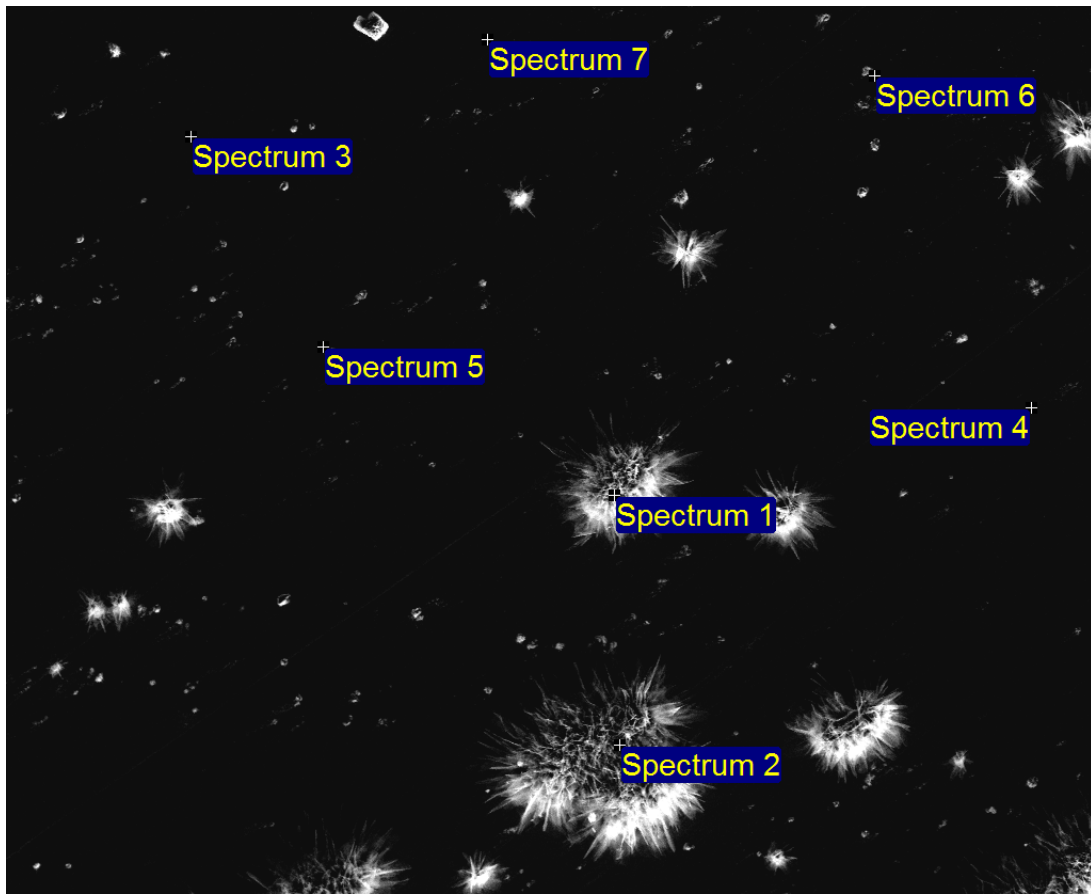


Figure A.6: EDX image of sample e) after 336 hours.

Table A.4: EDX analysis of sample e) after 336 hours, elements in weight%.

	O	Si	Cr	Fe
Spectrum 1	61		4	34
Spectrum 2	47		5	48
Spectrum 3	9	1	18	72
Spectrum 4	9	1	17	72
Spectrum 5	9	1	17	72
Spectrum 6	8	1	18	72
Spectrum 7	10	1	18	71

A.4 650°C exposure

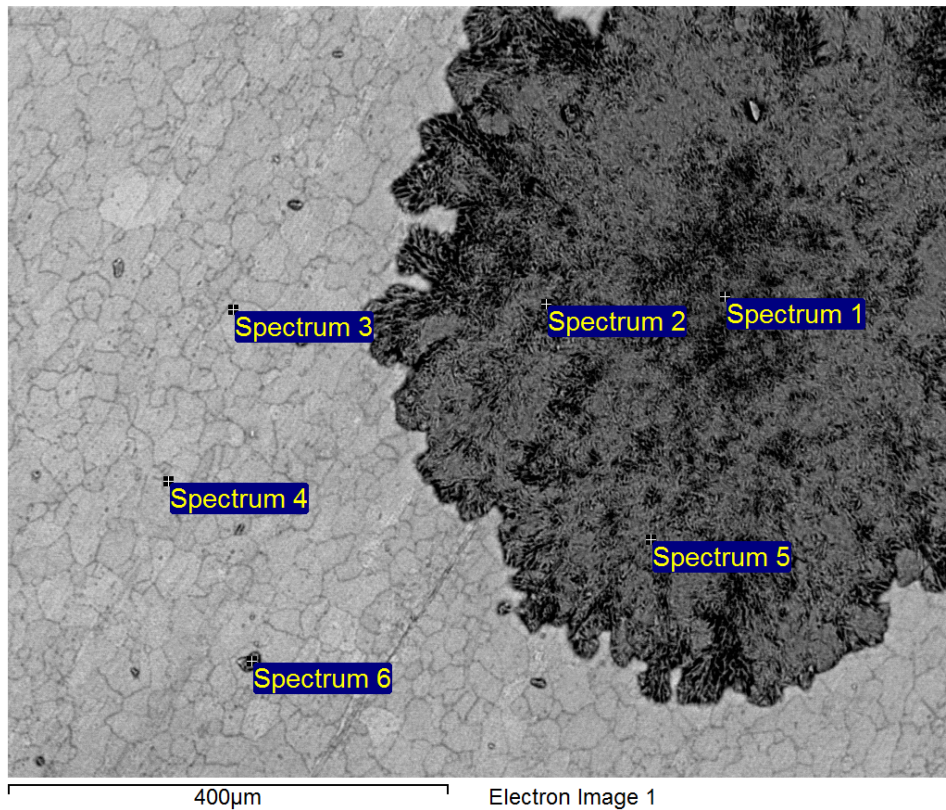


Figure A.7: EDX of sample a) after 336 hours.

Table A.5: EDX analysis of sample a) after 336 hours, elements in weight%.

	C	O	Si	Cr	Mn	Fe
Spectrum 1	1	22		10		67
Spectrum 2	3	30		10		57
Spectrum 3	3	13	1	19	2	62
Spectrum 4	2	12	1	18	2	65
Spectrum 5	2	24		11	1	62
Spectrum 6	2	26		7		65

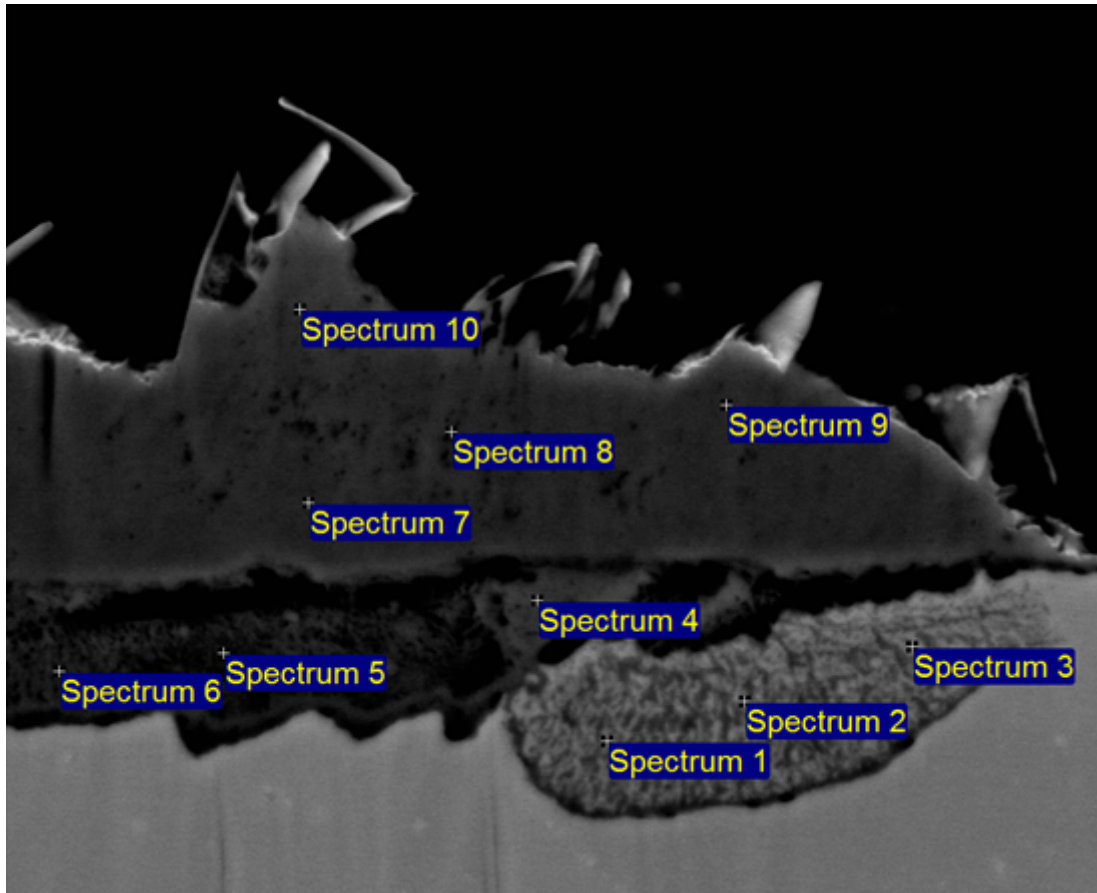


Figure A.8: EDX of cross section of sample a) after 336 hours.

Table A.6: EDX analysis of cross section of sample a) after 336 hours, elements in weight%.

	O	Si	Ti	Cr	Mn	Fe
Spectrum 1	11	1		18		70
Spectrum 2	11	1		19		68
Spectrum 3	8	1		13		78
Spectrum 4	24	1		15		60
Spectrum 5	23	1	1	34	1	40
Spectrum 6	23	1		31	1	44
Spectrum 7	24			5		71
Spectrum 8	24			6	1	70
Spectrum 9	24			5	1	70
Spectrum 10	24			4		71

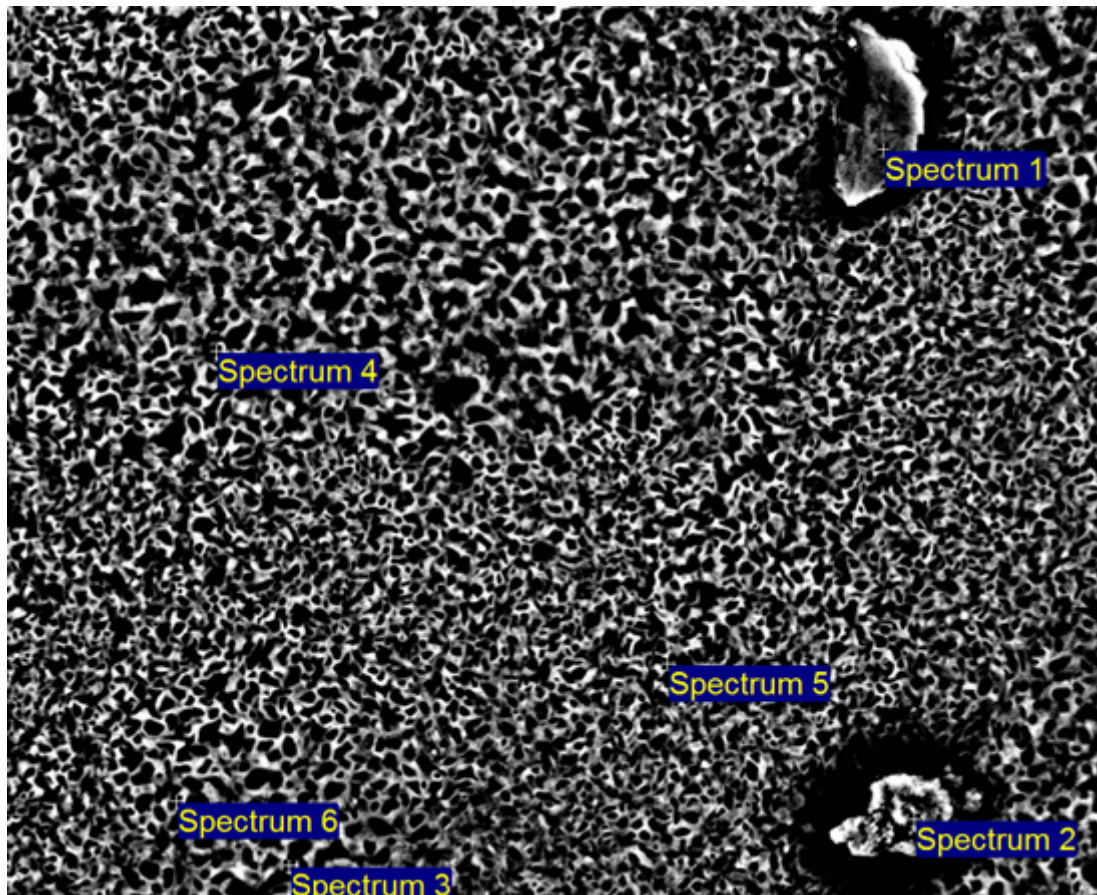


Figure A.9: EDX of sample e) after 336 hours.

Table A.7: EDX analysis of sample e) after 336 hours, elements in weight%

	C	O	Si	Cr	Mn	Fe
Spectrum 1	2	28	1	28	1	40
Spectrum 2	2	28	1	23	1	46
Spectrum 3	2	30		1		67
Spectrum 4	2	27		1	1	69
Spectrum 5	1	24		2	1	72
Spectrum 6	1	22		1	1	75

A.5 700°C exposure

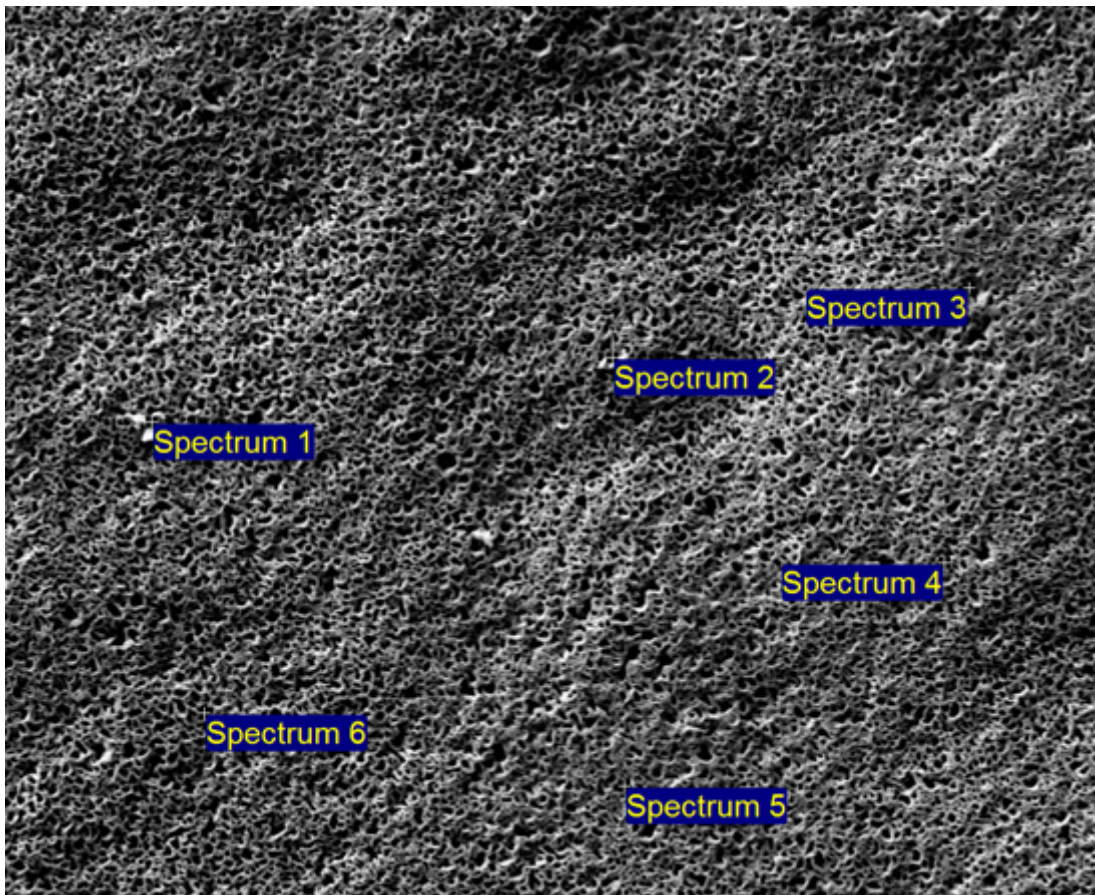


Figure A.10: EDX of sample e) after 336 hours.

Table A.8: EDX analysis of sample e) after 336 hours, elements in weight%

	C	O	Cr	Fe
Spectrum 1	11	19	19	51
Spectrum 2	29	17	3	50
Spectrum 3	26	12	10	52
Spectrum 4	26	15	5	54
Spectrum 5	36	16		48
Spectrum 6	16	13	14	56

A.6 800°C exposure

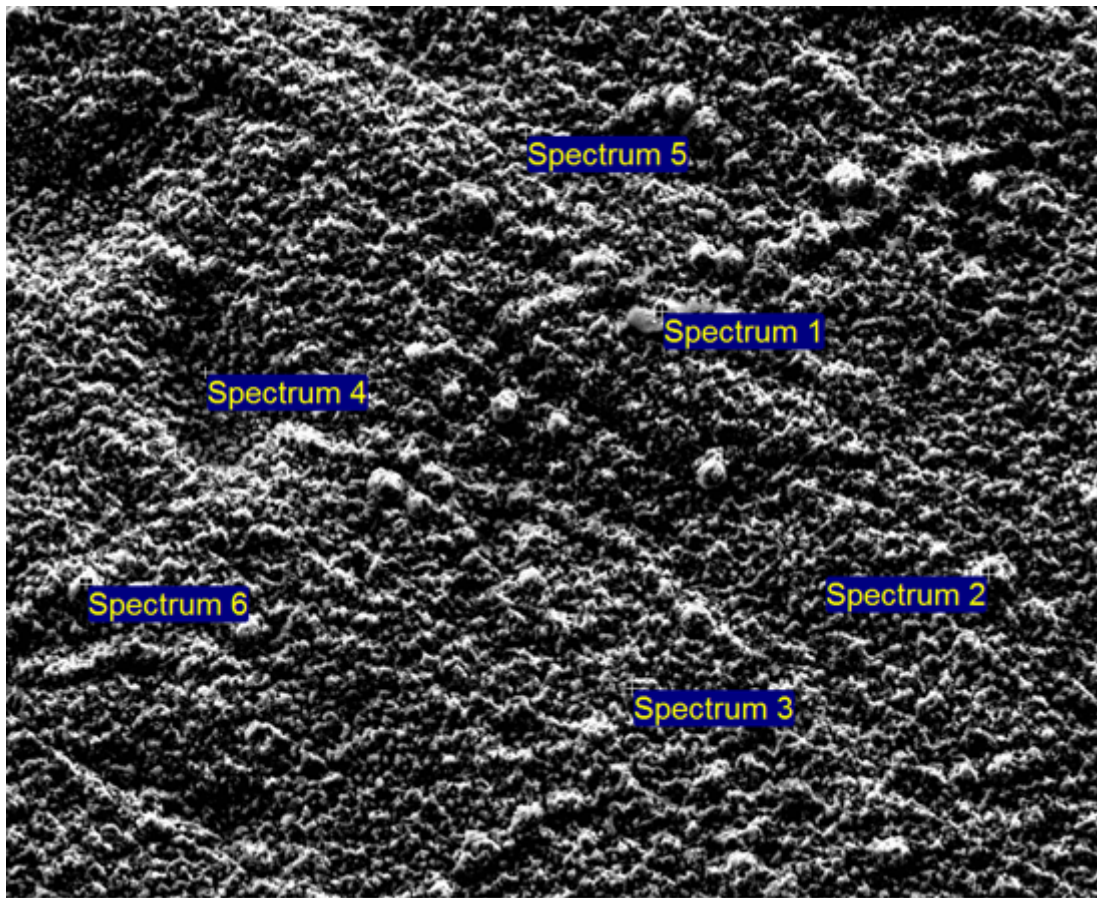


Figure A.11: EDX of sample a) after 336 hours.

Table A.9: EDX analysis of sample e) after 336 hours, elements in weight%

	C	O	Si	Ti	Cr	Mn	Fe
Spectrum 1	1	15	2		30	13	39
Spectrum 2	1	21		2	29	42	5
Spectrum 3	1	27		2	30	37	3
Spectrum 4		39		34	12	15	
Spectrum 5	1	23		1	29	42	4
Spectrum 6	1	20		2	27	44	5

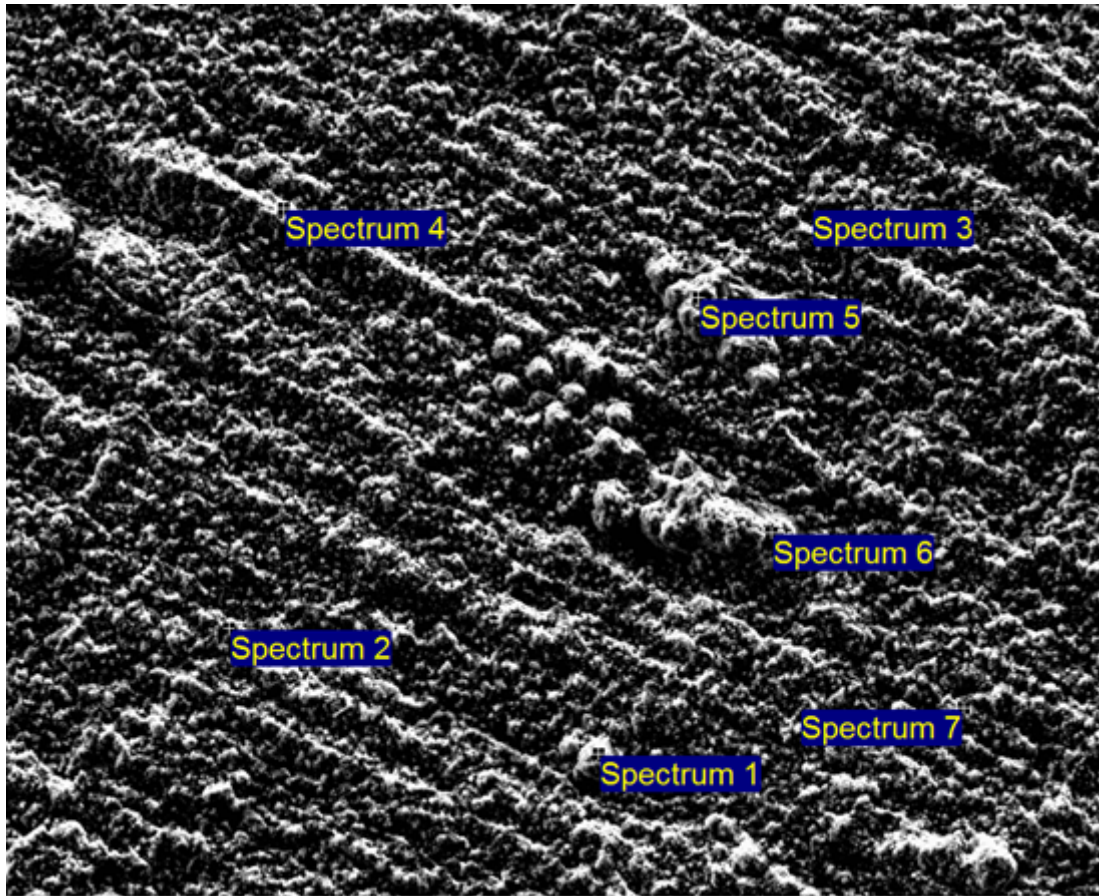


Figure A.12: EDX of sample c) after 336 hours.

Table A.10: EDX analysis of sample c) after 336 hours, elements in weight%

	C	O	Ti	Cr	Mn	Fe
Spectrum 1	1	21	1	28	43	5
Spectrum 2	1	20	3	28	43	5
Spectrum 3	1	22	3	29	40	4
Spectrum 4	1	27	13	25	31	3
Spectrum 5		41	52	3	4	
Spectrum 6	1	28	14	27	27	2

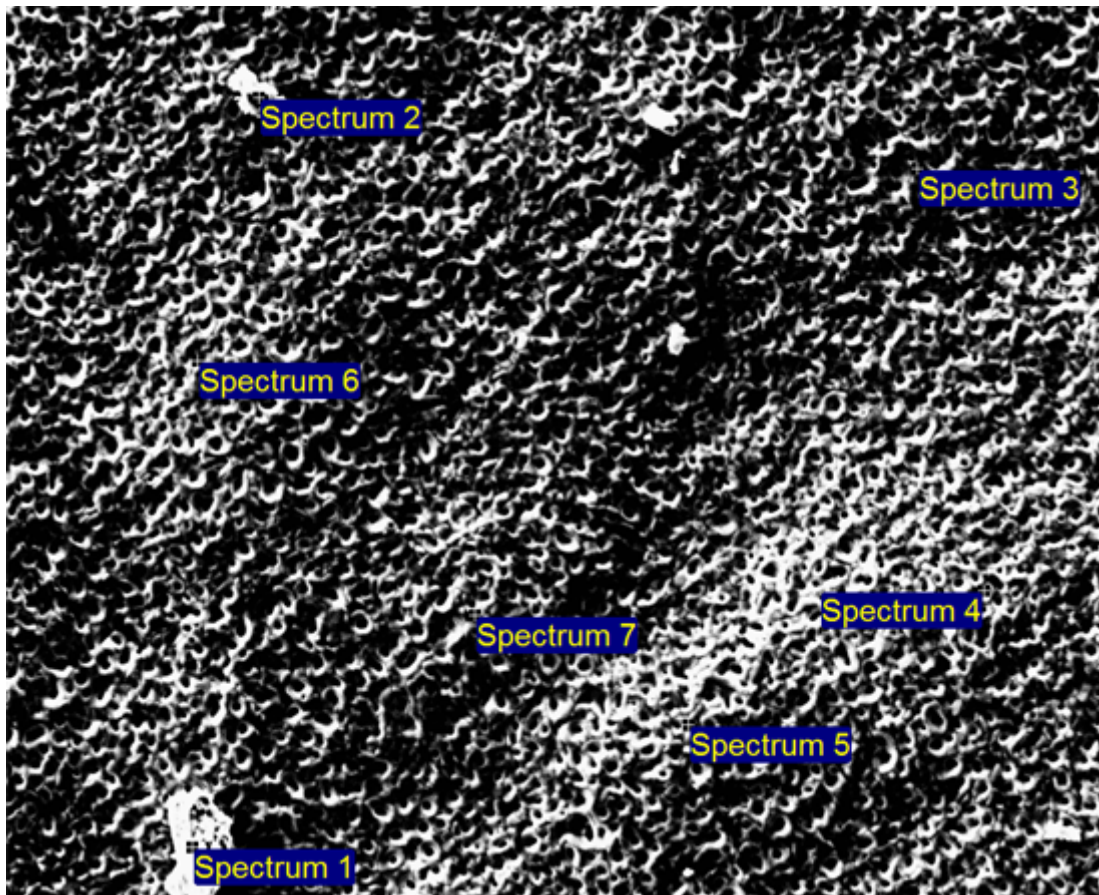


Figure A.13: EDX of sample e) after 336 hours.

Table A.11: EDX analysis of sample e) after 336 hours, elements in weight%

	C	O	Si	Cr	Fe
Spectrum 1	1	22	1	18	58
Spectrum 2	1	34	8	41	16
Spectrum 3	2	28			71
Spectrum 4	1	32			66
Spectrum 5	1	30			69
Spectrum 6	2	31			68
Spectrum 7	1	31			68